EVOLUTION OF AN INTERMONTANE BASIN ALONG THE MAACAMA FAULT, LITTLE LAKE VALLEY, NORTHERN CALIFORNIA

by

Gwendolyn Erickson

A Thesis

Presented to

The Faculty of Humboldt State University

In Partial Fulfillment

Of the Requirements for the Degree

Masters of Science

In Environmental Systems: Geology

May, 2008

EVOLUTION OF AN INTERMONTANE BASIN ALONG THE MAACAMA FAULT, LITTLE LAKE VALLEY, NORTHERN CALIFORNIA

by

Gwendolyn Erickson

Approved by the Master's Thesis Committee:

Harvey M. Kelsey, Major Professor Date

Victoria E. Langenheim, Committee Member Date

Kevin P. Furlong, Committee Member Date

Lori A. Dengler, Committee Member Date

Sharon Brown, Graduate Coordinator Date

Chris A. Hopper, Interim Dean for Research and Graduate Studies Date

ABSTRACT

EVOLUTION OF AN INTERMONTANE BASIN ALONG THE MAACAMA FAULT, LITTLE LAKE VALLEY, NORTHERN CALIFORNIA

Gwendolyn Erickson

Associated with the northern strands of the San Andreas fault system in California is a series of small intermontane basins. While it is tempting to ascribe their formation to simple 'pull-apart' tectonics along the dominantly strike-slip fault strands, direct evidence for basin genesis is lacking. In this study, a detailed gravity survey throughout the Little Lake Valley region (Willits, California) provides constraints on mechanisms of basin formation along this young segment of the San Andreas fault system. Interpretation of isostatic gravity anomaly data provides insight into fault geometry, basin structure, and thickness of Quaternary fill in Little Lake Valley, California. Although the active strike-slip Maacama fault zone diagonally trends through the southwest part of the valley, gravity and geologic interpretations indicate the valley conceals an earlier basin and faulting history.

Gravity models, mapped geology, and double-difference relocated seismicity data indicate that Little Lake Valley basin geometry records a tectonic history which includes subduction, extension, and presently, dextral strike-slip motion along the Maacama fault. The isostatic gravity anomaly of Little Lake Valley basin is negative (up to 13 mGals) and rhombic in shape. Modeling indicates two splays, less than a km apart,

of a reverse up-to-the-east East Valley fault. Cumulative vertical fault displacement along the East Valley fault increases in the southern portion of the valley. Gravity modeling and geology indicate two normal, up-to-the-northwest faults; one in the northwest portion of Little Lake Valley and the other to the south in Redwood Valley. Normal faults are presumed to be temporally related to Clear Lake volcanics (2 Ma to 10ka), located 45 km southwest of Little Lake Valley, and migration of the Mendocino triple junction to the north. While focal mechanisms of double-difference relocated seismicity indicate reverse and normal faults no longer accommodate significant vertical motion, portions of these structures are accommodating strike-slip motion. Consequently, the Maacama fault is occupying an upward-branching flower structure which takes advantage of pre-existing fault structures and may sole into a regional detachment at approximately 10 km depth. Although Little Lake Valley was not initiated as a strike-slip basin, development of the Maacama fault may evolve Little Lake Valley into a strike-slip basin.

ACKNOWLEDGEMENTS

I must first express my gratitude towards my major advisor Harvey Kelsey. His enthusiasm, support, and care floated me through this process. Vicki Langenheim, Kevin Furlong, and Gavin Hayes were always there when I needed an explanation, a computer program, a GMT script, or a glass of wine. They made this thesis possible. I would like to thank Lori Dengler for her guidance, and the opportunities she has given me through the years. Thank you Penn State and the U. S. Geological Survey for use of the gravimeters, and David Ponce of U. S. Geological Survey for processing the data. Janet Key, Gary Hensley, Paul Sunderberg, Vicki, and my Man, Todd Williams, generously donated time to help me in the field. Big love to Todd for the GMT lessons. Debt also owed to Cynthia Werner, Julie Bawcom, Bob McLaughlin, Darcy McPhee, Frey Vineyards, John Ford, Golden Vineyards, Mark Edwards, and Mendocino Redwood Company. Completing this thesis was comparable to a marathon. I'm sad it's over.

This is for my Mama.

TABLE OF CONTENTS

LIST OF TABLES

LIST OF FIGURES

LIST OF APPENDICES

INTRODUCTION

Field Area

Little Lake, Redwood, and Ukiah Valleys are three intermontane basins situated along the Maacama fault in the northern California Coast Ranges, approximately 100 km north-northwest of Santa Rosa, California (Figure 1). Collectively, the three basins span a north-south distance of approximately 50 km. The most common explanation for basins along the Maacama fault is that the basins are formed by slip along faults associated with the Maacama fault zone (Cardwell, 1965; Dickinson and Snyder, 1979; McLaughlin and Nilsen, 1982; Nilsen and McLaughlin, 1985; Nilsen and Clarke, 1989; Brady, 2003). However, structural models are not well developed and basins are best examined by evaluating their tectonic history.

Currently, Redwood and Ukiah Valleys are separated from the topographically higher Little Lake Valley by a 600 m step along the southern flank of the Laughlin Range (Figure 2A and 2B). The step of the Laughlin Range also forms part of the drainage divide between the Eel and Russian River watersheds. Pleistocene sediment in Little Lake Valley records a drainage reversal from south flowing to north flowing drainage through Little Lake Valley (Woolace, 2005), suggesting the drainage divide existed north of its current location during the Pleistocene. Tectonic processes related to the migration of the Mendocino triple junction may be accountable for the 600 m step in topography and Pleistocene drainage reversal (Lock et al., 2006).

Objectives

The objectives of this study are to better define geologic structure of Little Lake Valley, compare the structure to that of Redwood and Ukiah Valleys, and evaluate models of formation of Little Lake Valley. To evaluate bedrock geometries in each valley I collected gravity measurements and modeled and analyzed gravity anomaly data. Bedrock structures inferred from gravity models may lend insight to development of the Maacama fault zone and regional dynamic topography related to the passing of the Mendocino triple junction.

Regional Tectonics

Development of the western margin of North America has, in part, been controlled by interaction between the Pacific, North American, and Farallon (Gorda) plates (Figure 1) for the past 25 to 30 Ma (Atwater, 1970). Boundaries between the plates are the San Andreas fault zone, Mendocino fracture zone, and Cascadia subduction zone; the mutual intersection of these three plate boundaries is the Mendocino triple junction (circle on Figure 1).

The San Andreas fault zone is an approximately 1,200 km long, north-northwest growing transform plate boundary that develops in the wake of the Mendocino triple junction in northern California (Atwater, 1970). North of the latitude of San Francisco, the San Andreas fault zone plate boundary consists of three main faults that collectively are 110 km wide narrowing to approximately 70 km in the latitude of the Mendocino triple junction region (Figure 1). The three faults young to the northeast and from the

coast inland consist of the San Andreas fault, Maacama fault, and Bartlett Springs fault. Based on two-dimensional dislocation models of geodetic data between the latitudes of 38ºN and 40ºN, the slip rate across each of the three discrete faults decreases from 17 mm/yr on the coastal San Andreas fault to 8 mm/y along the Bartlett Springs fault in the east (Freymueller et al., 1999). The San Andreas fault is locked to 15 km depth, the Maacama fault is locked to 13 km depth with creep occurring in the upper 5 km, and the Bartlett Springs fault creeps at all depths (Freymueller et al., 1999). Rates are consistent along strike to the north, into the Mendocino triple junction region (Williams et al., 2006). In general, motion between the Pacific/North American Plates is distributed along the approximately 100 km wide San Andreas fault zone.

The Maacama fault is the central segment of the northern San Andreas fault zone and is a northward and right step continuation of the Rodgers Creek fault (Figure 1). The Maacama fault is mapped from approximately latitude 38º 50’ N to 39º 50’ N (Pampeyan et al., 1981; Upp, 1982) as a series of unconnected and en echelon faults and lineaments varying in azimuth from N8º W to N47º W with an overall trend of approximately N27º W (Upp, 1989). The presence of multiple unconnected faults attests to the youthful age of the strike-slip Maacama fault. McLaughlin and Nilsen (1982) and Nilsen and McLaughlin (1985) suggested that structural basins along the San Andreas fault zone (including Ukiah Valley, Little Lake Valley and Round Valley) are consequences of oblique pull-apart extension between en echelon and branching splays of the major strike-slip fault zone. North of the Maacama fault, dextral motion related to the developing

transform plate boundary continues on the Garberville fault zone (Figure 1; Kelsey and Carver, 1988).

Geodetic data indicate higher dextral slip across the Maacama fault zone than do theodolite measurements of surface creep on the fault. Geodetic measurements across Maacama-fault-perpendicular transects through the towns of Willits and Ukiah, over a four-year period, indicate a far-field dextral slip rate of 13.9 mm/yr with creeping motion at the surface (Freymueller et al., 1999). Theodolite measurements during a 7.8 year period in Ukiah and a 9.3 year period in Willits indicate on-fault creep rates of 4.5 mm/yr and 6.6 mm/yr, respectively (Galehouse, 2002). The discrepancy between far-field geodetic and near-field theodolite measurements suggests that creep on discrete faults is accounting for less than one-half of the right lateral slip occurring across the Maacama fault zone.

Observations from paleoseismic investigations along various splays of the Maacama fault provide evidence for Holocene seismic activity. Fault trench studies within the Laughlin Range (Figure 2) and along Upp Creek in Little Lake Valley (Figure 3) conclude that at least two faulting events occurred in the last 16,200 years (Upp, 1989). A fault trench study near Haehl Creek in Little Lake Valley (Figure 3) documented two offset paleo-channels of Haehl Creek that indicate right-lateral strike-slip rates of 6.3 to 8.3 mm/yr and 9.2 to 11 mm/yr for the time frames of 700 and 2,800 years, respectively (Larsen, 2006). Near Lake Mendocino in Ukiah, Sickler (2003) used a 4,840 to 4,550 year old terrace riser which was offset 42 m to 61 m, to establish Holocene slip rates of 8.7 to 13.4 mm/yr on the Maacama fault. Slip rates inferred from

offset of the younger channel at Haehl Creek (584 to 704 years) (Larsen, 2006) are within the same order of magnitude as creep rates derived from theodolite measurements (Galehouse, 2002). In contrast, slip rates inferred from offset of the older channel at Haehl Creek (pre-2,544 years ago) (Larsen, 2006) and offset of the terrace riser in Ukiah (pre-4,550 years ago) both indicate slip rates similar to geodetic rates of 13 mm/yr (Freymueller et al., 1999).

The two tectonic regimes that have dominated development of the northern California Coast Range region are subduction and strike-slip tectonics. Deformation of the Franciscan complex records both regimes. The Franciscan complex consists of three belts increasing in age and metamorphic grade from west to east: Coastal, Central and Eastern belts (Blake et al., 1985). Fold axes and plunge measurements of Coastal belt rock in the Fort Bragg to Little Lake Valley (Kleist, 1974; Kramer,1976) and Laytonville (Gucwa 1974) areas indicate three periods of deformation: 1) deformation during deposition of soft sediments; 2) northwest-trending, east-dipping faulting and east-vergent folding and faulting related to subduction; and 3) east-west trending folds related to north-south transform compression. Coastal belt rocks show the deformational history of the Central and Eastern belts before the Central/Eastern belts were buried and tectonically disturbed (Kleist, 1981).

While structural fabric of the Franciscan complex provides evidence for the chronological order of deformation regimes, subduction and transform deformation in the northern California Coast Ranges are not mutually exclusive. Strike-slip faults currently are the dominant style of deformation in the northern California Coast Ranges south of

the Mendocino triple junction, but the landscape is still responding to deformation related to the passing of the Mendocino triple Junction (Lock et al., 2006). The rate of transform motion between Pacific and North American plates is approximately 46 to 48 mm/yr (DeMets et al., 1987; Bennett et al., 1999). Consequently, the Mendocino triple Junction, which migrates northward at the rate of transform motion, was approximately at the latitude of Little Lake Valley at 3 Ma and Point Reyes at 8 Ma (Figure 1; Atwater, 1970; Wilson, 1989; Hayes and Furlong, 2007a). As the Mendocino triple Junction migrates north, the southern edge of the subducted Gorda slab is replaced by upwelling asthenospheric material, creating a slab window (Figure 4; Atwater, 1970; Dickinson and Snyder, 1979). Recent regional geophysical studies support the model of a slab window that consists of high velocity material at relatively shallow depths (presumed to be hot asthenospheric material) approximately 150 km southeast of the Mendocino triple junction (Figures 1 and 4; Trehu et al., 1995; Beaudoin et al., 1996; Levander et al., 1998; Hayes et al., 2006; Hayes and Furlong, 2007a) and thermodynamic models and seismicity data predict the current location of the southern edge of the Gorda slab (Figure 1, SEDGE Furlong and Govers, 1999; Furlong and Schwartz, 2004; Pryor et al., 2007).

The Mendocino crustal conveyor model contends that both topography and tectonics south of the Mendocino triple junction are consequence of the northward migrating SEDGE (Furlong and Govers, 1999). The Mendocino crustal conveyor model assumes cooling asthenospheric material couples to both the upper face of the down going SEDGE and underside of the North American plate. Consequently, the North American plate thickens as it is pulled in on itself in advance of the Mendocino triple

junction and thins south of the Mendocino triple junction due to extension (Figure 4). As indicated by receiver function analyses (Hayes and Furlong, 2007a), the area between Ukiah and Little Lake Valley is within the area of crustal thinning as predicted by the Mendocino crustal conveyor model. Two hypothesized consequences of crustal thinning in the northern California Coast Ranges are crustal gravitational collapse (Liu and Furlong, 1994) and consolidation of multiple splays of the young Maacama fault zone into fewer but more continuous fault zones (Furlong et al., 1989).

Geology of the Little Lake Valley Area

Little Lake Valley lies at an elevation of approximately 400 m (USGS, 1991), within the Central belt of the Franciscan Complex (Figure 2) (Jenkins et al., 1960). The west side of Little Lake Valley consists of a mélange of greywacke and chert. Slopes are 7^{o} to 12^{o}, are landslide prone, and peak elevations reach 800 m. The east side of Little Lake Valley is more competent, and metavolcanics of Rocktree Valley and heavily fractured greywacke of Berry Canyon form steeper slopes, between 10^{o} and 25^{o}, and peak elevations reach 845 m.

Although Little Lake Valley drains north to the South Fork Eel River, imbricated clasts of Pleistocene gravel in the southern portion of Little Lake Valley indicate paleo-flow direction of high-energy streams to the south-southeast, indicating that Little Lake Valley previously drained to the Russian River (Woolace, 2005). Currently, small north-flowing creeks entering the south end of Little Lake Valley are incised in steeply walled canyons within the valley. In contrast, north of the latitude of Upp Creek and Berry

Canyon (Figure 3), the same creek channels shallow into an actively aggrading flood prone area that allows fine grained floodplain deposits (blue unit on Figure 3) to accumulate. Consequently, fluvial sediments in Little Lake Valley indicate a drainage reversal, then subsequent uplift and incision in the southern portion of the valley and provide evidence for a tectonically controlled basin (Woolace, 2005). Presently, the divide between the Eel and Russian Rivers is located approximately 5 km from the southern portion of Little Lake Valley (Figure 2).

Little Lake Valley sediment ranges in age from Holocene to Pliocene, although the age of oldest sediment fill is unknown (Cardwell, 1965). Youngest sediments are latest Holocene alluvial, colluvial, and lacustrine deposits derived from erosion of adjacent mountains and reworking of older sediments in the southern portion of the valley, and consist of clay, silt, sand, and gravel (blue unit on Figure 3; Woolace, 2005). Based on interpretations of soils recorded in California Water Resources well logs, Holocene deposits are absent on the hills in the southern portion of Little Lake Valley thickening to approximately 30 m in the northern portion of Little Lake Valley (Cardwell, 1965; Woolace, 2005). Pliocene- and Pleistocene-aged deposits underlie Holocene sediment in Little Lake Valley basin and also outcrop as erosional remnants at elevations between 425 m to 480 m and 425 m to 540 m on the east and south margins above Little Lake Valley, respectively (olive unit on Figure 3; Cardwell, 1965; Woolace, 2005). Pliocene and Pleistocene aged deposits consist of poorly sorted gravel, sand and sandstone, silty clay and diatomaceous shale (Cardwell, 1965) and are typical of fluvial, alluvial and lacustrine deposits. Three interbedded late Pleistocene tephras, including the

740 ka Thermal Canyon tephra, the approximately 575 ka Rockland tephra (Meyer et al., 1991; Lanphere et al., 1999) and an unnamed 110 ka tephra, have been identified in the southern portion of the valley (Woolace, 2005). Based on stratigraphic distributions of dated tephras, Woolace (2005) calculated an average Pleistocene sedimentation rate in Little Lake Valley of approximately 1.1 m/ka. Bedding of Pleistocene deposits in the southern portion of Little Lake Valley is tilted north 5º to 35 º with a mean dip of approximately 8º (Figure 3; Woolace, 2005) and these dips are in agreement with regional dips of 5º to 7º to the north in Ukiah Valley (Treasher, 1955; Cardwell, 1965). Based on depositional facies changes in Little Lake Valley, inferred from California Department of Water Resources well logs, the region began to undergo northward tilting during the middle Pleistocene (Woolace, 2005). Cardwell (1965) estimated Little Lake Valley fill deposits to be approximately 455 m thick in the southwestern part of the valley; however, he provided no basis for the estimate. In contrast, Woolace (2005) inferred that Little Lake Valley deposits were up to 1,100 m thick in the northern part of the valley based on post-depositional tilting observed in the southern portion of the valley.

The Maacama fault is well documented on the west side of Little Lake Valley (Figure 3; Jenkins et al., 1960; Pampeyan et al., 1981; Upp 1982, 1989; Woolace, 2005; Larsen, 2006) and the creeping fault can be traced through the town of Willits by its right-lateral offset and left-stepping en echelon cracks in pavement. North of Willits, geomorphology of Upp Creek appears to be structurally controlled by the Maacama fault (Pampeyan et al., 1981; Upp, 1989). Historical seismicity indicates the surface trace of

the Maacama fault mapped within Little Lake Valley is aseismic, assuming that the fault is vertical to seismogenic depths (Figure 3).

Little Lake Valley is bounded by North and East Valley faults (Woolace, 2005), but outside of geomorphic observations of fault-line scarps, little is understood about the fault style or timing. Depths to bedrock inferred from California Department of Water Resources well logs suggest both the North and East Valley faults exhibit at least 50 m up to the northwest and east displacements, respectively (Woolace, 2005). An isolated exposure of Pleistocene or older gravels at the Willits Airport at an elevation of 610 m (gray unit on Figure 3; Airport gravel of Woolace, 2005) is also consistent with an up-to-the-northwest North Valley fault (Woolace, 2005). Maps of Pampeyan et al. (1981) and Upp (1989) both indicate structures on the east margin of Little Lake Valley. Collectively, observations suggest faults on both the north and east margins of Little Lake Valley that accommodate vertical deformation (Pampeyan et al., 1981; Upp, 1989; Woolace, 2005). Earthquake epicenters for the Little Lake Valley area mostly occur east of the mapped trace of the Maacama fault in the vicinity of the East Valley fault (Castillo and Ellsworth, 1993). The associated focal mechanisms show right-lateral strike-slip motion that is consistent with the sense and slip on the Holocene-active Maacama fault (Castillo and Ellsworth, 1993). However, the strike-slip focal mechanisms are not compatible with the east-side-up fault-line scarp, nor with the magnitude of east-side-up bedrock offsets on the East Valley fault.

RESEARCH APPROACH

A gravity survey data set including 465 locations, was collected from March 2005 to April 2007 in order to evaluate Little Lake Valley basin geometry and compare with previous work on geologic structures in Little Lake, Redwood and Ukiah Valleys. Earth's gravity field is a function of three main components: 1) latitude; 2) elevation; and 3) mass distribution, or underlying rock density. Variations in any of these three components results in perturbations to the Earth's gravity field, or gravity anomalies. The aim of a gravity survey is to determine bedrock structure by means of the anomalies the bedrock produces to the Earth's gravity field at the Earth's surface. The gravity anomalies were then modeled to infer subsurface structures. Gravity models employ both data collected for this study and older data (Chapman, 1966, 1975; Roberts et al. 1990) and are constrained by rock density measurements (Chapman, 1975), 1-D velocity models (Castillo and Ellsworth, 1993; Hayes and Furlong, 2007a), well logs (unpublished logs from California Department of Water Resources; Cardwell, 1965; Woolace, 2005), and geomorphic evidence (Pampeyan et al., 1981; Upp, 1982, 1989; Woolace, 2005; Larsen, 2006; and Larsen and Kelsey, 2005a, b, c, d). With adequate constraints, gravity data provide insight to subsurface material density variations at depths beyond those reached by usual drilling and excavation methods. Double-difference relocated seismicity was used in conjunction with best-fit gravity model constructions (G. Hayes, written communication, December 2007; Waldhauser and Ellsworth, 2000, 2002) to define active fault geometries at depth.

METHODS

Gravity

A gravity survey of 465 gravity stations was completed (Figure 5) to evaluate density variations, subsurface bedrock geometry, intra-basin faults and basin-bounding faults. Gravity data supplemented existing regional data (crosses on Figure 6; Chapman, 1966, 1975; Roberts et al., 1990) and provided greater spatial coverage in the vicinity of Little Lake, Redwood and Ukiah Valleys to investigate basement structure details not discernable on current regional gravity maps (Roberts et al., 1990). Station spacing was between 100 to 400 meters (Figures 5 and 6), primarily along roads. Model profiles follow station transect lines W1, W2, W3, W4, LM1, U2, and U4 (Figure 5). Gravity data collection on gravity profiles W3, LM1, and U2 (Figure 5) was limited by property accessibility.

Gravity stations were tied into the existing gravity network using base station locations CH63 (Willits) and CH66 (Ukiah) originally established by Chapman (1966) (Figure 5), and adjusted to the International Gravity Standardization Network 1971 (IGSN-1971) gravity datum (Morelli, 1974). The exact location of base station CH63 in Willits City Park was not recovered; however, the station was re-established proximal to the original location (likely within 1-2 m) based on location and coordinate descriptions (Chapman, 1966). A third base station, Tomki, located in Redwood Valley (Figure 5), was established for this study and tied into the existing network by looping to Ukiah base

station CH66. Tomki is located at the base of a red post for the address 13000 Tomki Road (39º 19.580, 123º 13.489 NAD27) and the observed gravity value is 80014.61 mGal (Appendix 1). All three base stations, CH63, CH66, and Tomki, were used as daily local base stations depending on logistics and survey proximity (Figure 5). During the course of the current gravity survey five existing survey benchmarks were also occupied as gravity stations. Appendix 2 tabulates data from the five benchmarks, National Geodetic Survey permanent identification (PID) number and gravity data.

During the year 2006, gravity stations were collected with LaCoste Romberg model G gravity meter G425 (on loan from Pennsylvania State University). Stations were located in the NAD 27 reference frame using a Garmin ETrex handheld GPS unit connected to a real-time mapping program TOPO!. Elevations for these stations were estimated from Garmin ETrex locations, contours on the U.S. Geological Survey 7 ½ -minute topographic maps, and TOPO! program with estimated accuracy of 6 m. Comparison of the field determined elevations with the 30 m DEM by the U.S. Geological Survey, during gravity data processing, yielded seven stations (Stations 141, 305, 350, 513, 514, and 516) with unacceptable elevations. Consequently, interpolated elevations from the 30 m DEM were used for the seven stations (Appendix 1). Based on accuracy of 7 ½ -minute topographic maps and 30 m DEM, resultant observed gravity values may be in error up to approximately 1 mGal. Field terrain corrections to a radial distance of approximately 68 m were calculated in field as per Robbins and Oliver (1970). Tidal calculations were inadvertently omitted during the 2006 field collection process and resulting gravity data may be in error up to 0.2 mGal.

During the year 2007, gravity stations data were collected with LaCoste Romberg model G gravity meter G614 (on loan from the U.S. Geological Survey). Gravity stations were located using a Trimble GeoXT handheld GPS unit. Continually operating reference station CORS P164 (CORS, 2007) was used as a reference in post processing the Trimble GeoXT handheld data. Elevations from the 2007 gravity survey are accurate to approximately 2 m, which translates to an approximately 0.4 mGal error in the observed gravity measurement. Field terrain corrections were calculated in field per Robbins and Oliver (1970) and tidal corrections were completed by the U. S. Geological Survey during processing of the 2007 data.

All gravity data were processed by the U.S. Geological Survey for free air, Bouguer, terrain, and isostatic corrections (Appendix 1) and elevations used in the gravity reduction calculations are in the North American vertical datum 1929. Free air, Bouguer and isostatic corrections also have associated free air, Bouguer and isostatic gravity anomalies that are often modeled to give insight into their corrected effects. Specifically, the free-air correction removes the first order effect of elevation from sea level. The free air gravity anomaly reflects the gravitational field due to elevation and latitude of the gravity station point; as such, the greater the elevation the lower the gravity value. Consequently, if elevations are not accurately measured associated gravity values can be in error. Based on the accuracy of elevations measured during the 2006 survey, gravity values may be in error up to 1 mGal for the combined 2006 and 2007 data set.

The Bouguer correction accounts for the gravitational attraction of the mass between the gravity station and sea level and assumes an infinite horizontal slab of a

thickness coinciding with the elevation of the gravity station. As topography is rarely flat, the complete Bouguer gravity anomaly also takes into consideration local terrain effects. Terrain corrections are divided into three radial zones from each gravity station point: field (0 to 67 m), inner (68 to 590 or 2000 m) and outer (590 m or 2000 m to 167 km). Field zone corrections were described above. Inner zone terrain corrections were digitally calculated from 68 m to 590 m (2007 data) or 2000 m (2006 data) using 30-m DEMs derived from USGS 7.5' topographic maps (Plouff, U. S. Geological Survey, unpublished software, 2005). Outer zone terrain corrections were digitally calculated from 590 m or 2000 m to 167 km using a DEM derived from U. S. Geological Survey 1:250,000-scale topographic maps (Plouff, 1966; Plouff, 1977; Godson and Plouff, 1988). Gravity data were reduced to Bouguer anomalies using a density of 2.67 g/cm^3, and includes corrections for instrument drift, elevation, latitude, and terrain. Bouguer gravity anomalies show the effects of different rock densities in the subsurface.

Finally, the isostatic correction removes long wavelength gravitational effects from topographic loading unaccounted for in the Bouguer correction. An isostatic correction was calculated using a crustal density of 2.67 g/cm^3, a sea level crustal thickness of 25 km, and a mantle-crust density contrast of 0.40 g/cm^3. In general, isostatic and Bouguer anomalies exhibit comparable trends in the absence of topography; however, the isostatic anomaly tends to enhance shorter-wavelength anomalies. The resulting field, the residual isostatic gravity anomaly, reflects density variations within the middle and upper crust and most closely correlates with mapped geology (Jachens and Griscom, 1985; Simpson et al., 1986). This generally applies even if parameters for

the isostatic correction are modified. In particular, differing parameters for calculating the isostatic correction do not significantly change short-wavelength anomalies, but do effect the long-wavelength component (see Jachens and Griscom, 1985).

The forward modeling program GM-SYS® 4.9 (Northwest Geophysical Association, Inc, 2004) was used to calculate predicted isostatic residual gravity anomaly variations from density profiles and match to observed isostatic residual gravity anomaly variations.

1-D Velocity Models

1-D seismic velocity models can constrain horizontal density variations at depth and complement gravity models because gravity data best models vertical density variations. To evaluate the potential for distinct horizontal unit(s) at depth, four different 1-D velocity models for the northern Maacama area were evaluated (Table 1; Castillo and Ellsworth, 1993; Hayes and Furlong, 2007a). The 1-D velocity models I'm using are simple interpretations of velocity variations at depth, determined from U. S. Geological Survey relocated velocity models (Castillo and Ellsworth, 1993) and forward models of receiver functions (Hayes and Furlong, 2007a). The 1-D velocity model of MAN (Maacama north, Castillo and Ellsworth, 1993) is a model derived from the average of four different receiver locations and not a single point. Seismic receivers CVLO, KCPB, FREY, and HOPS are located in Round Valley, Laytonville, Redwood Valley and Hopland, respectively (Figure 1; Hayes and Furlong, 2007a). While seismic velocity models are sensitive to density and elastic properties of materials, the simple 1-D models

used here assume horizontal, homogenous layers with a constant Poisson's ratio (0.25). 1-D models generally extend 30 to 40 km in depth. Velocities within the upper 10 km were converted to densities using algorithms of Gardner et al. (1974) and Christensen and Mooney (1995). Gardner et al. (1974) used data from measurements of velocity and density of sedimentary deposits and rock to obtain their algorithm while the algorithm of Christensen and Mooney (1995) is based on worldwide compilation of velocity and density for basement/bedrock rocks. Regional bedrock maps indicate the field area is within the Central belt Franciscan (Jenkins et al., 1960), comprised primarily of greywacke and meta-volcanic rock (Blake et al., 1985). Calculated densities from these 1-D models were used to help constrain density models of isostatic gravity anomalies.

Rock Density Measurements

A total of thirty-four rock samples were collected from sixteen locations in and around the study area to determine rock densities and lithology (Figure 5 and Table 2). Measured rock densities were used to qualify densities of basement rocks when generating density models for isostatic gravity anomalies. Density measurement methods approximately followed American Society of Testing and Materials Standards (ASTM) C127 Specific Gravity and Absorption of Coarse Aggregate (ASTM, 2007).

Well Log Compilation

Well logs are useful to constrain depths to bedrock or deepest fill sediments for models of gravity anomaly data (Table 3). In addition to well logs presented by Cardwell

(1965) and Woolace (2005), I acquired and reviewed well logs archived by the California Department of Water Resources for northern Ukiah, Redwood, and Walker Valleys (T16N R12W S3-10, 14-18, T17N R12W S7, 8, 17-20, 27-34, and T17N R13W S15-17). Well logs were located using "Google Earth". Well logs recording valley axis depths to bedrock or minimum thickness of basin fill were used to constrain gravity models (Figure 2 and Table 3).

Relocated Seismicity

Relocated seismicity (G. Hayes, written communication, December 2007, per Waldhauser and Ellsworth, 2000, 2002) from the Northern California Earthquake Data Center (2006) was used to determine seismically active fault geometries at depth. Cross sections of 2 km wide swaths of double-difference relocated seismicity to a depth of 10 km (G. Hayes, written communication, December 2007) were applied to profiles W1, W2, W3, W4, LM1 and U4.

RESULTS

Densities Derived From 1-D Velocity Models

Results from density conversions of 1-D velocity models (Castillo and Ellsworth, 1993; Hayes and Furlong, 2007a) generally indicate two distinct materials above a depth of 10 km (Table 1). Although the average seismic velocity model of MAN (Castillo and Ellsworth, 1993) includes five distinct velocity intervals within the upper 10 km (0 km, 1.5 km, 3.5 km, 5 km, and 7 km, Table 1), density variations suggest this model represents only two distinct material intervals: surficial material (0 to 1.5 km), and material below 1.5 km. Additionally, 1-D velocity models of CVLO, FREY, HOPS and KCPB (Hayes and Furlong, 2007a) indicate only two distinct material intervals: surficial material (0 to approximately 3 km) and material below approximately 3 km.

Results from converting 1-D velocity models to densities do not constrain a distinct horizontal density contrast within the upper 10 km for gravity models. Velocities in surficial material (0 to approximately 3 km) may not be a good proxy for density because of the strong effect of fracturing on reducing velocities relative to densities (Stierman and Kovach, 1979) resulting in poor resolution of the 1-D models in the upper two to three km. Furthermore, surface materials include both rock and sediment, and are not homogenous as assumed in the 1-D velocity model. Density variations of surface materials are better constrained by field observations, mapped geology, and rock density measurements. Below approximately 3 km depth, density variations derived from seismic

velocity conversions from both the Gardner et al. (1974) and Christensen and Mooney (1995) methods range from 2.57 g/cm^3 to 2.80 g/cm^3. The 1-D velocity results indicate the average crustal density is 2.67 g/cm^3.

Rock Density Measurements

Rock density measurements conducted as part of this study (orange squares on Figure 5) are consistent with results from previous studies and are presented in Table 2. Rock density variations of greywacke, greenstone, and serpentine, between this and previous studies, are within 2σ of respective rock types (Bailey et al., 1964; Clement, 1965; Chapman and Bishop, 1974) (Table 2). The new rock density results indicate that densities of Coastal and Central belt Franciscan greywacke are nearly indistinguishable (2.59 and 2.60 g/cm^3, respectively). The average density of greywacke from the new and old studies ranges from 2.55 to 2.65 g/cm^3, with a standard deviation of 0.04 (Table 2). The largest data set for greywacke, 725 samples, has an average density of 2.65 g/cm^3 (Bailey et al., 1964).

Gravity

Isostatic residual gravity data collected for this study were merged with the existing regional data set (Chapman, 1966, 1975; Roberts et al., 1990; Figure 6B) and gridded at an interval of 300 m using the principle of minimum curvature (Briggs, 1974; unpublished U. S. Geological Survey program). In general, the addition of 465 gravity

locations to the existing data set indicates Little Lake Valley and Laughlin Range create greater isostatic residual gravity anomalies than previously recognized (Figure 6).

Seven cross sectional profiles (W1, W2, W3, W4, LM1, U2 and U4; Figure 5) of gridded gravity and topography (from 30 m DEM) were created for modeling in the GM-SYS program. Because the *student package* version of GM-SYS program was used, cross sectional gravity models are limited to thirty-five points and no more than seven density bodies. The overall procedure of gravity modeling includes adjusting geometries and densities of bedrock in the modeling program so that the calculated (modeled) anomaly matches observed anomalies. Consequently, a smoothed, gridded 2-D profile data set in which noise is alleviated is more preferential to model than the scattered isostatic residual gravity anomaly data values from the field profiles. A comparison of a gridded profile and isostatic residual gravity data for field profiles W2, LM1, and U2 indicate the gridded profile captures the gross gravity signature structure (Figure 7). Gravity models show bedrock density geometry solutions for each of the seven gravity profiles and I assumed near surface density contrasts extended to a depth of 10 km. Models were constrained by rock density variations, depths to bedrock inferred from well and borehole logs and mapped surface geology. Compatibility among models was also used for selection of bedrock density geometry solutions. Density contrast models for profiles W4, W1, W2, W3, LM1, U4 and U2 (Figures 9B through 15B, respectively) show the inferred geometry of the contact between Franciscan basement rock and valley fill to a depth of approximately 1 km.

Gravity models are not unique solutions; density contrast contacts at 10 km depth could vary up to 16º from vertical, and no appreciable change would occur to the model fit to observed gravity data (Figure 8). Consequently, to dissuade bias in the geometry of density contrast contacts in the Central belt of the Franciscan, all models were completed assuming vertical density contrast contacts extending to 10 km. Furthermore, density contrast contact locations could laterally vary, however, modeled locations are generally based on mapped geology and structures (Jenkins et al., 1960; Pampeyan et al., 1981; Upp, 1989; Woolace, 2005; Larsen and Kelsey, 2005a, b, c, d; Larsen; 2006).

Values presented in density contrast models are differential density ($\Delta\rho$) values based on the background bedrock density of 2.67 g/cm^3, which is consistent with average densities derived from 1-D velocity models and rock density measurements (Tables 1 and 2). Lateral variations in bedrock densities are based on field observations, geologic mapping (Jenkins et al., 1960; Pampeyan et al., 1981; Upp 1982, 1989; Woolace, 2005; Larsen and Kelsey, 2005a, b, c, d; Larsen, 2006), rock density measurements, and inverse gravity modeling. For example, the isostatic gravity high observed in the southernmost extent of profile W4 (Figure 9) fits and confirms the presence of higher density meta-volcanic rock (2.85 to 2.95 g/cm^3, personal communication J. McConnell of Northern Aggregate, June 2007; $\Delta\rho$ = 0.15 g/cm^3, Figure 9A and 9B) in the quarry along Highway 101, south of the Mendocino California Department of Forestry fire station. However, gravity anomaly highs with unresolved density units were inversely modeled and justified by a large crustal block of very small density variation (typically $\Delta\rho$ less than 0.03 g/cm^3). Without density constraints, isostatic residual gravity highs can be attributed to

either increased density of bedrock or uplifted crustal sections. Bedrock density can be attributed to multiple conditions such as pore size, fracturing, and chemical composition. Consequently, the primary focus of this study is to identify basement geometry and structures not apparent on the surface that would lend insight into tectonic evolution of Little Lake Valley and not to find/confirm small scale bedrock outcrops or rock types.

No direct measurements of density of Cenozoic basin fill deposits are available for the study area. Thus, densities of basin fill had to be assumed and were based on density values assigned to basin fill deposits near Clear Lake (Chapman, 1975), Point Reyes (Grove and Niemi, 2005), and Lake Pillsbury (Langenheim et al., 2007). Coarser-grained valley fill in Redwood and Ukiah Valleys was assigned a homogenous density contrast value of -0.3 g/cm^3 from the background bedrock density (2.67 g/cm^3) which equates to a basin fill density of 2.37 g/cm^3. To verify assigned density contrast values an infinite horizontal slab approximation, $\Delta g = 0.0419\ \Delta\rho\ L$ was used, where $\Delta\rho$ is the density contrast (g/cm^3), L is the material thickness (meters), and Δg is the resulting gravity anomaly. Based on the Quaternary fill thickness of 455 m, inferred form the Cardwell well (1965), and gravity contrast of 5 to 7 mGal (Figure 14A), reasonable density contrasts between bedrock and basin fill in Redwood and Ukiah Valleys range from -0.26 to -0.35 g/cm^3, which are consistent with the assigned density contrast value of -0.3 g/cm^3.

Alluvial, fluvial and lacustrine deposits forming the basin fill of Little Lake Valley are relatively finer-grained than fluvial derived basin fill of Redwood and Ukiah Valleys, therefore a density contrast greater than -0.3 g/cm^3 would be more appropriate

for Little Lake Valley basin fill. Consequently, a density contrast value of -0.4 g/cm^3 between bedrock and basin fill (which equates to a basin fill density value of 2.27 g/cm^3) was found to be the most compatible between profiles W1, W2, W3 and W4 during inverse modeling efforts. Because wells in Little Lake Valley do not confirm the thickness of basin fill anywhere in Little Lake Valley, the infinite slab approximation cannot be used to verify the assigned density value of -0.4 g/cm^3. However, in comparing a range of likely density contrast values (-0.4 to -0.6 g/cm^3), inferred depths of Little Lake Valley basin fill vary by approximately 33 percent with no significant effects occurring to modeled bedrock geometry. In particular, even with the possibility of lateral density variations of basin fill occurring from the north to the south ends of Little Lake Valley, the infinite slab approximation, using likely density contrasts, suggests that Little Lake Valley bedrock slopes to the south.

DISCUSSION

Little Lake Valley: Thickness of Valley Fill and Slope of Basement Floor

Because lowest gravity values in Little Lake Valley occur in the southern portion of the valley, Franciscan bedrock is deepest there (Figure 6). Using the assigned density contrast value of -0.4 g/cm^3, results from gravity models W1, W2, W3, and W4 indicate fill thickens from approximately 250 m in the northern portion of the valley to approximately 1,000 m in the southern portion of the valley (Figures 9 through 12). Gravity models indicate that the Franciscan basement floor of Little Lake Valley slopes towards the south (Figure 9), which is in contrast to the regional 5º to 8º north dip of the valley fill (Treasher, 1955; Cardwell, 1965; Woolace, 2005).

Structure of the East Valley fault based on Gravity, Seismicity, and Surface Morphology

A simple calculation of horizontal gravity gradients (Δg(mGal)/Δx(km)) along profiles W1, W2 and W3 within Little Lake Valley indicate gravity gradient maxima (up to 4.5 mGal/km) occur on the east side of Little Lake Valley suggesting that buried, near-vertical contacts separate materials of contrasting densities (Figures 10 through 12) (Blakely and Simpson, 1986). A linear gravity gradient along the east side of the valley provides geophysical evidence for the East Valley fault. Gravity models of profiles W1 through W3 incorporate a 3.5 km to 4.5 km wide block of slightly higher density material with a density contrast of 0.03 g/cm^3 (which equates to a density value of 2.70 g/cm^3), in

contact with valley fill on the east side of Little Lake Valley (Figures 10 through 12, panels A and B). Furthermore, gravity models for profiles W2 and W3 indicate that the East Valley fault zone is expressed by two faults with the western fault buried by valley fill (Figures 11 and 12). Vertical offset of the top of the greywacke is progressively greater to the southwest (Table 4, Figures 11 and 12). Vertical offset of buried bedrock associated with the East Valley fault along profile W1 is difficult to discern and is likely outside of the resolution of the data set; however, the gravity model suggests one fault at the eastern valley margin (Figure 10). Based on the magnitudes of the two vertical offsets along the East Valley fault in the southern portion of the valley, the East Valley fault is an up-to-the-east fault zone, branching from a single fault in the north to two faults further south.

Relocated seismicity (G. Hayes, written communication, 2007) along parallel profiles W1, W2, and W3 indicate seismicity generally occurs beneath the trace of the East Valley fault to a depth of 10 km. Seismicity occurs in two distinct near-vertical zones either above 5 km depth or below 7 km depth (Figures 10C through 12C). Seismicity below 7 km depth along profiles W1 and W2 generally indicate a single, narrow (<1 or 2 km wide), steeply east-dipping structure (Figures 10C and 12C). In contrast, seismicity along profile W3 shows two groups of hypocenters below 7 km, suggesting two separate east-dipping structures (Figure 12C): one that projects up towards the surface trace of the Maacama fault and the other approximately 1 km east of the East Valley fault. Based on seismicity patterns suggesting a single fault in profiles W1 and W2, and two faults in profile W3, I infer that the two faults of profile W3 join at

a depth below 10 km to form a single fault (Figure 12C). Seismicity, mapped surface faults, and gravity models together suggest a branching fault structure that is near-vertical with dips approximately 70º to 80º to the east (Figure 10C through 12C). Additionally, seismicity shallower than 5 km along profile W3 (Figure 12C) indicates a west-dipping fault that at depth may join the East Valley fault and at the surface may coincide with the density contrast contact east of the East Valley fault (Figure 12B).

Focal mechanisms for seismicity in the vicinity of the East Valley fault indicate mostly pure strike-slip motion, with infrequent oblique strike-slip events (cross sections A and B, Figure 16) (Castillo and Ellsworth, 1993; G. Hayes, written communication, December 2007). Relocated seismicity and focal mechanisms provide evidence that strike-slip motion on the developing Maacama fault appears to be using the older, east-dipping East Valley fault, at greater than approximately 8 km depth, as a preferential pathway to accommodate regional strain. The inference that the Maacama fault may merge with the East Valley fault at depth is consistent with Castillo and Ellsworth's (1993) assertion that preexisting structural fabric of northwest-trending reverse faults (i.e. the East Valley fault) strongly influence development of the San Andreas fault zone. In conclusion, the East Valley fault probably no longer accommodates much vertical slip, and slip along the East Valley fault is mostly strike-slip with occasional shallow oblique events. Seismicity indicates that the East Valley fault is Holocene-active at depth but the lack of fault scarps along the surface trace indicates Holocene slip has not propagated to the ground surface.

Structure of the North Valley fault based on Gravity, Seismicity and Surface Morphology

The gravity model of profile W1 (Figure 10) provides evidence for the North Valley fault (Woolace, 2005) with an approximately 2.3 km wide block of slightly higher density material with a density contrast of 0.02 g/cm^3 (which equates to a density value of 2.69 g/cm^3) in contact with valley fill on the northwest side of Little Lake Valley. Based on assigned density contrast values, vertical offset is inferred to be as much as 50 meters up-to-the-northwest (Figure 10A and 10B). Inferred vertical offset from the gravity model is in agreement with bedrock offsets determined by depths to bedrock in well logs (Woolace, 2005). If a larger basin fill density contrast is used (-0.6 g/cm^3 instead of -0.4 g/cm^3) in the gravity model, the inferred vertical offset would be decreased and beyond the resolution of this data set. However, assuming the isolated exposure of Pleistocene or older gravels at Willits Airport (Figure 3; 'Airport gravel' of Woolace, 2005), located at an elevation of 610 m, was deposited in Little Lake Valley basin, then motion on the North Valley fault has displaced gravel at least 200 m up to the northwest. Taking into account effects of exhumation on the uplifted Airport gravel would increase offset estimates. Thus, vertical displacement of the Airport gravel and in addition to approximately 50 m of bedrock offset (inferred from well logs and the gravity model) indicates a minimum of approximately 250 m of vertical separation on the North Valley fault. Additionally, Reeves Canyon, located north of the North Valley fault (Figure 3) is an abandoned backtilted valley, inferred to have originally contained a channel which flowed south into Little Lake Valley (Woolace, 2005). Based on local geomorphology, the North Valley fault is presumed to be the structure responsible for beheading and

accommodating northward tilt of the abandoned channel (Woolace, 2005). Bedrock displacements inferred from well logs, gravity data, elevation of the Airport gravel, and landforms to the north collectively provide evidence that the North Valley fault is an up-to-the-northwest normal fault. Based on gravity data and depths to bedrock inferred from well logs (Woolace, 2005), the North Valley fault appears to be confined to the northwest portion of Little Lake Valley and does not extend southwest across the surface trace of the Maacama fault nor northeast across the trace of the East Valley fault. Consequently, the North Valley fault likely merges with the Maacama fault to the west and East Valley fault to the east.

Initiation and timing of normal motion along the North Valley fault are poorly constrained, but Woolace (2005) inferred, from facies changes in Little Lake Valley fill, that initiation of normal slip on the North Valley fault occurred simultaneously with a decrease in vertical motion on the East Valley fault. Woolace (2005) suggested the transition in slip geometry from west-vergent reverse faulting to south-dipping normal faulting was tied to the northward migration of the Mendocino triple junction. Seismicity patterns down to a depth of 10 km in profiles W1 through W4 (Figures 9C through 12C) are not consistent with a seismically active fault in the vicinity of the North Valley fault.

Character of the Maacama fault in Little Lake Valley from Gravity and Seismicity

Relocated seismicity and inferred bedrock structures from gravity models in Little Lake Valley provide evidence for an approximately 5 to 10 km wide tectonically active Maacama fault zone that generally takes advantage of pre-existing structural fabric of

bedrock as determined from gravity models. While gravity models of profiles W1, W2, and W3 in Little Lake Valley indicate that bedrock is not vertically offset across the surface trace of the Maacama fault, vertical offset may be less than 30 to 40 m and beyond the resolution of the data set. Profile W1 is the only Little Lake Valley transect that has bedrock juxtaposed at the surface on both the east and west sides of the Maacama fault and while the gravity model indicates a density contrast of 0.02 g/cm^3, surface morphology does not indicate a local vertical offset across the Maacama fault (Figure 10A and 10B), suggesting the density contrast may be a result of strike-slip motion along the Maacama fault. Profiles W2 and W3 cross the surface trace of the Maacama fault within valley fill (Figure 5), and gravity models do not require buried vertical bedrock offsets or density contrasts across the Maacama fault (Figures 11B and 12B). Strike-slip features along the Maacama fault are not well developed and the fault cuts across major topographic features. In general, topography in the area, such as that associated with the East Valley fault and Laughlin Range, is still dominated by previous tectonic regimes associated with northerly migration of the Mendocino triple junction and attests to youthfulness of regional strike-slip tectonics.

Seismicity in Little Lake Valley provides evidence that principal strike-slip displacement along the Maacama fault zone occurs at depth, beneath the East Valley fault (Figures 10C, 11C, and 12C) approximately 5 km east of the surface trace of the Maacama fault. Based on seismicity locations, mapped surface geology, and density contrast contacts of gravity models, the Maacama fault zone in the Little Lake Valley area consists of upward branching faults (‘flower structures’ after Busby and Ingersoll,

1995) (Figures 10C, 11C, and 12C) rooted in the east to the East Valley fault. Focal mechanisms of seismicity in the area of profile W3 (Cross-section B, Figure 16) indicate that some translational motion is being accommodated along low-angle faults at depths of approximately 10 km. Although not constrained by gravity models, I speculate that the Maacama fault may root at depth (>10 km) in a low-angle fault that may be the southerly extension of the North Valley fault. Consequently, the Maacama fault in Little Lake Valley appears to be taking advantage of remnant structural fabric that first accommodated easterly convergence, then accommodated north-south extension.

Redwood Valley and northern Ukiah Valley: Thickness of Valley Fill and Slope of Basement Floor

Logs from two California Department of Water Resources wells (95412 and 3057F) and a borehole installed for the construction of the Coyote dam (Cardwell, 1965) (Table 3) provide constraints for the Redwood and Ukiah Valley gravity model of profile U4. The constrained gravity model provides evidence for basin fill thickness and depths to bedrock in Redwood and Ukiah Valleys. A density contrast of -0.3 g/cm^3 between the bedrock and basin fill (profile U4, Figure 13) produces the ~6 mGal anomaly relative to bedrock given a basin fill thickness of 455 m indicated at the Cardwell (1965) borehole. The depth to bedrock inferred from the gravity model along profile U2 is 250 m (Figure 14), and is approximately 200 m shallower than depth to bedrock recorded in the Cardwell (1965) bore log, located approximately 5 km to the north. Therefore, based on the depth to bedrock data inferred from well logs and constrained gravity models, the bedrock floor of Ukiah Valley slopes approximately 2º north, down towards Coyote Dam

(Figure 6). A 2º slope to the north is shallower, yet consistent with, regional valley fill bedding dips of 5º to 7º to the north (Treasher, 1955; Cardwell, 1965; Woolace, 2005).

Results from the gravity model of east-west profile U2, located in Ukiah Valley (Figure 5), indicate a broader, shallower valley than Little Lake Valley (Figure 14). Mapped east and west margins of Ukiah Valley fill (Larsen and Kelsey, 2005a, b, c, d) constrain the gravity model along profile U2 and the gravity model suggests that Ukiah valley fill is in depositional contact with shallowly-dipping bedrock on the east and west valley margins. Consequently, the Maacama fault does not appear to contribute significant vertical offset to bedrock nor does Ukiah Valley appear to be a fault-bounded basin.

The Laughlin Range, Redwood Valley, and northern Ukiah Valley: Evidence for the Laughlin Range fault

The gravity model of profile LM1 provides evidence of structure and depth to bedrock west of the Maacama fault, adjacent to Walker Valley, as well as suggests density variations within the Central belt Franciscan bedrock that make up the Laughlin Range, (Figure 15A and 15B). The mapped trace of the Maacama fault provides location constraints to density contrasts along the western flank of the Laughlin Range and assigned density values within the gravity model indicate approximately 50 m of east-side up vertical offset across the Maacama fault (Figure 15). Well logs and mapped geology (Pampeyan et al., 1981) indicate that landslide/earthflow deposits west of the Maacama fault extend downslope and merge with basin fill of Walker Valley (Figure 15). The minimum valley fill thickness in Walker Valley is 60 m (Table 3) and, based on the

gravity model for profile LM1 in the vicinity of Walker Valley, the valley fill thickness may be as great as 250 m and indicates that the lowest elevation of basement rock occurs near the east side of Walker Valley (Figure 15A and 15B).

Unlike the smooth nature of isostatic residual gravity variations/anomalies east of Little Lake Valley, the profile LM1 indicates finer-scale isostatic residual gravity anomalies which may indicate artifacts of elevation measurement inaccuracies and/or greater heterogeneity within the Central belt Franciscan in the Laughlin Range. While narrow bands (0.25 km to 0.55 km) of higher density rock ($\Delta\rho$ = 0.13 g/cm^3 to 0.16 g/cm^3) can account for isostatic residual gravity anomalies along profile LM1, west of the inferred rock quarry material (Figure 15) locations of the higher density rock in contact with other variably dense rocks of the Laughlin Range may be in error and cannot be precisely accounted for due to potential elevation measurement inaccuracies (Figure 14B and 15B).

Despite the absence of significant topography on the floor of Redwood Valley, a gentle, 7-mGal gravity gradient over a distance of 7 km is observed longitudinally north-south through Redwood Valley along profile U4 (Figure 13). While geophysical studies indicate higher density material in the upper 25 km in the area of Redwood Valley (Hayes et al., 2006; Hayes and Furlong, 2007a), and shallow asthenospheric material near Clear Lake (Chapman, 1975) and Lake Pillsbury (Trehu et al., 1995; Beaudoin et al., 1996), the resultant gravity gradient from these effects would be anticipated to be much longer wavelength than what is observed in profile U4. Consequently, the isostatic residual gravity data in the area of Redwood Valley indicate an anomaly that appears

coincident with changes in local bedrock topography, likely concealed beneath the valley. Because the gravity model U4 is constrained by depths to bedrock observed in local well logs 95412 and Cardwell (1965), the assigned basin fill density contrast of -0.3 g/cm^3 accounts for a majority of the 7-mGal anomaly within the depth to bedrock constraints. However, the rest of the 7-mGal gravity anomaly along profile U4 is modeled to be caused by a 360 m up-to-the-north vertical step in bedrock located in the middle of Redwood Valley (Figure 13B), at approximately the same latitude as the southern boundary of the Laughlin Range, located west of Redwood Valley (Figure 2). Using the assumption that isostatic residual gravity anomalies correlate with structures in the middle and upper crust (Jachens and Griscom, 1985; Simpson et al., 1986), the bedrock offset in Redwood Valley inferred from the gravity model may be a structure which accommodates crustal thinning.

Gravity data collected between the peak of Laughlin Range and its southern flank, located west and nearly parallel to gravity profile U4 (Figure 5), indicate a similar gravity gradient over the same 39.27º N to 39.33º N latitude range as in Redwood Valley (Figures 13 and 17). Gravity data from the southern flank of the Laughlin Range were not "smoothed" for modeling in GM-SYS because the data only represent a gravity gradient, and did not reach background gravity values necessary to constrain the model. While it would be simple to attribute increasing southward thickness of basin fill, as modeled on profile U4, to the southern flank profile to account for the gravity anomaly, the southern flank profile was completed over a large elevation change (approximately 890 m down to 350 m) in an area without any basin fill. Therefore, a laterally

unconstrained bedrock density contrast must occur along the southern flank profile to contribute to the observed gravity gradient. To determine the magnitude of the required density contrast ($\Delta\rho$), I used the infinite slab approximation, $\Delta g = 0.0419\ \Delta\rho\ L$. Assuming bedrock extends to 10 km (L), which is the assumption for all other gravity models in this study, and the gravity gradient (Δg) may be between 4 and 7 mGals (background not reached) from the northern to southern ends, then the infinite slab approximation estimates a density contrast value for bedrock along the southern flank profile to be between approximately 0.009 to 0.017 g/cm^3. Topography of the Laughlin Range suggests this density contrast may be due to a faulted crustal section. Because the same gravity gradient is seen on U4, without the large topographic relief of the southern flank profile, I infer that a change in structural style or geology must occur between the two profiles. Preliminary results from applying this density contrast value (0.009 to 0.017 g/cm^3) between bedrock at the bottom of the gravity gradient along modeled profile U4 would require either that the density contrast value between bedrock and basin fill (-0.3 g/cm^3) should be less or that the basin fill is thinner, thereby a component of the gradient would decrease the amount of buried bedrock offset in Redwood Valley. However, neither one of these conditions seems valid. The Cardwell well (Cardwell, 1965) constrains basin fill thickness and a decrease in the density contrast between bedrock and basin fill of Ukiah and Redwood Valley does not seem reasonable given other regional basin fill density contrasts (Chapman, 1975; Grove and Niemi, 2005; Langenheim et al., 2007). In summary, the density contrasts between the southern flank profile and modeled gravity profile U4 are not resolved, but the linear trend of observed gravity anomaly

values of both profiles (Figure 17) suggest a structure, approximately east-west in strike, that I speculatively define to be the Laughlin Range fault (Figures 6, 13 and 17).

Relocated seismicity plotted north-south along profile U4 generally indicates increased seismic activity in the area of the inferred Laughlin Range fault relative to seismicity north and south of the Laughlin Range fault. Seismicity and focal mechanisms plotted parallel to the Laughlin Range fault (cross section C, Figure 16) (G. Hayes, written communication, December 2007) indicate an approximately 10 km wide zone of seismicity that occurs primarily east of the mapped surface trace of the Maacama fault. From the focal mechanisms, several slip planes suggest low-angle faults at approximately 10 km depth. These low angle faults could be part of the Laughlin Range fault. Because the fault dip accommodating strike-slip motion of the Maacama fault appears to shallow at approximately 10 km depth, the Maacama fault at depth may be occupying the remnant Laughlin Range fault and transition to a regional low-angle detachment.

The isostatic residual gravity anomaly of profile U4 does not indicate a significant gravity signature, or inferred bedrock offset, associated with the Calpella fault (Figure 13). Geomorphic evidence suggests the east-west Calpella fault exhibits a fault line scarp, up-to-the-north on the north end of Lake Mendocino capped with uplifted fluvial terraces of the Russian River (Larsen and Kelsey, 2005b). Seismicity in the vicinity of the Calpella fault does not indicate an active fault (Figure 13C). Based on geomorphic evidence and inferred tectonic setting, the Calpella fault is a historically inactive normal fault whose period of activity may have been contemporaneous with initiation of the Laughlin Range fault.

Speculations on the Tectonic Evolution of Little Lake Valley

Based on evaluation of stratigraphy (Cardwell, 1965; Woolace, 2005) and bedrock structure in the context of a dynamic tectonic setting, Little Lake Valley is a polyhistory basin (Kingston et al., 1983; Klein, 1987; Busby and Ingersoll, 1995). Three tectonic settings sequentially have dominated the region and contributed to structures and stratigraphy within Little Lake Valley. The tectonic settings were (1) west-vergent reverse faulting, followed by (2) north-south extension, and finally (3) northwest-trending, dextral strike-slip motion. The basin was initiated by flexural subsidence on the footwall of east-dipping East Valley fault when east-west contraction dominated the plate boundary (back calculated to be approximately 5 Ma). During reverse faulting, bedrock offset along the East Valley fault appears to be greatest in the southern portion of the valley (Table 4). Therefore, accommodation space for fluvial deposition by a high-energy, south-flowing paleo-Russian River (Woolace, 2005) was greatest in the area now occupied by southern Little Lake Valley. As the Mendocino triple junction migrated north, easterly contraction related to the convergent margin ceased sometime during the late Pliocene to early Pleistocene, and vertical motion along the East Valley fault became less active.

Subsequent to the convergence dominated tectonic setting of the early Pliocene, Clear Lake volcanics (late Pliocene to early Holocene) were initiated approximately 45 km to the southeast, indicative of a tectonic setting characterized by local shallow intrusion of asthenospheric material and regional gravitational collapse (Liu and Furlong, 1994). Regional, north-south gravitational collapse was accommodated in Little Lake and

Ukiah Valley areas by normal slip on the North Valley fault, the Laughlin Range fault and, to a lesser extent, on the Calpella fault (Figures 18 and 19). Based on topography, drainage reversal history of Little Lake Valley, and focal mechanism data to 10 km depth, the Laughlin Range fault appears to have been the main fault accommodating a regional north-south crustal thinning near Ukiah and Redwood Valleys. Crustal thinning at this latitude in the California Coast Ranges is predicted by the Mendocino crustal conveyor model (Furlong and Govers, 1999; Furlong and Schwartz, 2004) and by geophysical imaging studies of Trehu et al. (1995) and Hayes and Furlong (2007a). The Laughlin Range fault likely intersects a low angle detachment at approximately 10 km depth (Figures 13C, 16, and 19). Although the Laughlin Range fault had little influence on inception of Little Lake Valley, the Laughlin Range fault appears to be the primary structure which back-tilted Little Lake Valley and the Laughlin Range to the north, consequently defeating southerly drainage of Little Lake Valley into the Russian River and promoting drainage of Little Lake Valley to the Eel River.

The young dextral-Maacama fault is presently the only active structure at the surface in Little Lake Valley. The Maacama fault is the central segment in the developing transform San Andreas fault zone plate boundary system and is comprised of many discontinuous and en-echelon surface faults. Based on mapped geomorphology, seismicity, and gravity models in Little Lake Valley, stresses related to the developing Maacama fault are preferentially being accommodated along pre-existing faults such as the East Valley and North Valley faults. As orientations of the pre-existing structures vary from north-south and east-west, strike-slip stress accommodation is complicated by

unknown paths of least resistance and localized dominant stress regimes. In particular, stresses related to the developing Maacama fault in Little Lake Valley are inferred to be accommodated on a complex flower structure that exhibits zones of both seismic and creep motion. The shape of this flower structure is inferred to be trans-tensional (Busby and Ingersoll, 1995), suggesting Little Lake Valley may be developing into a strike-slip basin, even though Little Lake Valley was not initiated as a strike-slip basin.

CONCLUSIONS

An additional 465 gravity station points were added to the existing regional gravity network and provide much higher resolution of isostatic residual gravity anomalies associated with Little Lake Valley and the Laughlin Range. When bedrock structural interpretations of Little Lake, Redwood and Ukiah Valleys are put into a regional context and compared with relocated seismicity and focal mechanism data, these data provide evidence for the tectonic evolution of Little Lake Valley and faults accommodating crustal thinning. Faults inferred from gravity models, mapped geology, and relocated seismicity (Figures 18 and 19) record the changing tectonic setting related to passage of the Mendocino triple junction and evolving San Andreas fault zone.

Stratigraphy and structure of the Little Lake Valley region record a tectonic history of subduction to extension to strike-slip motion. Based on fault geometry, buried bedrock relief and elevations of peaks on the east side of Little Lake Valley, genesis of Little Lake Valley is by west-vergent reverse motion on branching splays of the East Valley fault when subduction-related tectonics dominated the region. Maximum sediment fill thickness occurs in the southern portion of the Little Lake Valley and attests to increased vertical motion on the southern end of the East Valley fault relative to the northern portion of the valley where valley fill is inferred to be much thinner.

To the west, northward migration of the Mendocino triple junction resulted in the cessation of vertical motion along the East Valley fault and a transition to extension and initiation of slip on the North Valley and Laughlin Range faults. Bedrock displacement

from well logs, gravity data, elevation of the Airport gravel, and landforms to the north provide evidence that the North Valley fault is an up-to-the-northwest normal fault. However, current seismicity patterns indicate the North Valley fault is no longer active.

Gravity data across parallel profiles U4 and the southern flank of the Laughlin Range are the primary evidence for the Laughlin Range fault. Seismicity patterns and focal mechanisms in the area of the Laughlin Range fault, however, suggest a component of normal motion may still be active in Redwood Valley. The Laughlin Range fault was the main fault in the region accommodating north-south extension and is responsible for uplift of the Laughlin Range with a vertical offset that likely exceeds 360 m, and back tilt of Little Lake Valley basin. Backtilt of the basin defeated southerly flow of Little Lake Valley and reversed drainage of the valley to the north. The Laughlin Range fault is responsible for the current position of the Eel and Russian River divide. Geophysical data are consistent with the inference that valley-bounding normal faults (North Valley and Laughlin Range faults) merge with the Maacama fault to the west.

The transition to a dextral strike-slip tectonic setting during the late Pliocene has been accommodated over a wide area, but more locally by pre-existing fault planes of weakness. Regional topography primarily reflects previous tectonic regimes and the developing Maacama fault cuts this topography. In the area of Little Lake Valley, the developing Maacama fault comprises a branching flower structure that generally occupies east-dipping faults that were part of the former easterly convergent plate boundary. The Maacama fault roots in remnants of extensional faults. Although Little Lake Valley was

not initiated as a strike-slip basin, development of the Maacama fault may advance Little Lake Valley into a strike-slip basin.

REFERENCES

ASTM, 2007. ASTM Standard C 127 2007, Standard Test Method for Density, Relative Density (Specific Gravity), and Absorption of Coarse Aggregate, ASTM International, West Conshohocken, PA, www.astm.org.

Atwater, T. 1970. Implications of plate tectonics for the Cenozoic tectonic evolution of western North America: Geological Society of America Bulletin, v. 81 p. 3513-3536.

Bailey, E. H., Irwin, W. P., Jones, D. L., 1964. Franciscan and related rocks and their significance in the geology of western California: California Division of Mines and Geology Bulletin 183, p. 177.

Beaudoin, B. C., Godfrey, N. J. , Klemperer, S. L. Lendl, C., Trehu, A. Henstock, T. J. Levender, A., Holl, J. E., Metzler, A. S., Luetgert, J. H., Mooney, W. D., 1996. Transition from slab to slabless: Results from the 1993 Mendocino triple junction seismic experiment. Geology, v. 24, no. 3, p. 195-199.

Bennett, R. A., Davis, J. L. and Wernicke, B. P., 1999. Present-day of Cordilleran deformations in the Western United States. Geology, v. 27, no. 4, p. 371-374.

Blake, M. C. Jr., Jayko, A. S., McLaughlin, R. J., 1985. Tectonostratigraphic Terranes of the Northern Coast Ranges, California. Earth Science Series, Number 1, Circum-Pacific Council for Energy and Mineral Resources, Houston, TX.

Blakely, R.J., and Simpson, R.W., 1986, Approximating edges of source bodies from magnetic or gravity anomalies. Geophysics, v. 51, p. 1494-1498.

Brady, R. J., 2003. Active Transtensional Basin Formation Along The Maacama Fault Zone, Northern California Coast Range Abstracts with Programs - Geological Society of America, v. 35, no. 6, p. 547.

Briggs, I.C., 1974. Machine contouring using minimum curvature. Geophysics, v. 39, p. 39-48.

Busby, C. J., Ingersoll, R. V., eds., 1995. Tectonics of Sedimentary Basins. Blackwell Science, Inc., Cambridge, Massachusetts 1995. p. 425-458.

Cardwell, G. T., 1965. Geology and groundwater in Russian River valley areas and in Round, Laytonville and Little Lake Valleys, Sonoma and Mendocino Counties, California, U.S. Geological Survey Water-Supply Paper 1548, 154 p.

Castillo, D. A., and Ellsworth, W. L., 1993. Seismotectonics of the San Andreas Fault System Between Point Arena and Cape Mendocino in Northern California: Implications for the Development and Evolution of a Young Transform. Journal of Geophysical Research, v. 98, no. B4, p. 6543-6560.

Chapman, R. H., 1966. The California Division of Mines and Geology gravity base station network: California Division of Mines and Geology Special Report 90, 49p.

Chapman, R. H., 1975. Geophysical Study of the Clear Lake Region, California. Special Report 116. California Division of Mines and Geology

Chapman, R. H., Bishop, C. C., 1974. Gravity map of California, Santa Rosa sheet: California Division of Mines and Geology, scale 1:250,000

Christensen, N.I., and Mooney, W.D., 1995. Seismic velocity structure and composition of the continental crust: A global view: Journal of Geophysical Research, v. 100, p.9761-88.

Clement, W. G., 1965. Complete Bouguer map of the northern part of San Francisco Bay area and its geophysical interpretation: U.S. Geological Survey Geophysical Investigations Map GP-468, 6 p. text, scale 1:125,000

CORS, 2007. http://www.ngs.noaa.gov/CORS/Data.html

DeMets, C., Gordon, R. G., Stein, S, and Argus, D. F., 1987. A revised estimate of Pacific-North American plate boundary zone tectonics. Geophysical Research Letters, v. 14, p. 911-914.

Dickinson, W. R, and Snyder, W. S., 1979. Geometry of Triple Junctions Related to San Andreas Transform. Journal of Geophysical Research, v. 84, no. B2, p. 562-572.

Freymueller, J. T., Murray, M. H., Segall, P., Castillo, D., 1999. Kinematics of the Pacific-North America plate boundary zone, Northern California. Journal of Geophysical Research, v. 104, no. B4, p. 7419 -7441.

Furlong, K. P., Hugo, W. D, and Zandt, G., 1989. Geometry and Evolution of the San Andreas Fault Zone in Northern California. Journal of Geophysical Research, v. 94, no. B3, p. 3100-3110.

Furlong, K. P. and Govers, R., 1999. Ephemeral crustal thickening at a triple junction: The Mendocino crustal conveyor. Geology, v. 27, p. 127-130.

Furlong, K. P. and Schwartz, S. Y., 2004. Influence of the Mendocino Triple Junctions and the Tectonics of Coastal California. Annual Review of Earth and Planetary Science, v. 32, p. 403-433.

Galehouse, J. S., 2002. Data from Theodolite Measurements of Creep Rates on San Francisco Bay Region Faults, California: 1979–2001. US Department of the Interior, USGS Open-file report 02-225, 94 p.

Gardner, G. H. F, Gardner, L. W., Gregory, A. R., 1974. Formation Velocity and Density-The Diagnostic Basics for Stratigraphic Traps, Geophysics, v. 39, p. 770-780.

Godson, R.H., and Plouff, Donald, 1988. BOUGUER version 1.0, a microcomputer gravity–terrain–correction program. U.S. Geological Survey Open-File Report 88-644-A, Documentation, 22 p.; 88-644-B, Tables, 61 p., 88-644-C, 5 1/4 - in diskette.

Grove, K., and Niemi, T.M., 2005. Late Quaternary deformation and slip rates in the northern San Andreas fault zone at Olema Valley, Marin County, California. Tectonophysics, vo. 401, p. 231-250.

Gucwa, P. R., 1974. Geology of the Covelo/Laytonville Area, northern California. PhD dissertation, The University of Texas at Austin, 82 p.

Hayes, G. P., Johnson, C. B., Furlong, K. P., 2006. Evidence for melt injection in the crust of northern California. Earth and Planetary Science Letters, v. 248, p. 638-649.

Hayes, G. P., Furlong, K. P., 2007a. Abrupt changes in crustal structure beneath the Coast Ranges northern California – developing new techniques in receiver function analysis. Geophysical Journal International, v. 170, no. 1, p. 313-336.

Jachens, R. C. and Griscom, A., 1983. Three-Dimensional Geometry of the Gorda Plate Beneath Northern California. Journal of Geophysical Research, v. 88, no. B11, p. 9375-9392.

Jachens, R. C. and Griscom, A., 1985. An isostatic residual gravity map of California – A residual map for interpretation of anomalies from intracrustal sources, in The Utility of Regional Gravity and Magnetic Anomaly Maps, edited by W. J. Hinze, W. J. Society of Exploration Geophysicists, p. 347-360.

Jenkins, O. P., Jennings, C. W, and Strand, R. G., 1960 (third printing 1992). Geologic Map of California Ukiah Sheet, Scale 1:250,000. California Division of Mines and Geology.

Kelsey, H. M., and Carver, G. A., 1988. Late Neogene and Quaternary Tectonics Associated with Northward Growth of the San Andreas Transform Fault, Northern California. Journal of Geophysical Research, v. 93, no. B5, p. 4797-4819.

Kingston, D. R., Dishoon, C. P., Williams, P. A., 1983. Global basin classification system. American Association of Petroleum Geologist Bulletin, v. 67, p. 2175-2193.

Klein, G. deV., 1987. Current aspects of basin analysis. Sedimentary Geology, v. 50, p. 95-118.

Kleist, J. R., 1974. Geology of the Coastal Belt, Franciscan Complex, near Ft. Bragg, California. PhD dissertation, University of Texas at Austin, Austin, TX, United States. 1974

Kleist, J. R. ed, 1981. The Franciscan Complex and The San Andreas Fault from the Golden Gate to Point Reyes, California. Field trip guide. The Pacific Section of American Association of Petroleum Geologists. May 29, 1981.

Kramer, J. C., 1976. Geology and Tectonic Implications of the Coastal Belt Franciscan Fort Bragg-Willits Area, Northern Coast Ranges, California. Ph.D. Dissertation, University of California, Davis. 128 p. + illustrations. June 1976.

Lanphere, M. A., Champion, D. E., Clynne, M. A., Muffler, L. P., 1999. Revised age of the Rockland tephra, northern California: Implications for climate and stratigraphic reconstructions in the western United States. Geology, v. 27, p. 135-138.

Langenheim, V.E., Jachens, R.C., Morin, R.L., and McCabe, C.A., 2007. Preliminary gravity and magnetic data of the Lake Pillsbury region, northern Coast Ranges, California: U.S. Geological Survey Open-File Report2007-1368, 24 p. (http://pubs.usgs.gov/of/2007/1368 last accessed 3/31/08)

Larsen, M., 2006. Late Holocene Slip Rate Investigation of the Maacama fault at the Haehl Creek Site, Willits, California. Masters Thesis; Humboldt State University, Arcata, California; May 2006.

Larsen, M., and Kelsey, H., 2005a. Geologic Map of the Redwood Valley Quadrangle, Mendocino County, California; scale 1:24,000 EDMAP Agreement No. 04HQAG0081

Larsen, M., and Kelsey, H., 2005b. Geologic Map of the Ukiah Quadrangle, Mendocino County, California; scale 1:24,000 EDMAP Agreement No. 04HQAG0081

Larsen, M., and Kelsey, H., 2005c. Geologic Map of the Elledge Peak Quadrangle, Mendocino County, California; scale 1:24,000 EDMAP Agreement No. 04HQAG0081

Larsen, M., and Kelsey, H., 2005d. Geologic Map of the Purdys Garden Quadrangle, Mendocino County, California; scale 1:24,000 EDMAP Agreement No. 04HQAG0081

Levander, A., Henstock, T. J., Metzler, A. S. Beaudoin, B. C. Trehu, A. M., Klamperer, S. L., 1998. Fluids in the lower crust following Mendocino triple junction migration: Active basaltic intrusion? Geology, v. 26, no. 2, p. 171-174.

Liu, M., and Furlong, K. P., 1994. Intrusion and underplating of mafic magmas; thermal-rheological effects and implications for Tertiary tectonomagmatism in the North American Cordillera. Tectonophysics, v. 237, no. 3-4, p. 175-187.

Lock, J., Kelsey, H., Furlong, K., Woolace, A., 2006. Late Neogene and Quaternary landscape evolution of the northern California Coast Ranges: Evidence for Mendocino triple junction tectonics. Geological Society of America Bulletin, v. 118, p. 1232-1246.

McLaughlin, R. J, and Nilsen, T, 1982. Neogene non-marine sedimentation and tectonics in small pull-apart basins of the San Andreas fault system, Sonoma County, California. Sedimentology, v. 29, p. 865-876.

Meyer, C. E., Sarna-Wojcicki, A. M., Hillhouse, J. W., Woodward, M. J., Slate, J. L. Sorg, D. H., 1991. Fission-track age (400,000 yr) of the Rockland tephra, based on inclusion of zircon grains lacking fossil fission tracks. Quaternary Research, v. 35, p. 367-382.

Morelli, C., ed, 1974, The International Gravity Standardization Net 1971: International Association of Geodesy Special Publication no. 4, 194 p.

Nilsen, T. H., and McLaughlin, R. J., 1985 Comparison of tectonic framework and depositional patterns of the Hornelen strike-slip basin of Norway and the Ridge and Little Sulphur Creek strike-slip basins of California. Special Publication - Society of Economic Paleontologists and Mineralogists, v.37, p.79-103.

Nilsen, T. H. and Clarke, S. H., 1989. Late Cenozoic Basins of Northern California. Tectonics, v. 8, no. 6, p. 1137-1158.

Northern California Earthquake Data Center (NCEDC), 2006. Northern California Seismic Network; U.S. Geological Survey, Menlo Park; Berkeley Seismological Laboratory,

University of California, Berkeley; Advanced National Seismic System (ANSS) (http://www.ncedc.org/anss/catalog-search.html).

Pampeyan, E. H, Harsh, P. W., Coakley, J. M., 1981. Preliminary map showing recently active breaks along the Maacama fault zone between Laytonville and Hopland, Mendocino County, California, scale 1:24000, U.S. Geological Survey. Miscellaneous Field Study Map 1217.

Plouff, Donald, 1966. Digital terrain corrections based on geographic coordinates [abs.]. Geophysics, v. 31, no. 6, p. 1208.

Plouff, Donald, 1977. Preliminary documentation for a FORTRAN program to compute gravity terrain corrections based on topography digitized on a geographic grid. U.S. Geological Survey Open-File Report 77-535, 45 p.

Pryor, I., McPherson, R., Williams, T., 2007. Seismicity and Plate Geometry of the Mendocino Triple Junction Region, Northern California, 1986 to 2006. EOS Transactions AGU, 88 (52), Fall Meeting Supplemental Abstract S43A-1046.

Robbins, S. L., Oliver, H. W., 1970. On making inner-zone terrain corrections to gravity data. United States Department of the Interior Geologic Survey. October 1970.

Roberts, C. W., Jachens, R., C., Oliver, H., W., 1990. Isostatic residual gravity map of California. California Division of Mines and Geology Geologic Data Map no. 7, scale 1:750,000.

Sickler, R., 2003. A paleoseismic study of the Maacama Fault, near Ukiah, Mendocino County, California. Masters Thesis; Humboldt State University, Arcata, California; December 2003.

Simpson, R.W., Jachens, R.C., Blakely, R.J., and Saltus, R.W., 1986, A new isostatic residual gravity map of the conterminous United States with a discussion on the significance of isostatic residual anomalies. Journal of Geophysical Research, v. 91, p. 8348-8372.

Stierman, D.J., and Kovach, R.L., 1979, An in-situ velocity study: the Stone Canyon well. Journal of Geophysical Research, v. 84, no. B2, p. 672-678.

Treasher, R. C. 1955. Areal geology of the Coyote Dam Site, Mendocino County, California: Geological Society of America Bulletin, v. 66, no. 12, p. 1666-1667.

Trehu, A. M. and the Mendocino Working Group, 1995. Pulling the Rug out From Under California: Seismic Images of the Mendocino Triple Junction Region. EOS, v. 76, no.38, p. 369, 380, 381.

Upp, R. R., 1982. Holocene activity on the Maacama fault, Mendocino County, California. PhD dissertation, Stanford University, Stanford, California, 112 p.

Upp, R. R., 1989. Holocene activity and tectonic setting of the Maacama Fault Zone, Mendocino County, Ca: in Johnson, A.M. Burnham, C.W., Allen, C.R., and Muehlberger, W. eds., Richard H. Jahns memorial volume: Engineering Geology, v. 27, p. 375-412.

USGS, 1991. Willits Quadrangle, California Mendocino Co. 7.5 minute Series (topographic). Scale 1:24,000. U.S. Department of Interior, U.S.G.S.

USGS, 2006. USGS and California Geological Survey, Quaternary fault and fold database for the United States, accessed 2007, from USGS website: http//earthquakes.usgs.gov/regional/qfaults/.

USGS, 2007. http://seamless.usgs.gov

Waldhauser, F., Ellsworth, W. L., 2000. A Double Difference Earthquake Laoction Algorithm: Method and Application to the Northern Hayward Fault, California. Bulletin of the Seismological Society of America, v. 90, no. 6, p. 1353-1368.

Waldhauser, F., Ellsworth, W. L., 2002. Fault Structure and mechanics of the Hayward Fault, California, from double-difference earthquake locations. Journal of Geophysical Research, v. 107, no. B3.

Williams, T., Kelsey, H., Freymueller, J., 2006. GPS-derived strain in northwestern California: termination of the San Andreas fault system and convergence of the Sierra Nevada-Great Valley block contribute to southern Cascadia forearc contraction. Tectonophysics, v. 413, p. 171-184.

Wilson, D. S., 1989. Deformation of the So-Called Gorda Plate. Journal of Geophysical Research, v. 94, no. B3, p. 3065-3075.

Woolace, A., 2005. Late Neogene and Quaternary Stratigraphy and Structure of Little Lake Valley, Northern Coast Range, California. Masters Thesis; Humboldt State University, Arcata, California; May 2005.

TABLES

Table 1: 1-D Velocity Model to Density Conversions

1-D Velocity Model ID	Depth (km)	Velocity (km/sec)	Calculated Density per Gardner* (g/cm^3)	Calculated Density per Christensen and Mooney** (g/cm^3)
CVLO[1]	0	4.00	2.45	2.15
	3	5.75	2.68	2.65
FREY/HOPS[1]	0	4.00	2.45	2.15
	2.5	6.00	2.71	2.72
KCPB[1]	0	4.00	2.45	2.15
	1.5	5.25	2.62	2.51
	3	5.00	2.59	2.43
	8	6.25	2.74	2.80
MAN[2]	0	4.36	2.50	2.25
	1.5	5.46	2.65	2.57
	3.5	5.60	2.66	2.61
	5	5.63	2.67	2.62
	7.5	5.66	2.67	2.63

* density = 0.23(3208.84V)^0.25 where V in feet/s (Gardner et al., 1974)

** density = (989.3 + 289.1V)/1000 where V in km/s (Christensen and Mooney, 1995)

[1] Hayes and Furlong, 2007a

[2] Average velocity structure of four stations from the U. S. Geological Survey seismic network (Castillo and Ellsworth, 1993)

Table 2: Rock Density Measurements

Rock Unit and Type	Source of Data	No. Samples	Density Range (g/cm^3)	Average Density (g/cm^3)
Upper Cretaceous greywacke*	Bailey et al., 1964	78	---	2.55 (median value)
Lower Cretaceous greywacke*		71	---	2.57 (median value)
Franciscan Formation greywacke*		725	---	2.65 (median value)
Coastal belt greywacke	this study	8	2.50-2.66	2.59
Central belt greywacke		13	2.53-2.66	2.60
Franciscan Formation greenstone*	Clement, 1965	---	2.38-2.89	2.78
Franciscan Formation greenstone*	Chapman and Bishop, 1974	3	2.70-3.14	2.95
Central belt greenstone	this study	7	2.57-3.01	2.79
Serpentine*	Chapman and Bishop, 1974	3	---	2.53
Serpentine (Susceptibility 13.175-17.975)	this study	6	2.29-2.39	2.32

*From Table 1, Chapman, 1975.

Table 3: Well Log Compilation*

Location	Well ID	Total Depth (m)	Reference
Little Lake Valley	A1	107	Woolace, 2005
Little Lake Valley	A2	160	Woolace, 2005
Walker Valley	97456	61	well log on file with CA Department of Water Resources, unpublished
Redwood Valley	95412	40**	well log on file with CA Department of Water Resources, unpublished
Redwood Valley	3057F	132	well log on file with CA Department of Water Resources, unpublished
northern Ukiah Valley	Cardwell	455**	Cardwell, 1965

* Well locations presented on Figure 2, all wells drilled in Quarternary or late Neogene deposits

** Indicates depth to bedrock, total depth of well extends beyond

Table 4: Approximate Vertical Offsets Along Splays of the East Valley fault

Cross section	Western splay (m)	Eastern splay (m)	Cumulative (m)
W1 (Figure 10)	---	25	25
W2 (Figure 11)	160	30	190
W3 (Figure 12)	250	210	460

Inferred bedrock offset based on assigned density contrast value for basin fill -0.4 g/cm^3

FIGURES

Figure 1

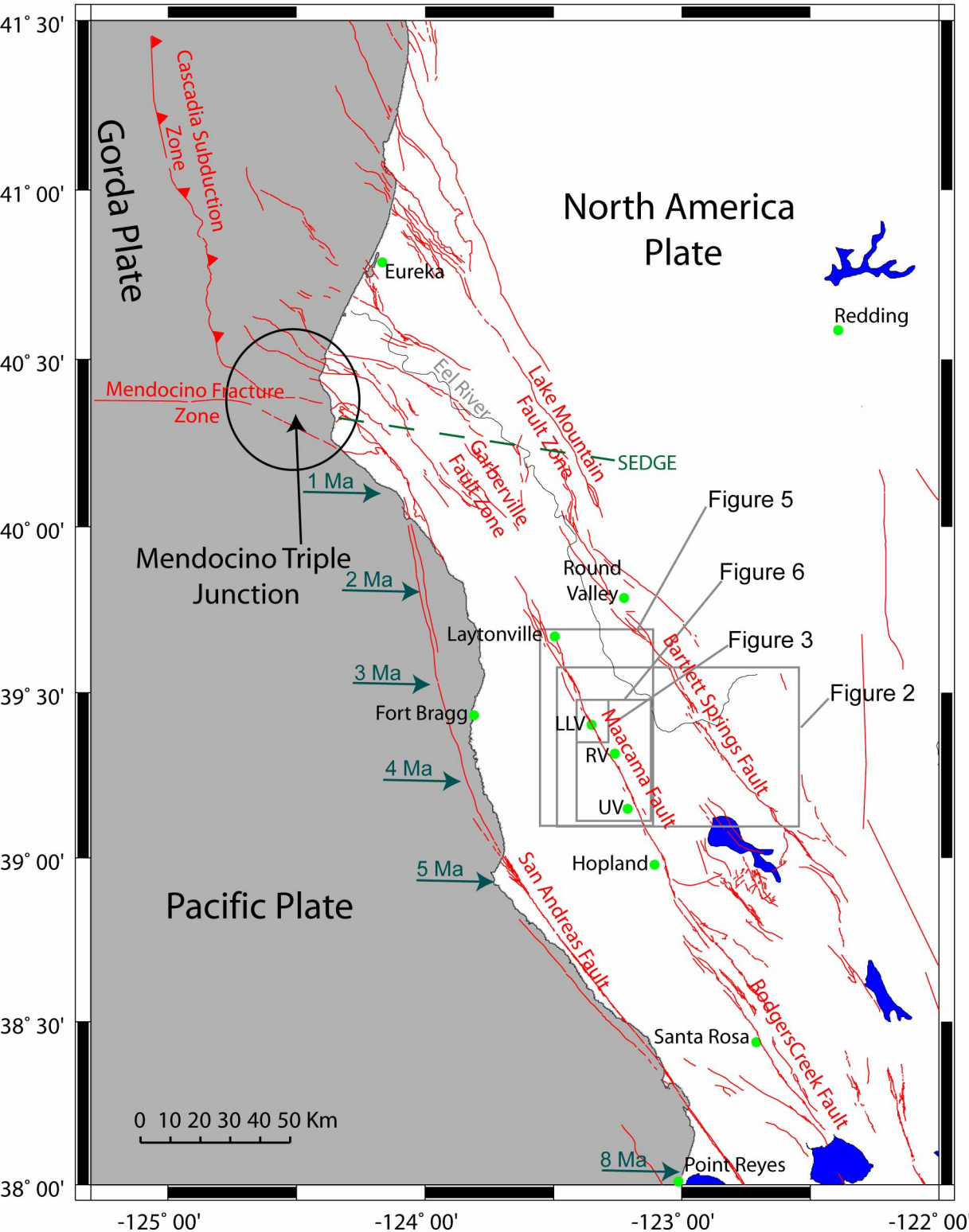
41° 30'
41° 00'
40° 30'
40° 00'
39° 30'
39° 00'
38° 30'
38° 00'
-125° 00'
-124° 00'
-123° 00'
-122° 00'
Gorda Plate
Cascadia Subduction Zone
North America Plate
Pacific Plate
Eureka
Redding
Mendocino Fracture Zone
Eel River
Lake Mountain Fault Zone
Garberville Fault Zone
SEDGE
1 Ma
2 Ma
3 Ma
4 Ma
5 Ma
8 Ma
Mendocino Triple Junction
Figure 5
Figure 6
Figure 3
Figure 2
Round Valley
Laytonville
Bartlett Springs Fault
Fort Bragg
LLV
RV
UV
Maacama Fault
Hopland
San Andreas Fault
Santa Rosa
Bodgers Creek Fault
Point Reyes
0 10 20 30 40 50 Km

Figure 1: Index map showing geographic locations, faults, major tectonic boundaries, and study area. Mapped surface fault locations from Quaternary faults and folds database (USGS, 2006) are shown in red. Green dashed line shows southern edge of subducted Gorda Plate (SEDGE) after Furlong and Govers (1999) and Pryor et al. (2007). Blue arrows and time indicate past approximate locations of the Mendocino Triple Junction (MTJ; Wilson, 1989); large black circle indicates current position. Thin black line is the Eel River. LLV: Little Lake Valley; RV: Round Valley; UV: Ukiah Valley.

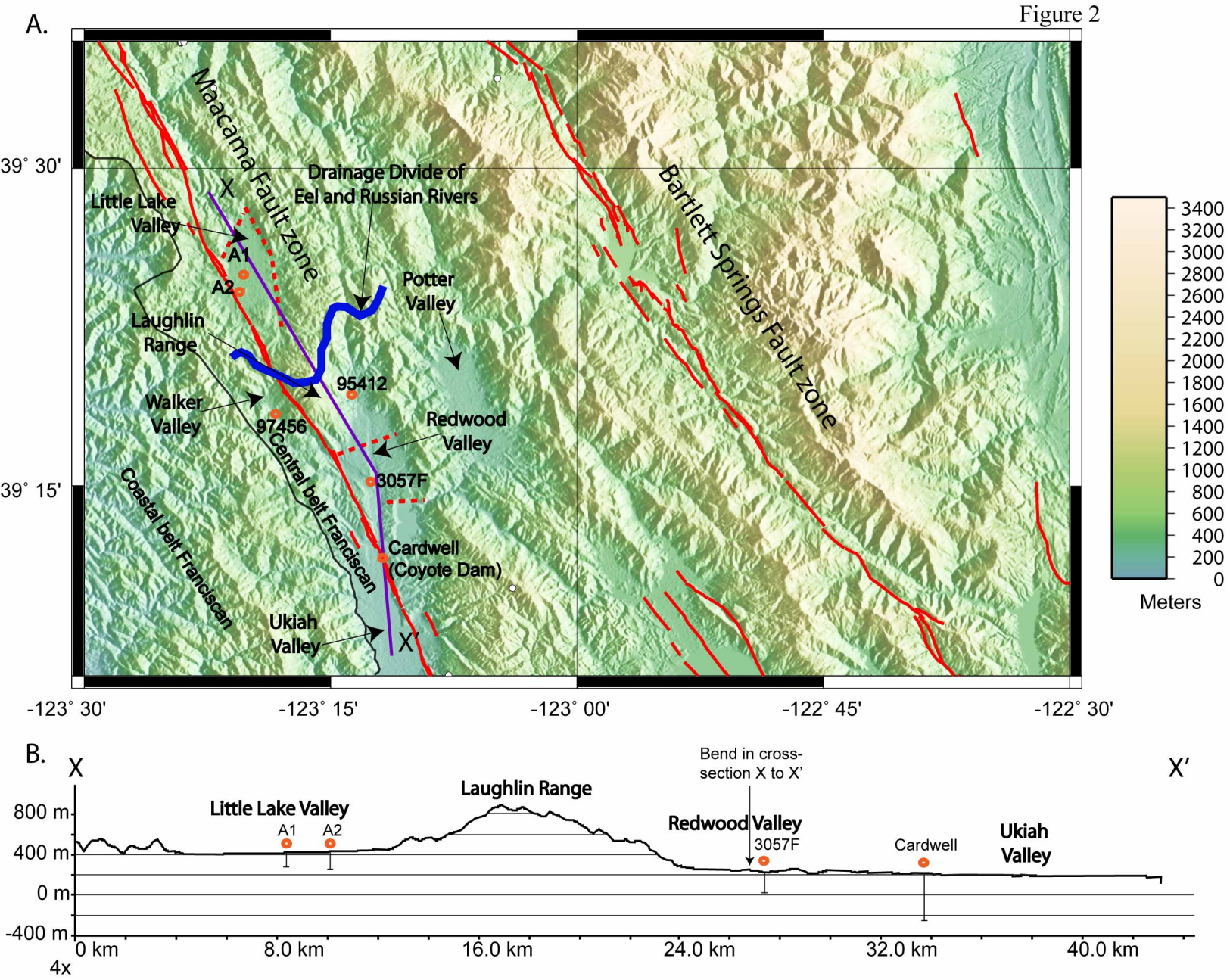
A.
Maacama Fault zone
Drainage Divide of
Eel and Russian Rivers
Little Lake
Valley
X
A1
A2
Potter
Valley
Laughlin
Range
Bartlett Springs Fault zone
95412
Walker
Valley
97456
Redwood
Valley
3057F
Central belt Franciscan
Coastal belt Franciscan
Cardwell
(Coyote Dam)
Ukiah
Valley
X'
39° 30'
39° 15'
-123° 30'
-123° 15'
-123° 00'
-122° 45'
-122° 30'
3400
3200
3000
2800
2600
2400
2200
2000
1800
1600
1400
1200
1000
800
600
400
200
0
Meters
B.
X
X'
Bend in cross-
section X to X'
Laughlin Range
Little Lake Valley
A1
A2
Redwood Valley
3057F
Cardwell
Ukiah
Valley
800 m
400 m
0 m
-400 m
0 km
8.0 km
16.0 km
24.0 km
32.0 km
40.0 km
4x

Figure 2: A. Regional shaded-relief topographic map with cross-section. USGS data product (USGS, 2007) 3-arc second DEM from latitude 39.1^{o} N to 39.6^{o} N and longitude -123.5 W to -122.5 W. Red lines are mapped surface fault locations from Quaternary faults and folds database (USGS, 2006) with dashed faults in Little Lake and Redwood Valley areas based on this study. Strong blue line is major drainage divide between the Eel and Russian Rivers. Orange circles are well locations from Cardwell (1965), Woolace (2005), and unpublished logs from California Department of Water Resources (2007). Purple line shows location of cross-section X-X' shown in B. B. Cross section X-X' showing topographic elevation between Little Lake and Ukiah Valley. Topographic cross section developed in a topographic mapping program TOPO!. Vertical bars for wells A1, A2, and 3057F show total depths of wells and are minimum thickness of Quaternary fill. Cardwell well shows depth to top of Franciscan bedrock. Wells 95412 and 97456 are located off the cross-section X to X'.

Figure 3

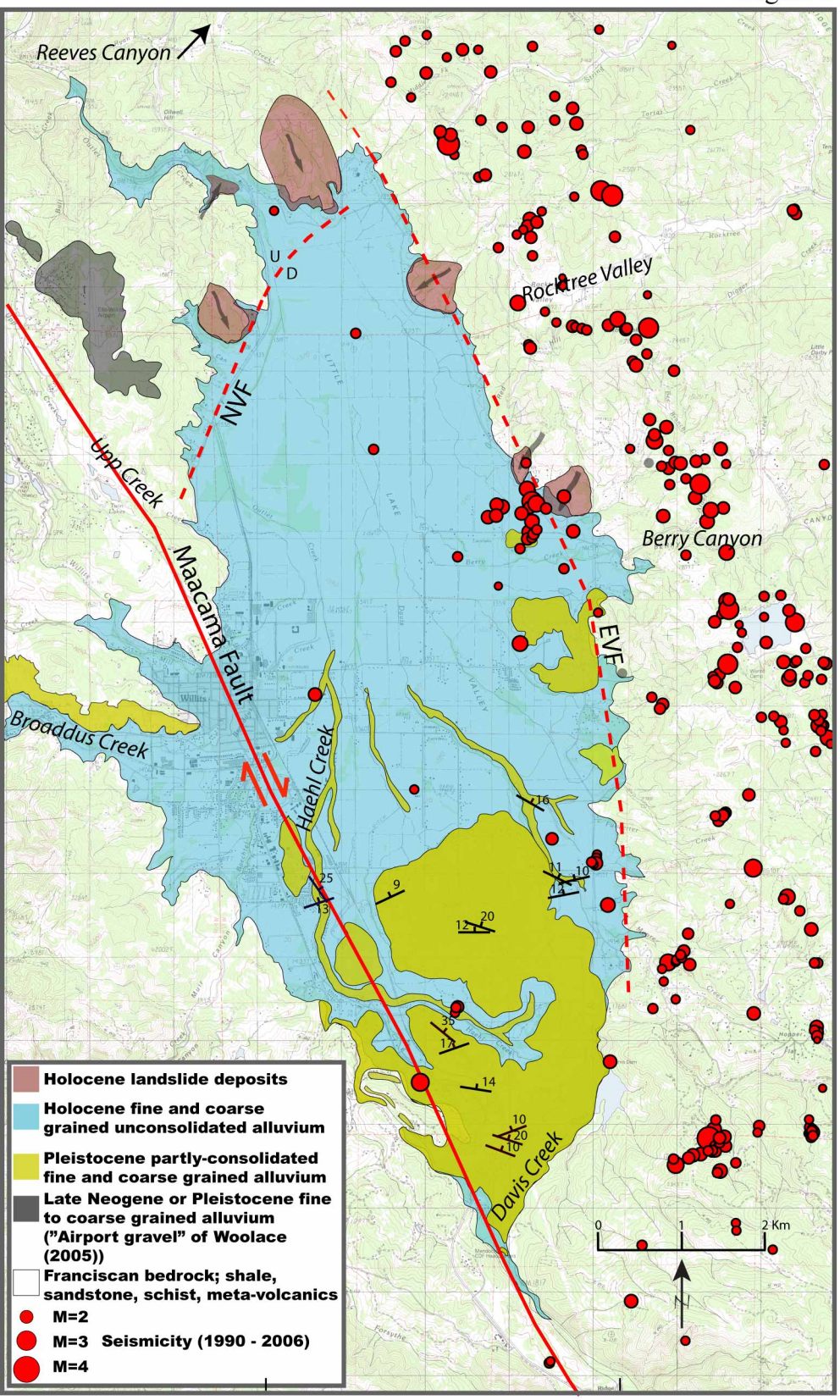
Reeves Canyon
U
D
NVF
Rocktree Valley
Upp Creek
Maacama Fault
Berry Canyon
EVF
Broaddus Creek
Haehl Creek
Davis Creek
Holocene landslide deposits
Holocene fine and coarse grained unconsolidated alluvium
Pleistocene partly-consolidated fine and coarse grained alluvium
Late Neogene or Pleistocene fine to coarse grained alluvium ("Airport gravel" of Woolace (2005))
Franciscan bedrock; shale, sandstone, schist, meta-volcanics
M=2
M=3 Seismicity (1990 - 2006)
M=4
0
1
2 Km
N

Figure 3: Geologic map of Little Lake Valley (modified from Woolace, 2005). Red circles are double-difference relocated seismicity with magnitude from 1990 to 2006 (G. Hayes, written communication, December 2007; Waldhauser and Ellsworth, 2000, 2002). Red lines are approximate locations of mapped surface fault locations and dashed faults NVF and EVF locations are inferred from Woolace (2005). NVF: North Valley fault; EVF: East Valley Fault.

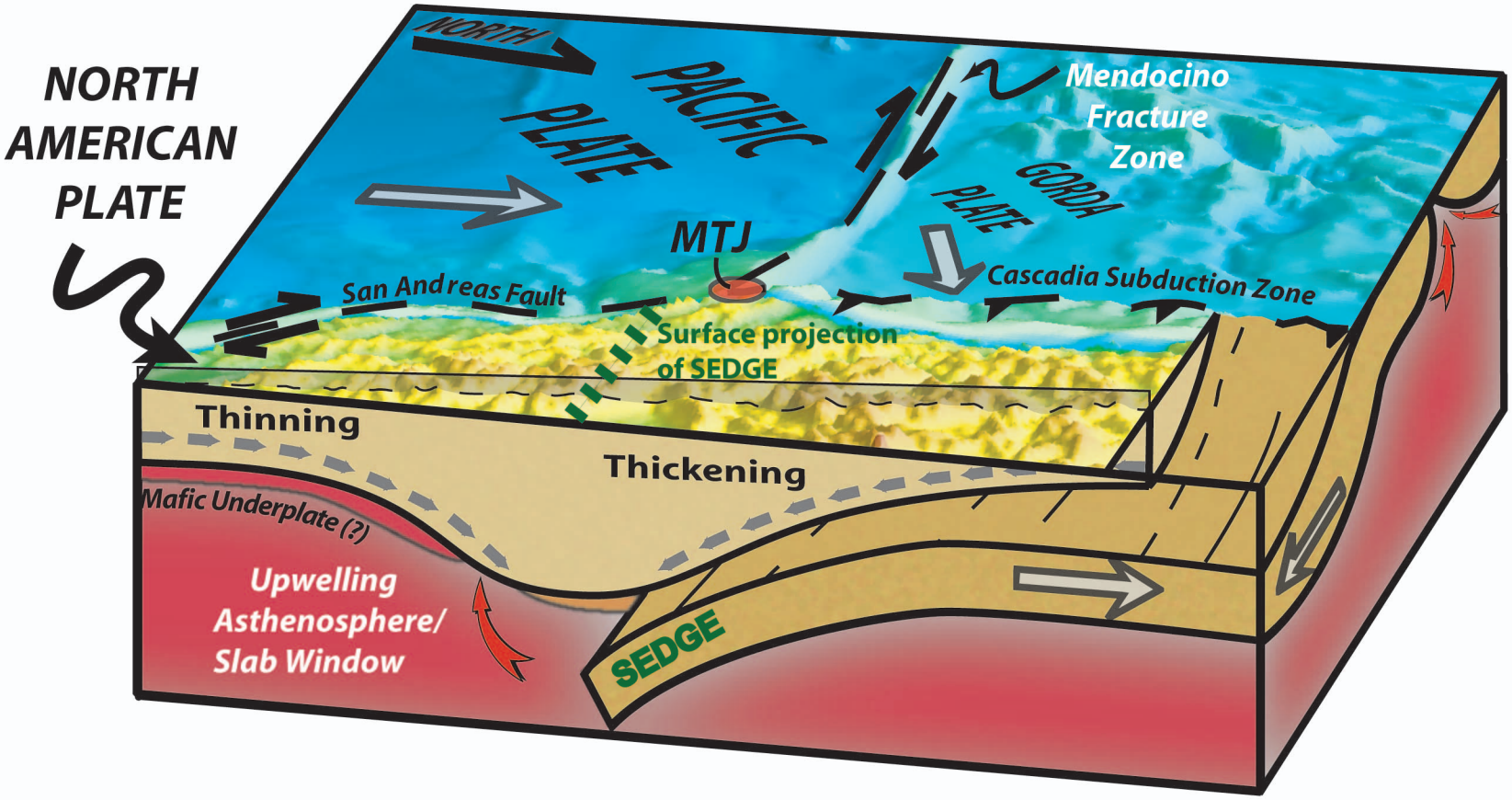
NORTH AMERICAN PLATE
NORTH PACIFIC PLATE
Mendocino Fracture Zone
GORDA PLATE
MTJ
San Andreas Fault
Cascadia Subduction Zone
Surface projection of SEDGE
Thinning
Thickening
Mafic Underplate (?)
Upwelling Asthenosphere/ Slab Window
SEDGE

Figure 4: Slab window and Mendocino crustal conveyor model (modified from Hayes and Furlong, 2006). Black dashed lines indicate plate boundaries and large gray arrows show plate motions. Green dotted line is projected SEDGE. As upwelling asthenosphere accretes to the base of the North American plate (mafic underplating) and upper face of the SEDGE, coupling causes thickening north of the MTJ and thinning in its wake (Furlong and Govers, 1999).

Figure 5

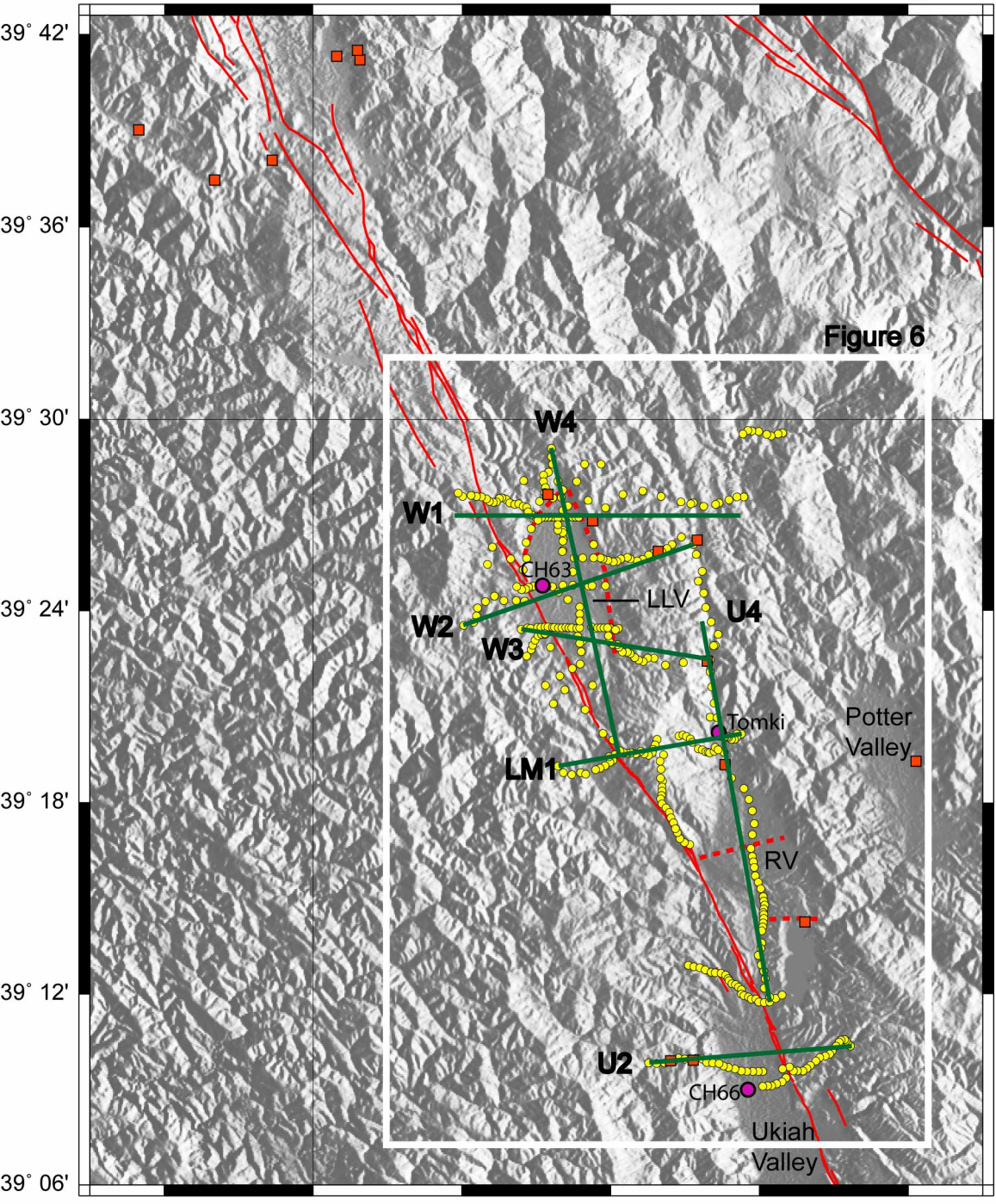
39° 42'
39° 36'
39° 30'
39° 24'
39° 18'
39° 12'
39° 06'
-123° 36'
-123° 30'
-123° 24'
-123° 18'
-123° 12'
-123° 06'
Figure 6
W4
W1
CH63
LLV
U4
W2
W3
Tomki
Potter
Valley
LM1
RV
U2
CH66
Ukiah
Valley

Figure 5: Shaded-relief topographic map showing gravity station locations (yellow dots) and modeled cross sections (green lines). Topography from USGS data product (USGS, 2007) 3-arc second DEM from latitude 39.1° N to 39.71° N and longitude -123.65° W to -123.05°W. See Figures 9 through 15 for models of profiles W1, W2, W3, W4, LM1, U2, and U4. Purple circles are base station locations; CH63 and CH66 were established by Chapman (1966), and Tomki was established for this study. Orange squares are rock sample locations for density measurements (Table 2). Red lines are mapped surface fault locations from Quaternary faults and folds database (USGS, 2006) with dashed faults in Little Lake and Redwood Valley areas based on this study. LLV: Little Lake Valley; RV: Redwood Valley.

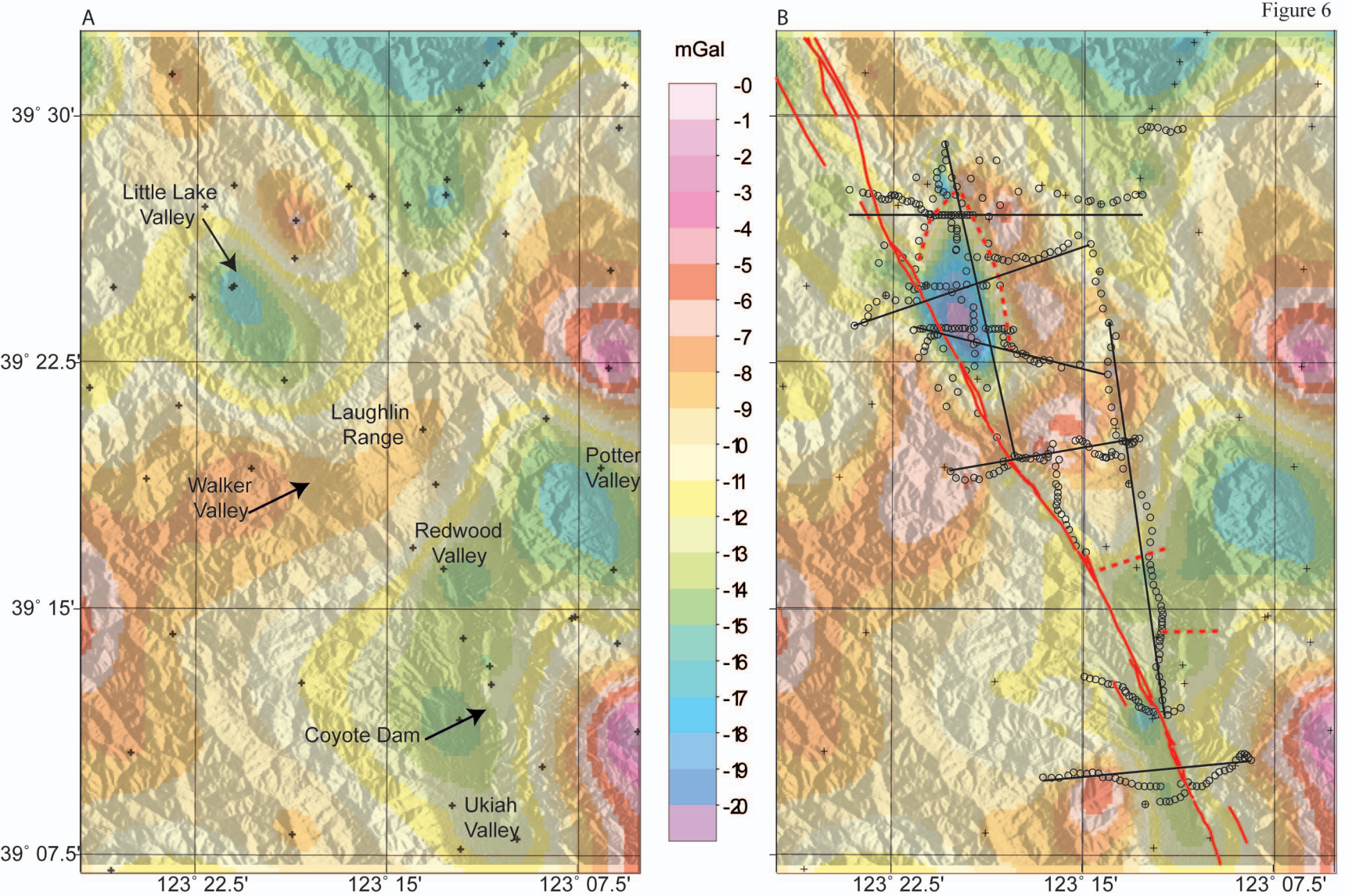
A
B
mGal
-0
-1
-2
-3
-4
-5
-6
-7
-8
-9
-10
-11
-12
-13
-14
-15
-16
-17
-18
-19
-20
39° 30'
39° 22.5'
39° 15'
39° 07.5'
123° 22.5'
123° 15'
123° 07.5'
Little Lake Valley
Laughlin Range
Potter Valley
Walker Valley
Redwood Valley
Coyote Dam
Ukiah Valley

Figure 6: Pre- and post-study isostatic residual gravity anomaly contour maps. A. Isostatic residual gravity data map from previous studies (Chapman, 1966, 1975; Roberts et al., 1990), laid over 3-arc second DEM, with geographic locations for study area. Black crosses are gravity station locations. B. Isostatic residual gravity contour map laid over 3-arc second DEM including new gravity station locations. Black circles are gravity station locations from this study, collected between March 2006 and April 2007. Black lines show locations of gridded and modeled profiles. Red lines are mapped surface fault locations from Quaternary faults and folds database (USGS, 2006) with dashed faults in Little Lake and Redwood Valley areas based on this study.

Figure 7

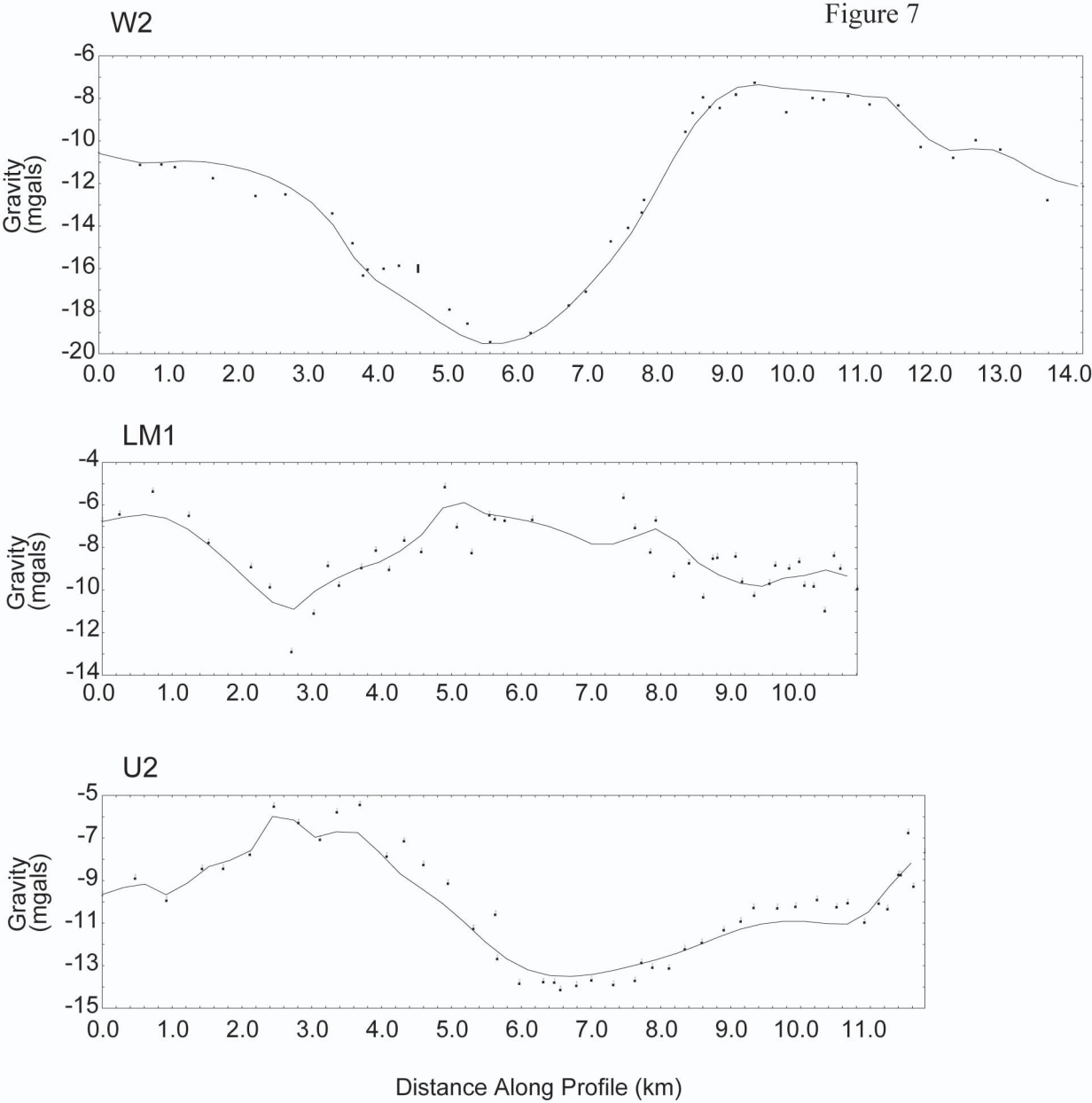
W2
Gravity (mgals)
-6
-8
-10
-12
-14
-16
-18
-20
0.0
1.0
2.0
3.0
4.0
5.0
6.0
7.0
8.0
9.0
10.0
11.0
12.0
13.0
14.0
LM1
Gravity (mgals)
-4
-6
-8
-10
-12
-14
0.0
1.0
2.0
3.0
4.0
5.0
6.0
7.0
8.0
9.0
10.0
U2
Gravity (mgals)
-5
-7
-9
-11
-13
-15
0.0
1.0
2.0
3.0
4.0
5.0
6.0
7.0
8.0
9.0
10.0
11.0
Distance Along Profile (km)

Figure 7: Profiles of gridded and observed gravity data for use in gravity models. Small dots are observed isostatic residual gravity anomaly values at each gravity station location projected onto profiles W2, LM1 and U2. Black lines represent gridded smoothed curve of isostatic residual gravity anomaly values.

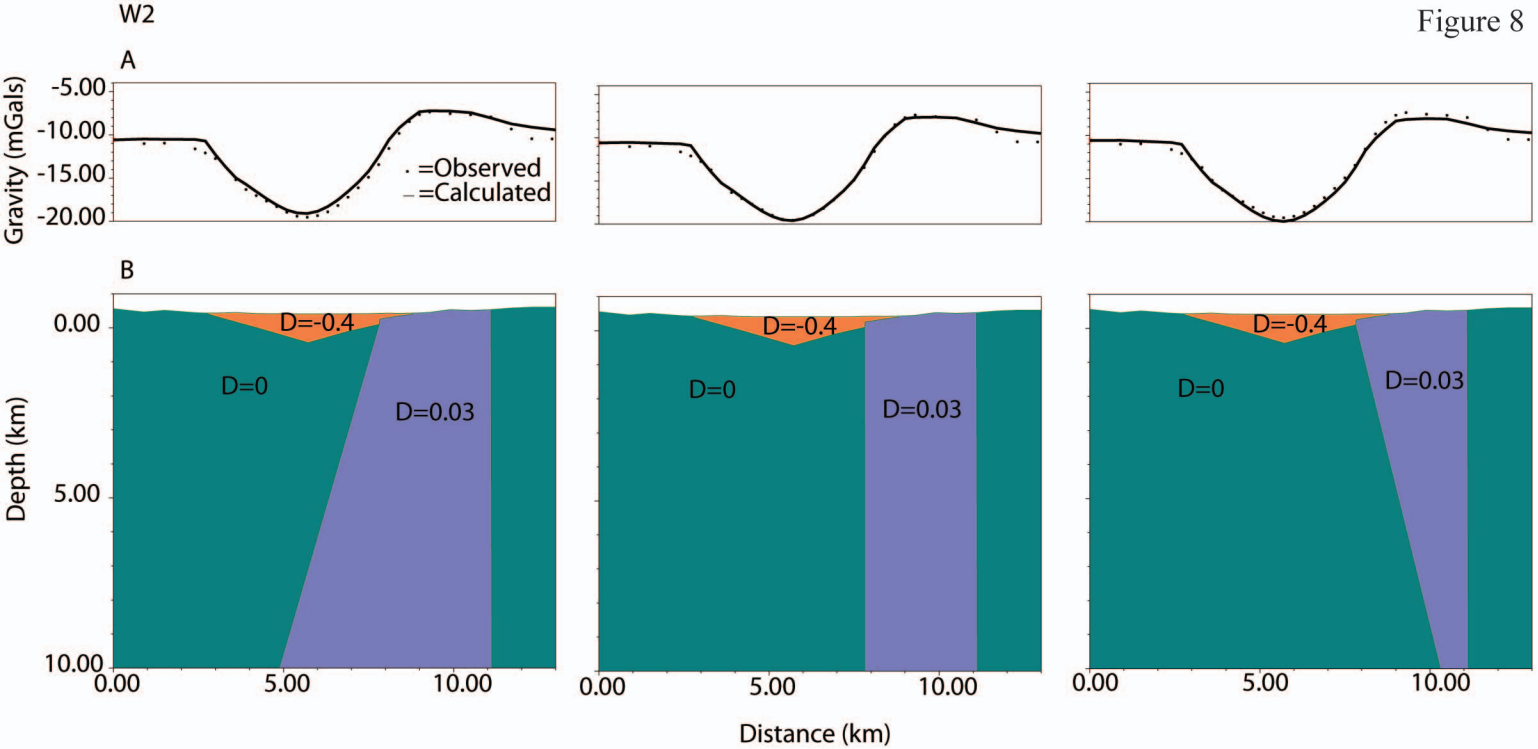
W2
A
Gravity (mGals)
-5.00
-10.00
-15.00
-20.00
=Observed
=Calculated
B
Depth (km)
0.00
5.00
10.00
D=-0.4
D=0
D=0.03
0.00
5.00
10.00
Distance (km)

Figure 8: Example of non-uniqueness of gravity model solutions. Three different gravity model output results of the same profile, W2, illustrating the effects of changing the dip of the bedrock density contrast on calculated gravity anomalies. A. Observed gridded and calculated residual isostatic anomalies. B. Density contrast model of cross section; topography from 30-m DEM; 0-value density corresponds to 2.67 g/cm^3 as assigned by GMSYS modeling program.

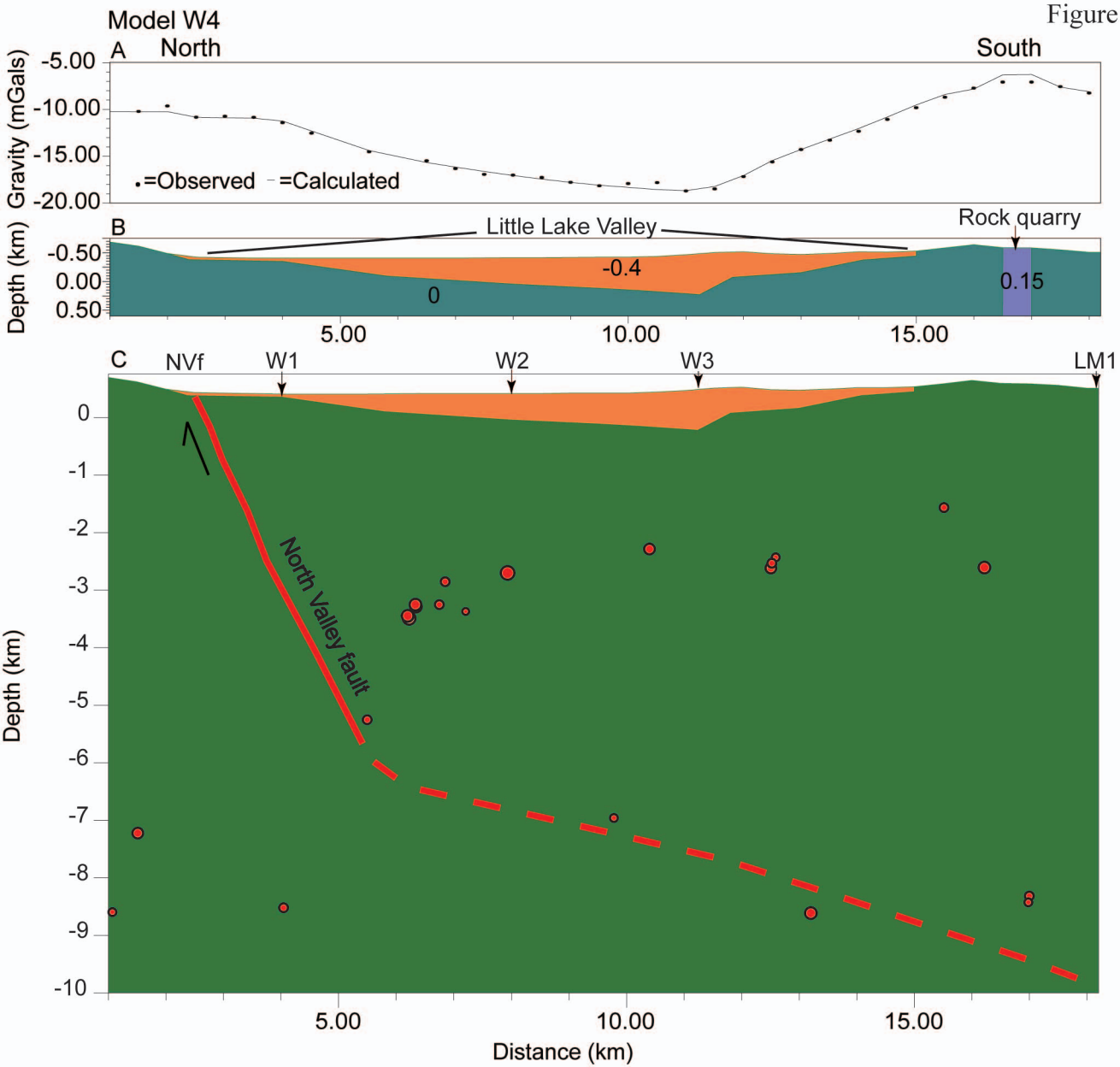
Model W4
A
North
South
-5.00
-10.00
-15.00
-20.00
Gravity (mGals)
•=Observed
=Calculated
B
Little Lake Valley
Rock quarry
-0.50
0.00
0.50
Depth (km)
-0.4
0
0.15
5.00
10.00
15.00
C
NVf
W1
W2
W3
LM1
0
-1
-2
-3
-4
-5
-6
-7
-8
-9
-10
Depth (km)
North Valley fault
5.00
10.00
15.00
Distance (km)

Figure 9: Model of gridded isostatic gravity anomaly data along cross section W4; refer to Figure 5 for cross-section location. A. Observed gridded and calculated residual isostatic anomalies. B. Density contrast model of cross section; topography from 30-m DEM; 0-value density corresponds to 2.67 g/cm^3 as assigned by GMSYS modeling program. C. Fault structure interpretation from surface geology, density contrast model, and double-difference relocated seismicity from 1990 to 2006 (G. Hayes, written communication, December 2007; Waldhauser and Ellsworth, 2000, 2002) down to 10 km depth. Projected seismicity is a 2-km wide swath along profile. Dashed line inferred to be intersection of southerly extension of North Valley fault with Maacama fault. Maacama fault is subparallel to trend of profile W4. No vertical exaggeration. NVf: North Valley fault.

Figure 10

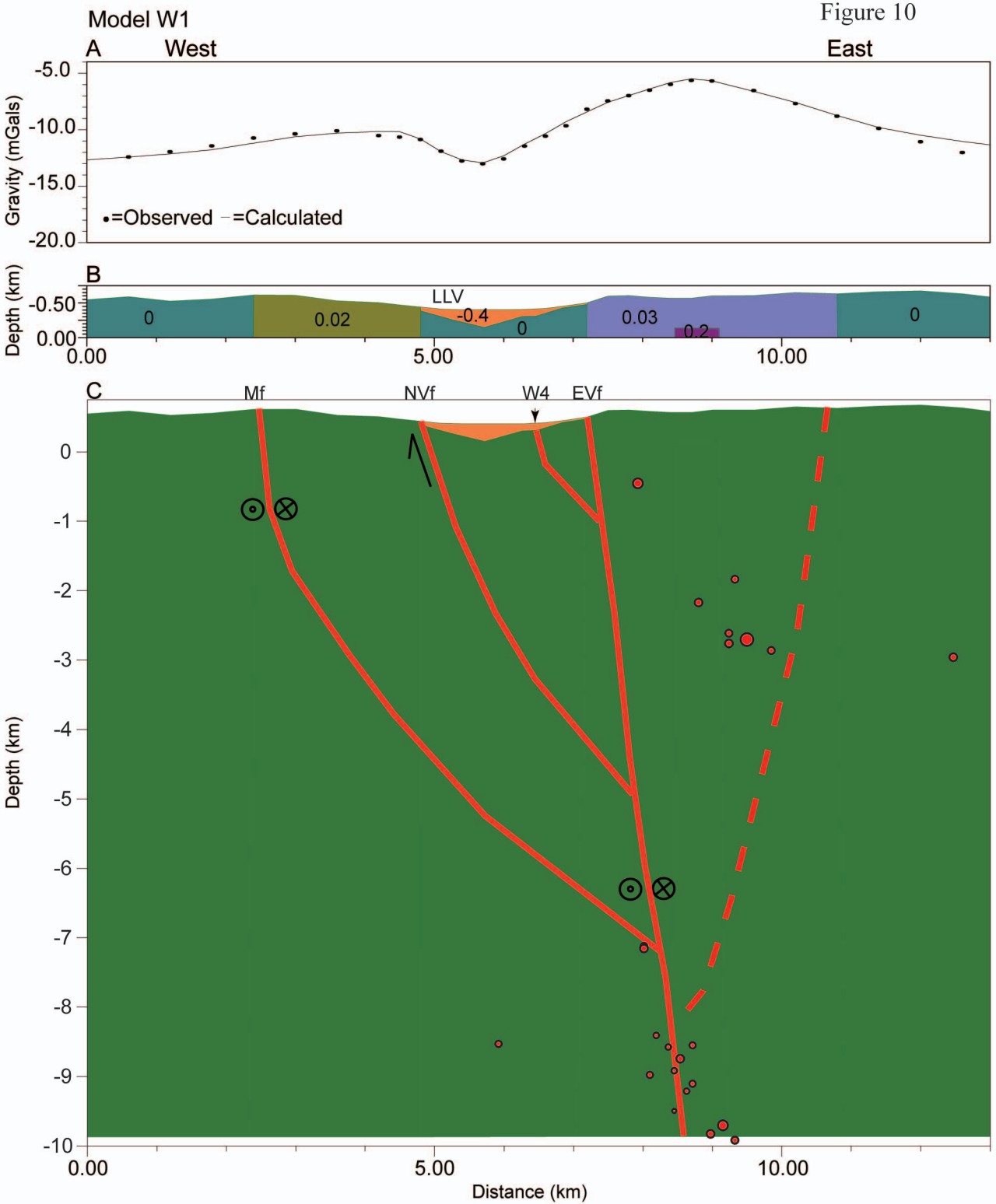
Model W1
A
West
East
Gravity (mGals)
-5.0
-10.0
-15.0
-20.0
•=Observed –=Calculated
B
Depth (km)
-0.50
0.00
LLV
0
0.02
-0.4
0
0.03
0.2
0
0.00
5.00
10.00
C
Mf
NVf
W4
EVf
Depth (km)
0
-1
-2
-3
-4
-5
-6
-7
-8
-9
-10
0.00
5.00
10.00
Distance (km)

Figure 10: Model of gridded isostatic gravity anomaly data along cross section W1; refer to Figure 5 for cross-section location. A. Observed gridded and calculated residual isostatic anomalies. B. Density contrast model of cross section; topography from 30-m DEM; 0-value density corresponds to 2.67 g/cm^3 as assigned by GMSYS modeling program. C. Fault structure interpretation from surface geology, density contrast model, and double-difference relocated seismicity from 1990 to 2006 (G. Hayes, written communication, December 2007; Waldhauser and Ellsworth, 2000, 2002) down to 10 km depth. Projected seismicity is a 2-km wide swath along profile. No vertical exaggeration. LLV: Little Lake Valley, Mf: Maacama fault, NVf: North Valley fault, EVf: East Valley fault.

Model W2

Figure 11

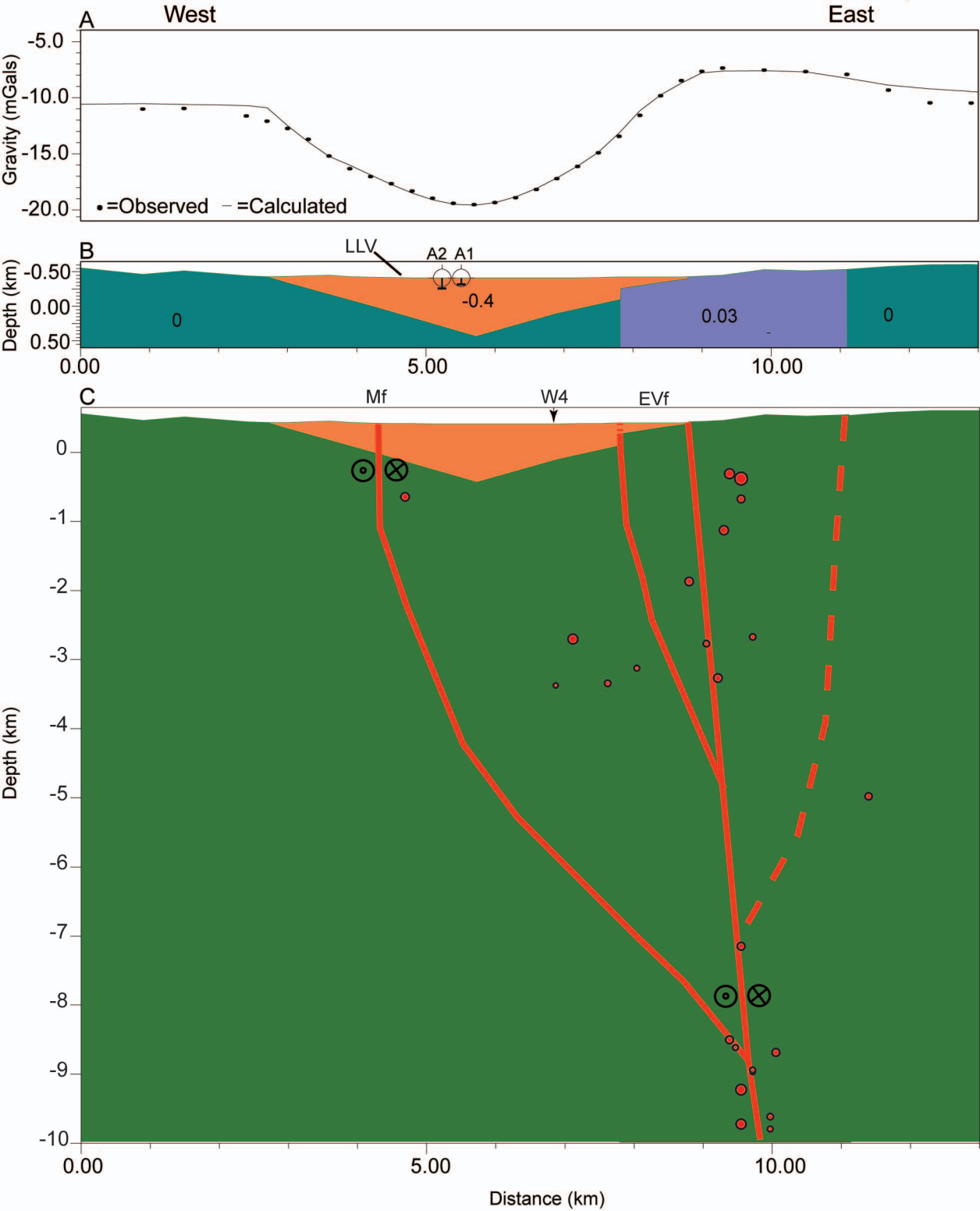

Figure 11: Model of gridded isostatic gravity anomaly data along cross section W2; refer to Figure 5 for cross-section location. A. Observed gridded and calculated residual isostatic anomalies. B. Density contrast model of cross section; topography from 30-m DEM; 0-value density corresponds to 2.67 g/cm^3 as assigned by GMSYS modeling program. Data from well logs A1 and A2 indicate minimum depths of valley fill (Woolace, 2005). C. Fault structure interpretation from surface geology, density contrast model, and double-difference relocated seismicity from 1990 to 2006 (G. Hayes, written communication, December 2007; Waldhauser and Ellsworth, 2000, 2002) down to 10 km depth. Projected seismicity is a 2-km wide swath along profile. No vertical exaggeration. LLV: Little Lake Valley, Mf: Maacama fault, EVf: East Valley fault.

Figure 12

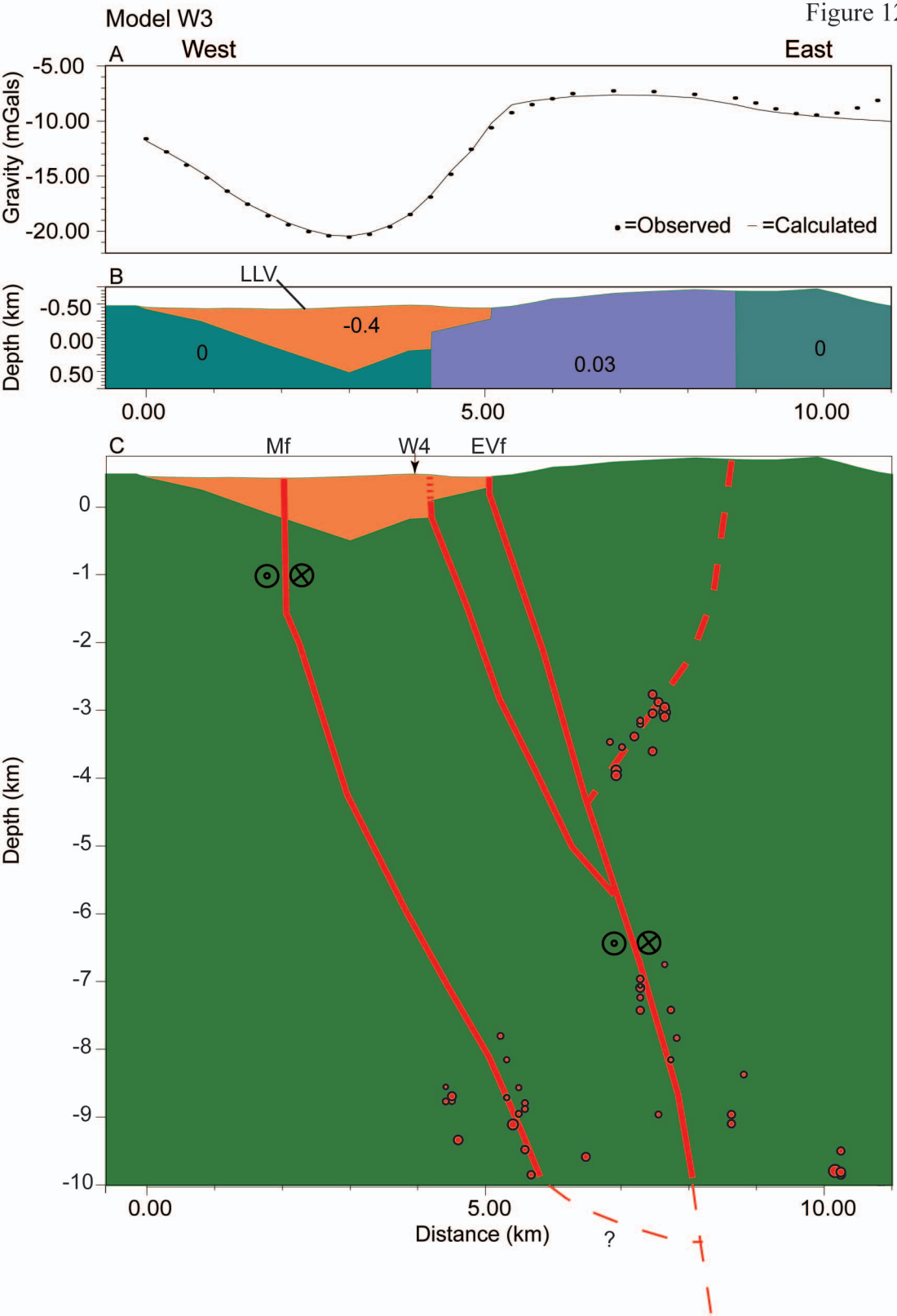
Model W3
A
West
East
-5.00
-10.00
-15.00
-20.00
Gravity (mGals)
•=Observed –=Calculated
B
LLV
-0.50
0.00
0.50
Depth (km)
-0.4
0
0.03
0
0.00
5.00
10.00
C
Mf
W4
EVf
0
-1
-2
-3
-4
-5
-6
-7
-8
-9
-10
Depth (km)
0.00
5.00
10.00
Distance (km)
?

Figure 12: Model of gridded isostatic gravity anomaly data along cross section W3; refer to Figure 5 for cross-section location. A. Observed gridded and calculated residual isostatic anomalies. B. Density contrast model of cross section; topography from 30-m DEM; 0-value density corresponds to 2.67 g/cm^3 as assigned by GMSYS modeling program. C. Fault structure interpretation from surface geology, density contrast model, and double-difference relocated seismicity from 1990 to 2006 (G. Hayes, written communication, December 2007; Waldhauser and Ellsworth, 2000, 2002) down to 10 km depth. Projected seismicity is a 2-km wide swath along profile. No vertical exaggeration. LLV: Little Lake Valley, Mf: Maacama fault, EVf: East Valley fault.

Figure 13

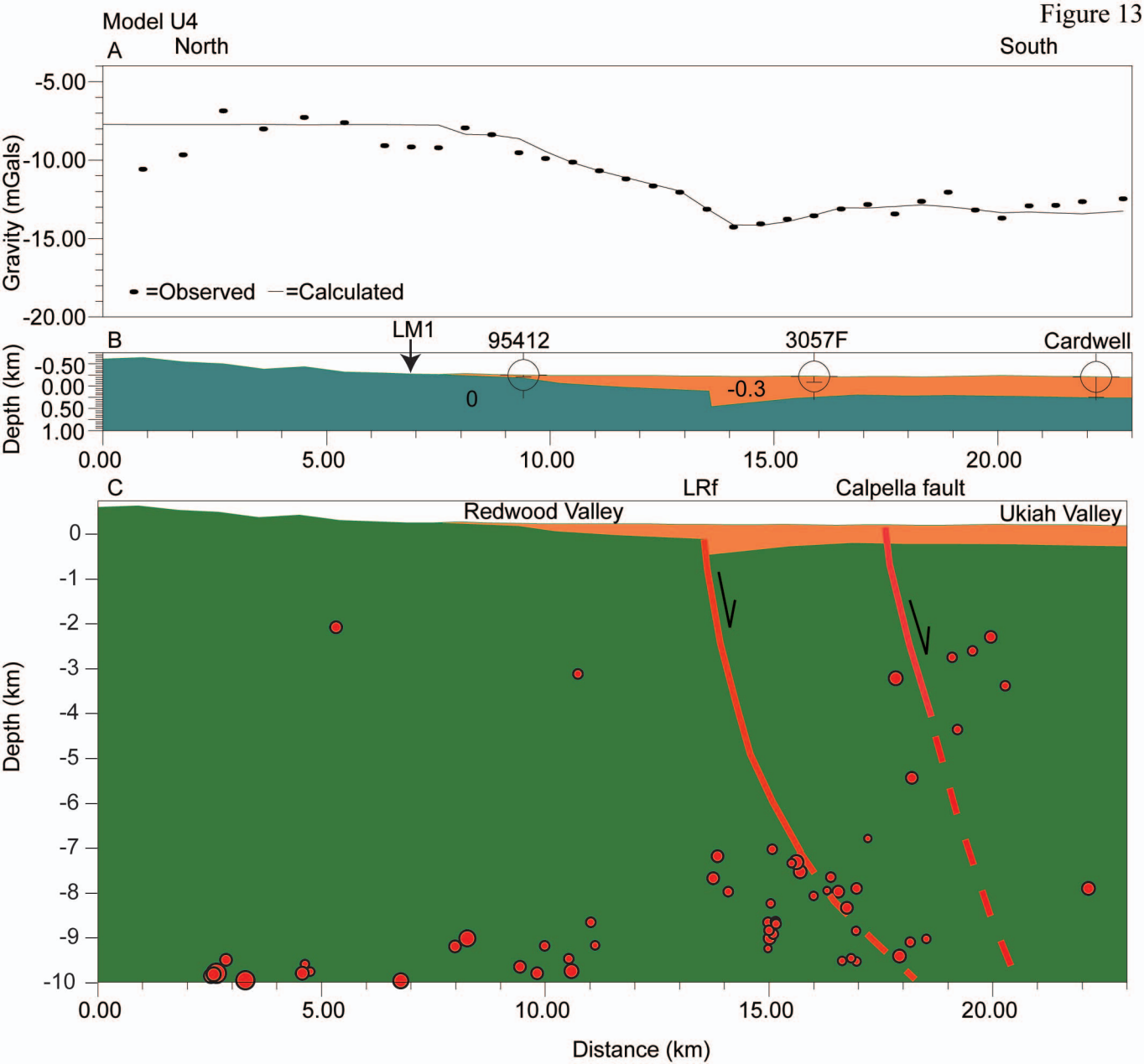
Model U4
A
North
South
-5.00
-10.00
-15.00
-20.00
Gravity (mGals)
=Observed
=Calculated
B
LM1
95412
3057F
Cardwell
-0.50
0.00
0.50
1.00
Depth (km)
0
-0.3
0.00
5.00
10.00
15.00
20.00
C
LRf
Calpella fault
Redwood Valley
Ukiah Valley
0
-1
-2
-3
-4
-5
-6
-7
-8
-9
-10
Depth (km)
0.00
5.00
10.00
15.00
20.00
Distance (km)

Figure 13: Model of gridded isostatic gravity anomaly data along cross section U4; refer to Figure 5 for cross-section location. A. Observed (from grid) and calculated residual isostatic anomalies. B. Density contrast model of cross section; topography from 30-m DEM; 0-value density corresponds to 2.67 g/cm^3 as assigned by GMSYS modeling program. Data from well log 3057F indicates minimum depth of valley fill (California Department of Water Resources, unpublished well logs). Data from well logs Cardwell and 95412 indicate depth to top of bedrock (Cardwell, 1965; California Department of Water Resources, unpublished well logs). C. Fault structure interpretation from surface trace of Calpella fault (Larsen and Kelsey, 2005b), density contrast model, and double-difference relocated seismicity from 1990 to 2006 (G. Hayes, written communication, December 2007; Waldhauser and Ellsworth, 2000, 2002) down to 10 km depth. Projected seismicity is a 2-km wide swath along profile No vertical exaggeration. LRf: Laughlin Range fault.

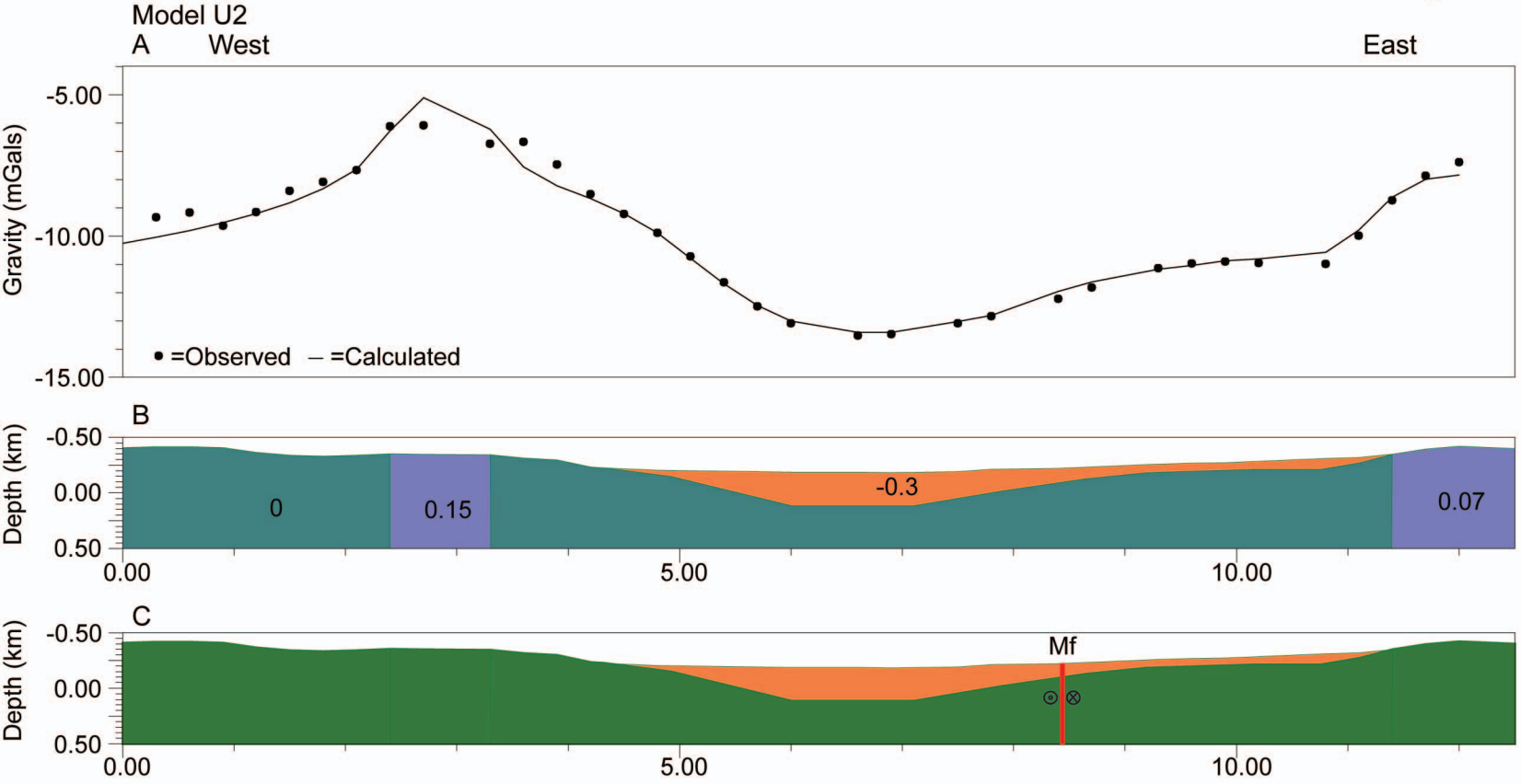
Model U2
A
West
East
-5.00
-10.00
-15.00
Gravity (mGals)
• =Observed — =Calculated
B
-0.50
0.00
0.50
Depth (km)
0
0.15
-0.3
0.07
0.00
5.00
10.00
C
-0.50
0.00
0.50
Depth (km)
Mf
0.00
5.00
10.00

Figure 14: Model of gridded isostatic gravity anomaly data along cross section U2, refer to Figure 5 for cross-section location. A. Observed gridded and calculated residual isostatic anomalies. B. Density contrast model of cross section; topography from 30-m DEM; 0-value density corresponds to 2.67 g/cm^3 as assigned by GMSYS modeling program. C. Geologic interpretation from density contrast model down to 0.50 km. No vertical exaggeration. Mf: Maacama fault.

Figure 15

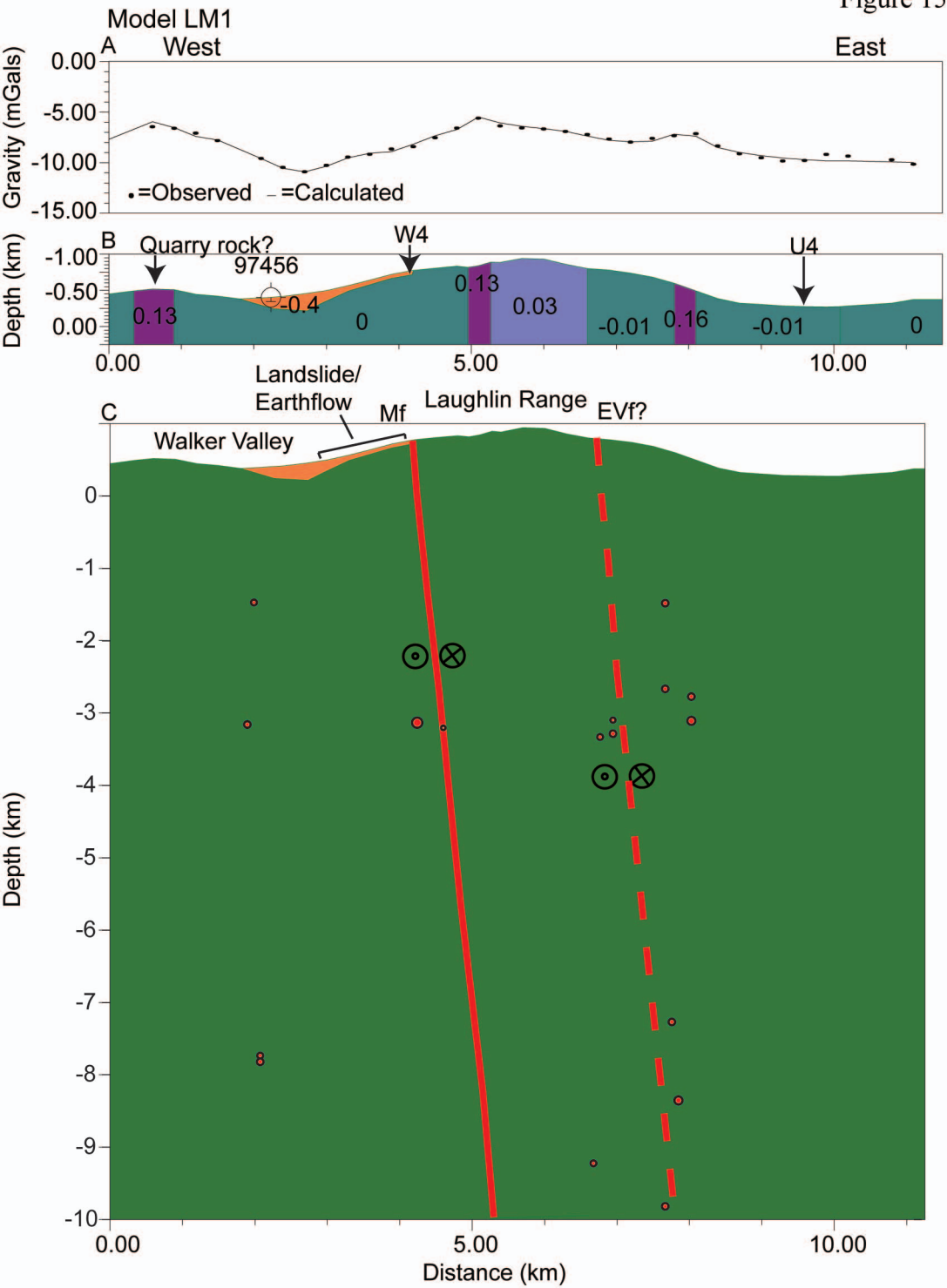
Model LM1
A
West
East
Gravity (mGals)
0.00
-5.00
-10.00
-15.00
•=Observed
–=Calculated
B
Quarry rock?
97456
W4
U4
Depth (km)
-1.00
-0.50
0.00
0.13
-0.4
0
0.13
0.03
-0.01
0.16
-0.01
0
0.00
5.00
10.00
C
Landslide/
Earthflow
Mf
Laughlin Range
EVf?
Walker Valley
Depth (km)
0
-1
-2
-3
-4
-5
-6
-7
-8
-9
-10
0.00
5.00
10.00
Distance (km)

Figure 15: Model of gridded isostatic gravity anomaly data along cross section LM1, refer to Figure 5 for cross-section location. A. Observed gridded and calculated residual isostatic anomalies. B. Density contrast model of cross section; topography from 30-m DEM; 0-value density corresponds to 2.67 g/cm^3 as assigned by GMSYS modeling program. Data from well log 97456 indicates minimum depth of valley fill (California Department of Water Resources, unpublished well logs). C. Fault structure interpretation from surface geology, density contrast model, and double-difference relocated seismicity from 1990 to 2006 (G. Hayes, written communication, December 2007; Waldhauser and Ellsworth, 2000, 2002) down to 10 km depth. Projected seismicity is a 2-km wide swath along profile. EVf location based on eastern cluster of seismicity and density contrast material $\Delta\rho$=0.03 g/cm^3, which correlates with similar material along profiles W1, W2, and W3. No vertical exaggeration. Mf: Maacama fault, EVf: East Valley fault.

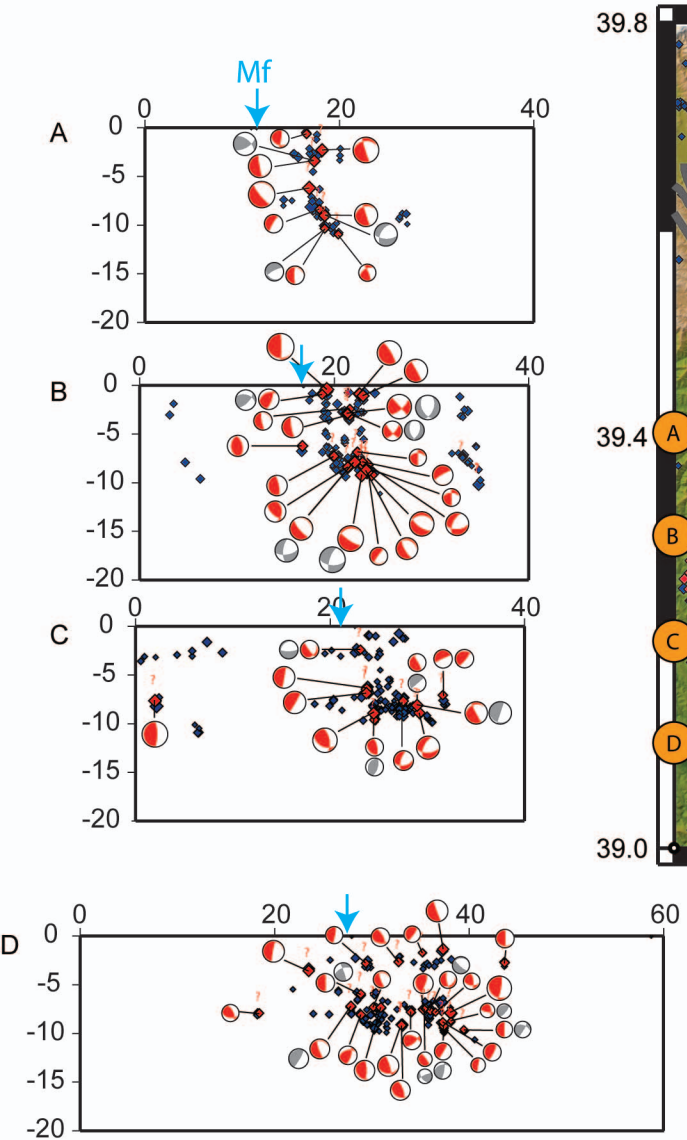

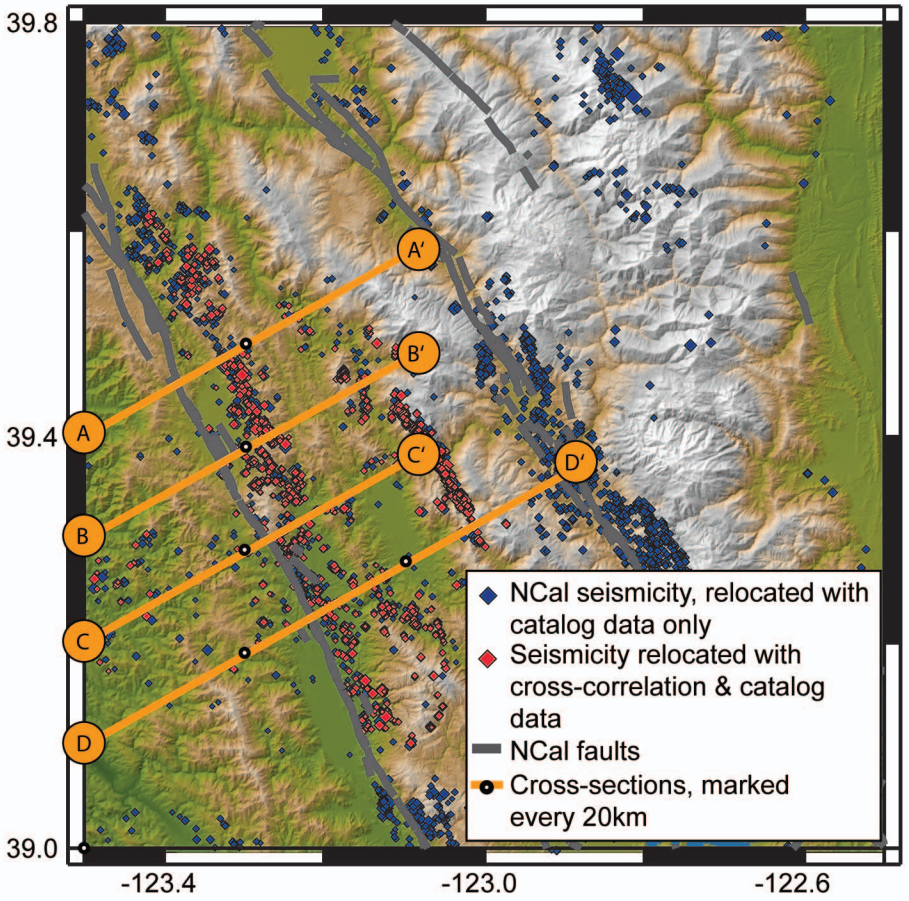

Modified from from unpublished figure of G. Hayes

Figure 16: Relocated seismicity (1990 to 2006, G. Hayes, written communication, December 2007; Waldhauser and Ellsworth, 2000, 2002) and cross-sections of focal mechanisms perpendicular to the Maacama fault. Red diamonds are catalog seismicity data relocated with cross-correlation technique (Waldhauser and Ellsworth, 2000, 2002) and corresponding focal mechanisms are red. Blue diamonds are catalog seismicity and corresponding focal mechanisms are gray. Cross sections show seismicity projected within 10 km of the profile. Focal projection is perpendicular to the Maacama fault. Figure modified from unpublished figure from G. Hayes (written communication, December 2007). Blue arrows indicate surface location of the Maacama fault along the cross-section. Mf: Maacama fault.

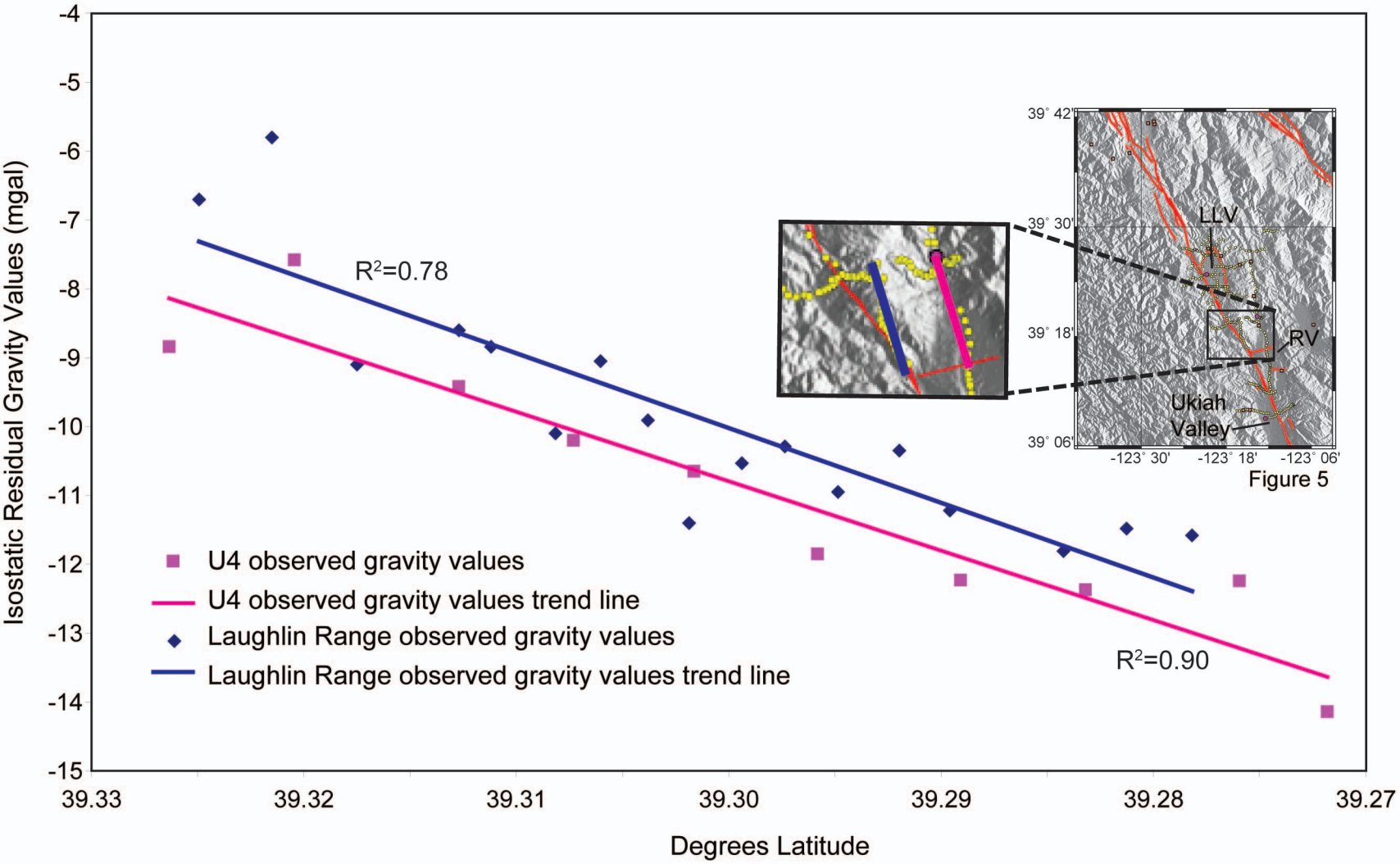
Isostatic Residual Gravity Values (mgal)
-4
-5
-6
-7
-8
-9
-10
-11
-12
-13
-14
-15
39.33
39.32
39.31
39.30
39.29
39.28
39.27
Degrees Latitude
R²=0.78
R²=0.90
U4 observed gravity values
U4 observed gravity values trend line
Laughlin Range observed gravity values
Laughlin Range observed gravity values trend line
39° 42'
39° 30'
39° 18'
39° 06'
-123° 30'
-123° 18'
-123° 06'
LLV
RV
Ukiah
Valley
Figure 5

Figure 17: Parallel transects of observed isostatic residual gravity data values plotted with linear regression lines from approximately latitude 39.33º to 39.27º, indicating consistent gravity gradients. Pink squares are observed isostatic residual gravity values along part of modeled cross section U4; completed down the longitudinal axis of Redwood Valley. Blue diamonds are observed isostatic residual gravity values along an un-modeled cross section completed from the peak of Laughlin Mountain down its southern flank. Trend lines indicate a similar gravity gradient occurs over the two distinctly different topographic cross sections; U4 is along the valley floor and the southern flank is down the Laughlin Range. Locations of the gravity gradient suggest the Laughlin Range fault trends approximately east from the south flank of the Laughlin Range across the floor of Redwood Valley (map inset).

Figure 18

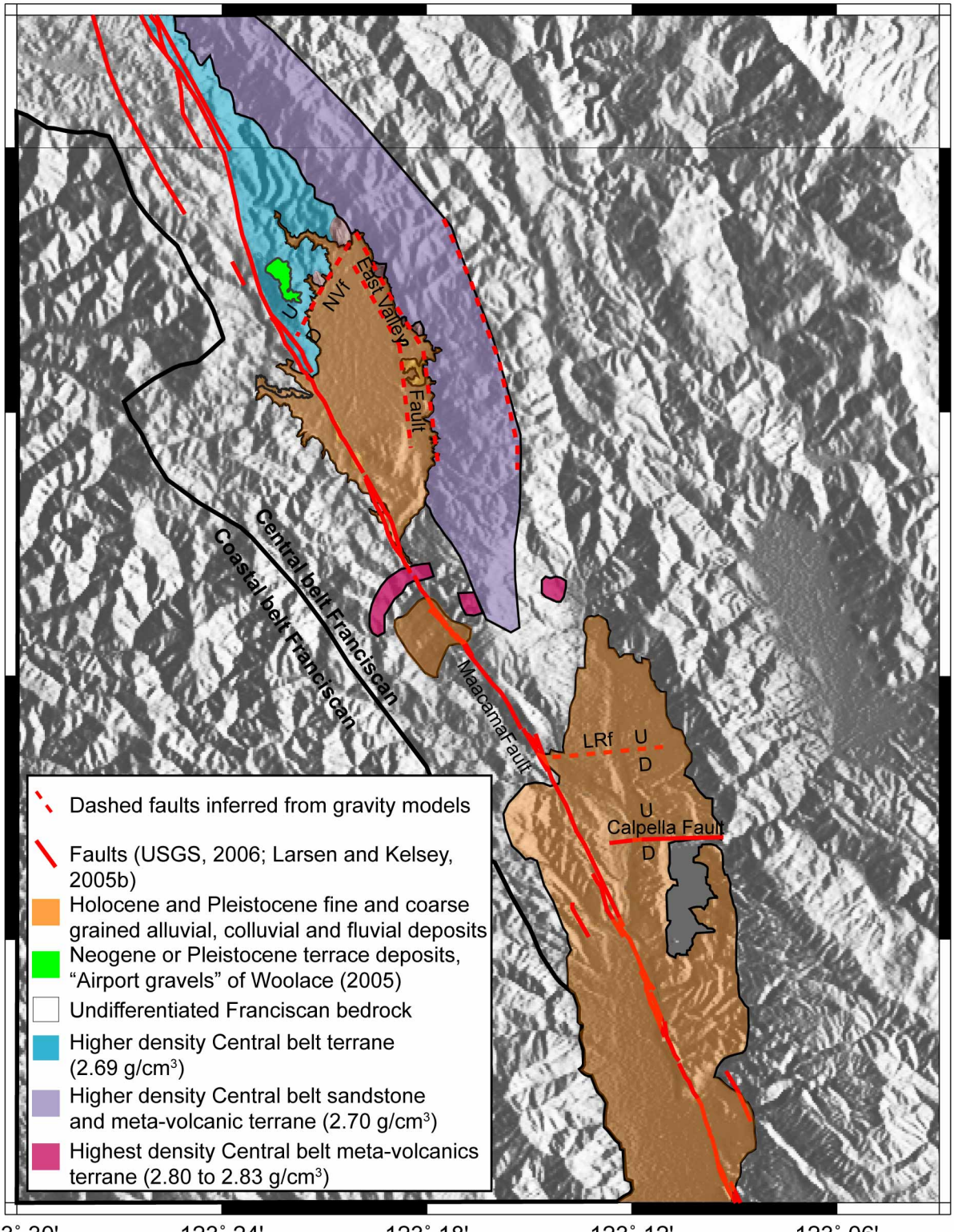
39° 30'
39° 24'
39° 18'
39° 12'
39° 06'
-123° 30'
-123° 24'
-123° 18'
-123° 12'
-123° 06'
NVf
East Valley
Fault
U
D
Central belt Franciscan
Coastal belt Franciscan
Maacama Fault
LRf
U
D
U
Calpella Fault
D
Dashed faults inferred from gravity models
Faults (USGS, 2006; Larsen and Kelsey, 2005b)
Holocene and Pleistocene fine and coarse grained alluvial, colluvial and fluvial deposits
Neogene or Pleistocene terrace deposits, "Airport gravels" of Woolace (2005)
Undifferentiated Franciscan bedrock
Higher density Central belt terrane (2.69 g/cm3)
Higher density Central belt sandstone and meta-volcanic terrane (2.70 g/cm3)
Highest density Central belt meta-volcanics terrane (2.80 to 2.83 g/cm3)

Figure 18: Interpretive geologic map from gravity models overlaid on USGS data product (USGS, 2007) 3-arc second DEM from latitude 39.1^{o} N to 39.55^{o} N and longitude -123.5 ^{o} W to -123.05 ^{o} W. Red lines are mapped surface fault locations from Quaternary faults and folds database (USGS, 2006) and inferred from gravity models. Quaternary and Tertiary aged units from Woolace (2005) and Larsen and Kelsey (2005a, b, c, d). Bedrock units interpreted from gravity models. NVf: North Valley fault, LRf: Laughlin Range fault. Fault locations of NVf, East Valley fault, and LRf inferred from isostatic gravity anomaly data. Calpella fault location from Larsen and Kelsey (2005b).

Figure 19

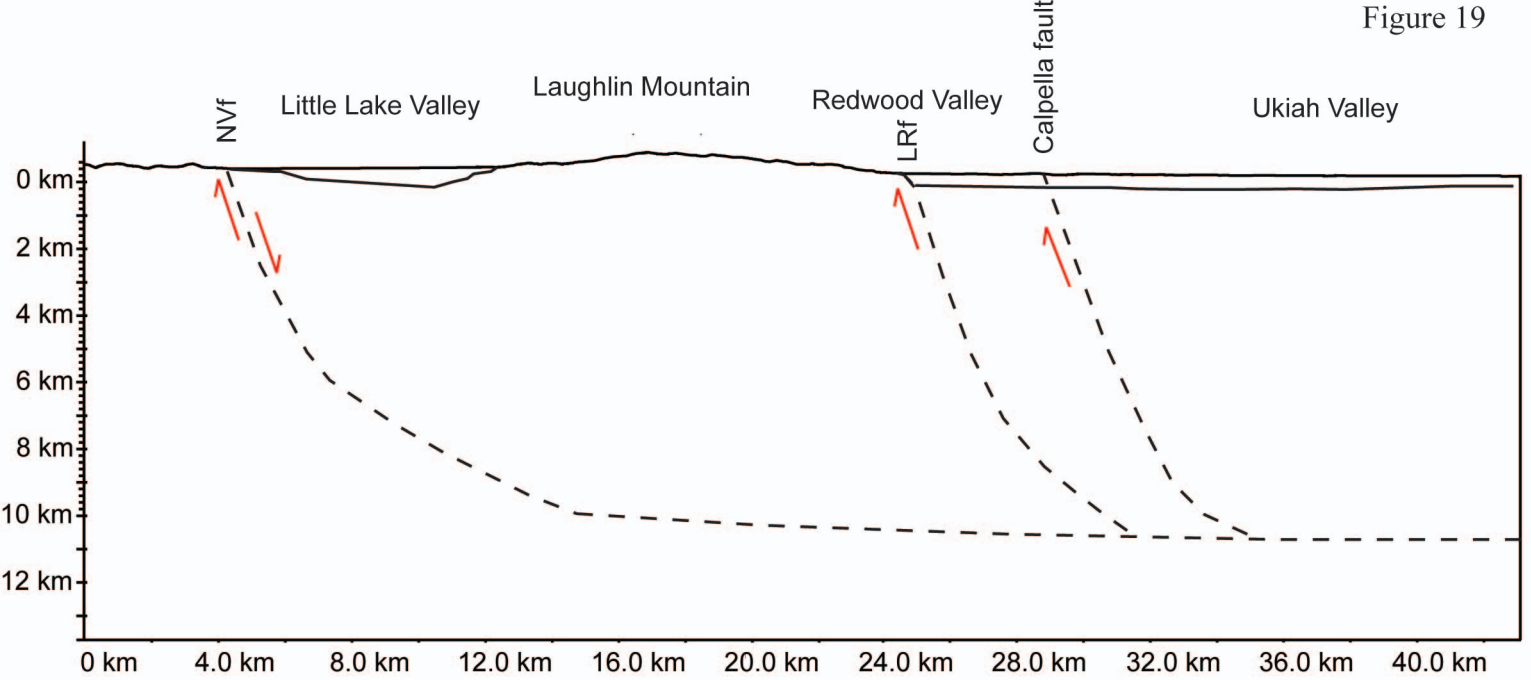
NVf
Little Lake Valley
Laughlin Mountain
Redwood Valley
LRf
Calpella fault
Ukiah Valley
0 km
2 km
4 km
6 km
8 km
10 km
12 km
0 km
4.0 km
8.0 km
12.0 km
16.0 km
20.0 km
24.0 km
28.0 km
32.0 km
36.0 km
40.0 km

Figure 19: Fault structure model indicating locations of paleo-extensional faulting in study area. Cross section showing topography modified from Figure 2 and basement surface from gravity; no vertical exaggeration. NVf: North Valley fault, LRf: Laughlin Range fault. NVf, LRf and Calpella fault are major tectonic regional faults likely linked to deeper detachment fault below 10 km depth.

APPENDIX

APPENDIX 1: U. S. Geological Survey processed gravity data

Station ID	Area	Latitude Degrees	Latitude minutes	Longitude Degrees	Longitude minutes	Elevation (feet)	Absolute Observed Gravity[#] (mGal)	Free-air Anomaly (mGal)	Simple Bouguer anomaly (mGal)	Inner-Zone terrain correction to 68 m (mGal)	Total terrain correction to 166.7 km (mGal)	Complete Bouguer anomaly reduced for density 2.67g/cm^3 (mGal)	Isostatic gravity anomaly reduced for density 2.67g/cm^3 (mGal)
CH63	LLV	39	24.79	123	21.10	1370	79991.2	3.25	-43.47	0.05	1.93	-42.09	-15.96
101	LLV	39	26.08	123	14.65	1660	79969.1	6.52	-50.1	1.73	3.71	-47.04	-12.14
102	LLV	39	26.33	123	15.14	1725	79964.52	7.68	-51.16	2.61	4.5	-47.33	-12.78
103	LLV	39	26.09	123	15.53	1880	79958.65	16.74	-47.38	2	3.83	-44.27	-10.4
104	LLV	39	25.96	123	15.73	1900	79957.74	17.9	-46.9	2.32	4.17	-43.45	-9.96
105	LLV	39	25.85	123	15.92	1940	79956.22	20.31	-45.86	0.75	2.64	-43.96	-10.79
106	LLV	39	25.82	123	16.25	1805	79964.54	15.97	-45.59	1.31	3.19	-43.09	-10.28
107	LLV	39	25.76	123	16.46	1745	79970.28	16.16	-43.35	1.25	3.17	-40.86	-8.33
108	LLV	39	25.62	123	16.70	1690	79973.54	14.46	-43.18	1.43	3.41	-40.43	-8.28
109	LLV	39	25.58	123	16.91	1630	79977.54	12.87	-42.72	1.54	3.57	-39.78	-7.89
110	LLV	39	25.63	123	17.19	1585	79980.25	11.28	-42.78	1.64	3.71	-39.69	-8.06
111	LLV	39	25.68	123	17.33	1550	79982.88	10.54	-42.32	1.34	3.44	-39.49	-7.98
112	LLV	39	25.64	123	17.59	1450	79987.4	5.72	-43.74	2.26	4.48	-39.83	-8.65
113	LLV	39	25.56	123	17.74	1430	79990.34	6.9	-41.88	1.7	3.92	-38.52	-7.59
114	LLV	39	25.54	123	17.88	1420	79992.16	7.8	-40.63	0.99	3.19	-38	-7.26
115	LLV	39	25.59	123	18.10	1405	79993.41	7.57	-40.35	0.38	2.56	-38.35	-7.81
116	LLV	39	25.63	123	18.29	1390	79994.02	6.71	-40.7	0.28	2.44	-38.81	-8.45
117	LLV	39	25.66	123	18.41	1385	79994.55	6.73	-40.51	0.25	2.39	-38.67	-8.41
118	LLV	39	25.67	123	18.67	1366	79994.94	5.31	-41.27	0.18	2.3	-39.52	-9.57
119	LLV	39	25.67	123	19.11	1350	79993.38	2.25	-43.79	0.06	2.13	-42.2	-12.77
120	LLV	39	25.67	123	19.46	1339	79992.59	0.42	-45.24	0.02	2.04	-43.73	-14.72
121	LLV	39	25.24	123	19.53	1342	79990	-1.25	-47.02	0	1.96	-45.6	-17.08
122	LLV	39	24.81	123	19.92	1355	79987.6	-1.79	-48	0	1.88	-46.66	-19.02
123	LLV	39	24.77	123	20.57	1355	79988.82	-0.51	-46.72	0.01	1.88	-45.38	-18.58
124	LLV	39	24.77	123	20.76	1355	79989.7	0.37	-45.84	0.02	1.9	-44.48	-17.92
125	LLV	39	24.76	123	21.29	1380	79990.88	3.92	-43.15	0.08	1.97	-41.73	-15.86
126	LLV	39	24.69	123	21.42	1395	79989.96	4.51	-43.07	0.08	1.98	-41.64	-16
127	LLV	39	24.67	123	21.58	1395	79990.04	4.62	-42.96	0.14	2.05	-41.46	-16.04

128	LLV	39	24.76	123	21.78	1405	79990.9	6.29	-41.63	0.22	2.14	-40.05	-14.8
129	LLV	39	24.32	123	21.47	1395	79989.37	4.47	-43.11	0.16	2.09	-41.57	-16.32
130	LLV	39	24.33	123	21.80	1430	79990.44	8.81	-39.96	0.36	2.29	-38.23	-13.4
131	LLV	39	24.34	123	22.30	1430	79991.5	9.86	-38.91	0.73	2.77	-36.71	-12.51
132	LLV	39	24.48	123	22.68	1430	79992.2	10.35	-38.42	0.46	2.56	-36.42	-12.58
133	LLV	39	24.30	123	23.05	1440	79992.57	11.93	-37.18	0.66	2.82	-34.94	-11.75
134	LLV	39	24.10	123	23.36	1460	79992.05	13.59	-36.21	0.77	2.95	-33.84	-11.23
135	LLV	39	23.85	123	23.39	1480	79990.72	14.51	-35.97	0.93	3.12	-33.44	-11.1
136	LLV	39	23.66	123	23.53	1500	79988.62	14.57	-36.59	1.89	4.09	-33.09	-11.12
137	LLV	39	23.56	123	23.92	1550	79987.11	17.91	-34.96	1.4	3.68	-31.89	-10.54
138	LLV	39	22.40	123	15.06	2250	79935.17	33.51	-43.23	1.78	4.26	-39.8	-8.98
139	LLV	39	22.31	123	15.78	1960	79956.29	27.49	-39.36	0.77	2.93	-37.18	-7.16
140	LLV	39	22.53	123	16.25	2080	79948.93	31.09	-39.85	0.73	2.95	-37.69	-8
141*	LLV	39	22.54	123	16.50	2164	79944.53	34.57	-39.23	0.39	2.74	-37.3	-7.91
142	LLV	39	22.43	123	16.67	2200	79940.09	33.68	-41.35	0.85	3.28	-38.89	-9.81
143	LLV	39	22.48	123	16.85	2160	79942.31	32.06	-41.6	1.02	3.38	-39.03	-10.09
144	LLV	39	22.54	123	17.01	2100	79947.72	31.74	-39.88	1.02	3.31	-37.36	-8.53
145	LLV	39	22.67	123	17.19	1995	79954.83	28.79	-39.25	0.93	3.09	-36.92	-8.14
146	LLV	39	22.73	123	17.32	1925	79959.56	26.85	-38.81	1	3.1	-36.43	-7.73
147	LLV	39	22.72	123	17.52	1810	79966.03	22.52	-39.21	0.67	2.73	-37.17	-8.69
148	LLV	39	22.87	123	17.65	1780	79968.4	21.85	-38.86	0.99	3.03	-36.52	-8.04
149	LLV	39	22.95	123	17.73	1660	79974.99	17.03	-39.58	1.11	3.16	-37.07	-8.58
150	LLV	39	22.97	123	17.92	1515	79983.44	11.82	-39.85	0.73	2.87	-37.58	-9.26
151	LLV	39	23.04	123	18.04	1440	79987.01	8.23	-40.88	0.66	2.86	-38.59	-10.32
152	LLV	39	23.46	123	17.68	1630	79976.62	15.09	-40.5	1.52	3.53	-37.61	-8.59
153	LLV	39	23.45	123	17.92	1565	79980.82	13.19	-40.19	0.84	2.88	-37.91	-9.15
154	LLV	39	23.48	123	18.03	1480	79985.79	10.12	-40.35	0.53	2.64	-38.3	-9.63
155	LLV	39	23.24	123	18.07	1450	79986.54	8.41	-41.05	0.48	2.64	-38.98	-10.58
156	LLV	39	23.43	123	21.60	1480	79988.22	12.63	-37.85	0.64	2.62	-35.81	-11.55
157	LLV	39	23.48	123	21.33	1500	79984.55	10.76	-40.4	0.56	2.51	-38.48	-13.84
158	LLV	39	23.47	123	21.22	1435	79989.18	9.3	-39.65	0.61	2.59	-37.63	-12.84
159	LLV	39	23.50	123	20.95	1405	79987.4	4.65	-43.27	0.11	2.07	-41.75	-16.58
160	LLV	39	23.50	123	20.80	1415	79986.52	4.71	-43.55	0.07	2.01	-42.1	-16.74
161	LLV	39	23.51	123	20.64	1450	79982.54	4.01	-45.45	0.16	2.07	-43.95	-18.4
162	LLV	39	23.50	123	20.52	1400	79984.99	1.77	-45.98	0.13	2.07	-44.47	-18.77
163	LLV	39	23.50	123	20.34	1390	79984.58	0.42	-46.99	0.03	1.97	-45.57	-19.62

164	LLV	39	29.09	123	20.38	2150	79947.96	27	-46.33	1.25	3.64	-43.5	-12.71
165	LLV	39	28.83	123	20.38	2170	79943.8	25.1	-48.91	3.42	5.86	-43.86	-13.31
166	LLV	39	28.60	123	20.34	2060	79952.84	24.14	-46.12	2.77	5.05	-41.85	-11.45
167	LLV	39	28.35	123	20.51	1950	79957.4	18.73	-47.78	2.32	4.48	-44.04	-14.06
168	LLV	39	28.25	123	20.70	1795	79966.85	13.75	-47.47	1.01	3.07	-45.09	-15.39
169	LLV	39	28.06	123	20.70	1665	79972.34	7.3	-49.49	1.24	3.3	-46.84	-17.28
170	LLV	39	27.87	123	20.63	1535	79980.82	3.83	-48.52	1	3.13	-45.99	-16.48
171	LLV	39	27.72	123	20.65	1380	79990.19	-1.15	-48.22	0.57	2.88	-45.89	-16.5
172	LLV	39	27.55	123	20.31	1350	79992.12	-1.79	-47.83	0.34	2.69	-45.68	-16
173	LLV	39	27.64	123	20.45	1340	79991.8	-3.18	-48.89	0.43	2.81	-46.61	-17.02
174	LLV	39	27.15	123	19.92	1330	79983.01	-12.19	-57.55	0.36	2.68	-55.41	-25.61
175	LLV	39	25.90	123	19.93	1330	79991.18	-2.17	-47.53	0.01	2.03	-46.04	-17.38
176	LLV	39	26.26	123	19.91	1330	79993.74	-0.14	-45.51	0.03	2.12	-43.91	-14.89
177	LLV	39	26.53	123	19.91	1330	79995.41	1.13	-44.23	0.07	2.23	-42.54	-13.28
178	LLV	39	26.71	123	20.12	1320	79997.14	1.65	-43.37	0.05	2.25	-41.65	-12.48
179	LLV	39	26.93	123	20.13	1320	79998.42	2.6	-42.42	0.1	2.37	-40.58	-11.22
180	LLV	39	23.42	123	17.80	1590	79978.16	12.93	-41.3	1.05	3.09	-38.84	-9.98
181	LLV	39	22.60	123	21.39	1470	79990.62	15.31	-34.82	1.51	3.61	-31.79	-8
182	LLV	39	22.79	123	21.19	1420	79990.16	9.87	-38.56	1.1	3.2	-35.92	-11.7
183	LLV	39	22.94	123	21.14	1420	79990.47	9.96	-38.47	0.85	2.92	-36.11	-11.69
184	LLV	39	23.10	123	21.05	1420	79989.99	9.24	-39.19	0.43	2.47	-37.28	-12.6
185	LLV	39	23.24	123	20.92	1420	79987.88	6.93	-41.51	0.56	2.55	-39.52	-14.56
186	LLV	39	23.27	123	20.78	1415	79986.6	5.13	-43.13	0.11	2.08	-41.61	-16.44
187	LLV	39	23.29	123	20.65	1435	79984.85	5.23	-43.71	0.09	2.03	-42.25	-16.9
188	LLV	39	23.30	123	20.64	1435	79984.88	5.25	-43.7	0.09	2.03	-42.23	-16.86
189	LLV	39	23.50	123	20.25	1390	79984.01	-0.15	-47.56	0.03	1.96	-46.15	-20.1
190	LLV	39	23.48	123	20.10	1390	79983.71	-0.42	-47.83	0.04	1.97	-46.41	-20.19
191	LLV	39	23.49	123	19.96	1390	79983.23	-0.92	-48.32	0.05	1.98	-46.9	-20.5
192	LLV	39	23.49	123	19.81	1395	79982.61	-1.06	-48.64	0.09	2.01	-47.18	-20.6
193	LLV	39	23.49	123	19.67	1405	79982.09	-0.64	-48.56	0.11	2.03	-47.09	-20.35
194	LLV	39	23.49	123	19.57	1420	79981.57	0.25	-48.18	0.12	2.03	-46.72	-19.87
195	LLV	39	23.46	123	19.37	1470	79978.2	1.62	-48.51	0.18	2.08	-47.02	-19.97
196	LLV	39	23.48	123	19.23	1475	79979.43	3.29	-47.01	0.14	2.04	-45.56	-18.32
197	LLV	39	23.45	123	18.66	1530	79976.48	5.56	-46.62	0.27	2.23	-44.99	-17.12
198	LLV	39	23.50	123	18.77	1530	79977.27	6.28	-45.91	0.16	2.1	-44.41	-16.62
199	LLV	39	23.48	123	18.52	1410	79985.08	2.83	-45.26	0.34	2.45	-43.37	-15.27

200	LLV	39	23.48	123	18.40	1430	79986.24	5.87	-42.9	0.19	2.3	-41.16	-12.93
201	LLV	39	23.48	123	18.25	1435	79987.23	7.33	-41.61	0.27	2.4	-39.78	-11.37
202	LLV	39	23.48	123	18.12	1460	79986.85	9.3	-40.49	0.38	2.5	-38.57	-10.01
203	LLV	39	24.59	123	20.10	1355	79987.28	-1.78	-48	0	1.87	-46.66	-19.44
204	LLV	39	24.36	123	19.72	1365	79985.97	-1.81	-48.37	0	1.88	-47.03	-19.56
205	LLV	39	24.14	123	19.24	1385	79985.18	-0.4	-47.63	0.01	1.94	-46.25	-18.41
206	LLV	39	23.91	123	19.24	1390	79984.35	-0.42	-47.82	0.03	1.96	-46.42	-18.79
207	LLV	39	23.70	123	19.23	1405	79983.3	0.25	-47.66	0.09	2.03	-46.2	-18.75
208	LLV	39	23.22	123	19.32	1620	79968.84	6.72	-48.53	0.42	2.3	-46.87	-20.01
209	LLV	39	23.07	123	19.12	1635	79967.79	7.3	-48.46	0.44	2.34	-46.75	-19.8
210	LLV	39	23.00	123	19.24	1715	79962.69	9.83	-48.66	0.58	2.5	-46.82	-20.09
211	LLV	39	22.73	123	19.18	1530	79974.97	5.11	-47.07	0.32	2.27	-45.4	-18.78
212	UV	39	12.90	123	14.86	1150	79993.15	2.08	-37.14	1.02	2.86	-34.74	-11.76
213	UV	39	12.85	123	14.64	1020	80001.01	-2.21	-37	1.82	3.67	-33.74	-10.54
214	UV	39	12.82	123	14.41	940	80005.46	-5.24	-37.3	0.86	2.73	-34.95	-11.52
215	UV	39	12.76	123	14.17	890	80006.44	-8.87	-39.23	1.14	3.01	-36.58	-12.95
216	UV	39	12.68	123	13.93	890	80008.09	-7.11	-37.46	0.71	2.54	-35.28	-11.47
217	UV	39	12.67	123	13.77	790	80012.43	-12.16	-39.1	0.36	2.28	-37.14	-13.15
218	UV	39	12.65	123	13.54	690	80018.56	-15.4	-38.93	0.5	2.54	-36.68	-12.45
219	UV	39	12.59	123	13.35	670	80018.84	-16.91	-39.76	0.57	2.62	-37.43	-13.07
220	UV	39	12.48	123	13.26	670	80018.87	-16.72	-39.57	0.92	2.95	-36.9	-12.53
221	UV	39	12.42	123	13.22	670	80018.63	-16.87	-39.72	0.38	2.41	-37.6	-13.24
222	UV	39	12.32	123	13.10	670	80018.66	-16.7	-39.55	0.4	2.41	-37.41	-13.01
223	UV	39	12.29	123	12.96	655	80018.53	-18.19	-40.53	0.3	2.32	-38.49	-13.98
224	UV	39	12.21	123	12.84	680	80016.78	-17.47	-40.66	0.24	2.19	-38.75	-14.2
225	UV	39	12.14	123	12.73	700	80015.83	-16.44	-40.31	0.27	2.19	-38.41	-13.81
226	UV	39	11.99	123	12.71	675	80016.08	-18.32	-41.34	0.15	2.12	-39.5	-14.99
227	UV	39	11.96	123	12.61	665	80016.65	-18.64	-41.32	0.06	2.04	-39.56	-14.97
228	UV	39	11.90	123	12.44	660	80016.38	-19.3	-41.81	0.03	2.02	-40.06	-15.36
229	UV	39	11.85	123	12.32	650	80017.09	-19.45	-41.62	0.02	2.02	-39.88	-15.1
CH66	UV	39	9.02	123	12.45	635	80018.55	-15.23	-36.88	1.68	4.13	-33.01	-10.61
231	UV	39	11.84	123	12.14	600	80017.92	-23.31	-43.77	0.15	2.24	-41.78	-16.82
232	LLV	39	26.96	123	20.95	1330	79999.16	4.24	-41.12	0.42	2.55	-39.1	-10.75
233	LLV	39	26.96	123	21.02	1400	79996.22	7.88	-39.87	0.59	2.63	-37.79	-9.55
234	LLV	39	27.01	123	21.17	1480	79990.55	9.66	-40.81	0.56	2.53	-38.87	-10.8
235	UV	39	10.37	123	8.31	1430	79969.78	8.78	-39.99	3.3	5.79	-34.77	-7.69

236	UV	39	10.45	123	8.43	1160	79983.59	-2.92	-42.48	3.91	6.56	-36.39	-9.29
237	UV	39	10.46	123	8.58	1005	79993.95	-7.15	-41.43	3.23	6.07	-35.77	-8.74
238	UV	39	10.53	123	8.49	1170	79986.25	0.56	-39.34	3.33	5.92	-33.89	-6.77
239	UV	39	10.57	123	8.57	1200	79984.18	1.25	-39.67	1.81	4.33	-35.83	-8.75
240	UV	39	10.55	123	8.70	1130	79987.3	-2.18	-40.72	1.32	3.87	-37.31	-10.35
241	UV	39	10.49	123	8.78	1100	79989.58	-2.63	-40.15	1.11	3.66	-36.93	-10.09
242	UV	39	10.37	123	8.91	1090	79989.23	-3.75	-40.92	1.27	3.76	-37.6	-10.98
243	UV	39	10.20	123	9.06	890	80002.04	-9.49	-39.85	1.01	3.74	-36.47	-10.07
244	UV	39	10.11	123	9.16	870	80003.24	-10.04	-39.71	0.87	3.57	-36.5	-10.26
245	UV	39	10.05	123	9.35	835	80006.09	-10.4	-38.87	0.63	3.28	-35.94	-9.92
246	UV	39	10.01	123	9.56	790	80008.58	-12.08	-39.02	0.71	3.3	-36.05	-10.24
247	UV	39	9.90	123	9.73	765	80010.36	-12.49	-38.58	0.48	3.01	-35.89	-10.31
248	UV	39	9.75	123	9.95	750	80011.7	-12.34	-37.92	0.26	2.67	-35.55	-10.29
249	UV	39	9.66	123	10.07	725	80012.53	-13.73	-38.45	0.36	2.74	-36.01	-10.93
250	UV	39	9.58	123	10.23	715	80012.78	-14.3	-38.68	0.44	2.76	-36.22	-11.34
251	UV	39	9.58	123	10.45	700	80013.54	-14.95	-38.82	0.22	2.49	-36.63	-11.94
252	UV	39	9.59	123	10.62	690	80013.91	-15.53	-39.07	0.32	2.56	-36.79	-12.24
253	UV	39	9.70	123	10.79	650	80015.04	-18.33	-40.5	0.87	3.14	-37.63	-13.14
254	UV	39	9.65	123	11.06	630	80017.03	-18.15	-39.63	0.56	2.8	-37.09	-12.88
255	UV	39	9.37	123	10.92	605	80017.39	-19.72	-40.36	1.07	3.39	-37.22	-13.1
256	UV	39	9.24	123	11.08	590	80018.65	-19.68	-39.81	0.14	2.46	-37.59	-13.72
257	UV	39	9.18	123	11.29	590	80018.73	-19.51	-39.64	0.06	2.36	-37.53	-13.91
258	UV	39	9.11	123	11.50	595	80018.83	-18.84	-39.13	0.03	2.31	-37.07	-13.7
259	UV	39	9.11	123	11.65	600	80018.42	-18.78	-39.24	0.02	2.3	-37.19	-13.95
260	UV	39	9.10	123	11.87	605	80018.46	-18.26	-38.89	0.01	2.32	-36.82	-13.8
261	UV	39	9.57	123	11.86	605	80018.49	-18.92	-39.55	0.01	2.26	-37.55	-14.15
262	UV	39	9.57	123	12.03	610	80018.72	-18.22	-39.02	0.01	2.27	-37.01	-13.78
263	UV	39	9.57	123	12.27	610	80018.83	-18.11	-38.91	0.01	2.32	-36.85	-13.85
264	UV	39	9.57	123	12.49	635	80018.68	-15.91	-37.56	0.03	2.36	-35.47	-12.69
265	UV	39	9.58	123	12.73	650	80019.33	-13.86	-36.03	0.07	2.46	-33.85	-11.28
266	UV	39	9.65	123	12.99	660	80021.01	-11.34	-33.85	0.17	2.62	-31.51	-9.15
267	UV	39	9.70	123	13.24	670	80021.28	-10.21	-33.06	0.39	2.91	-30.43	-8.27
268	UV	39	9.75	123	13.44	690	80021.16	-8.52	-32.05	0.64	3.18	-29.16	-7.16
269	UV	39	9.84	123	16.46	1190	79990.09	7.3	-33.29	2.61	5.14	-28.63	-9.71
270	UV	39	9.82	123	16.13	1220	79989.53	9.59	-32.02	1.98	4.37	-28.14	-8.91
271	UV	39	9.83	123	15.82	1180	79990.01	6.3	-33.95	2.57	4.9	-29.52	-9.95

272	UV	39	9.89	123	15.47	1120	79994.91	5.46	-32.74	2.42	4.74	-28.45	-8.46
273	UV	39	9.99	123	15.27	1020	80000.01	1.01	-33.78	3.04	5.45	-28.74	-8.45
274	UV	39	9.96	123	15.00	940	80004.35	-2.13	-34.19	3.73	6.22	-28.35	-7.79
275	UV	39	9.95	123	14.76	950	80005.76	0.24	-32.16	3.79	6.22	-26.33	-5.53
276	UV	39	9.99	123	14.52	870	80009.09	-4.02	-33.69	4.16	6.65	-27.39	-6.3
277	UV	39	9.96	123	14.30	820	80011.84	-5.92	-33.89	3.32	5.85	-28.38	-7.09
278	UV	39	9.85	123	14.12	790	80015.07	-5.35	-32.3	2.87	5.43	-27.19	-5.8
279	UV	39	9.84	123	13.89	760	80017.6	-5.63	-31.55	2.24	4.78	-27.08	-5.45
280	UV	39	9.82	123	13.62	710	80018.43	-9.47	-33.69	1.67	4.21	-29.77	-7.88
281	UV	39	11.75	123	12.01	630	80017.79	-20.49	-41.97	0.03	2.07	-40.16	-15.15
282	UV	39	11.74	123	11.81	625	80019.53	-19.2	-40.52	0.05	2.1	-38.68	-13.48
283	UV	39	11.74	123	11.58	630	80019.44	-18.82	-40.31	0.57	2.63	-37.94	-12.51
284	UV	39	11.85	123	11.34	655	80019.48	-16.59	-38.93	0.12	2.16	-37.05	-11.32
285	UV	39	11.97	123	11.08	670	80017.45	-17.39	-40.24	0.2	2.26	-38.26	-12.2
286	UV	39	16.56	123	12.33	755	80016.51	-17.11	-42.86	0.18	2.22	-40.96	-12.24
287	UV	39	16.32	123	12.29	730	80016.05	-19.57	-44.47	0.04	2.07	-42.7	-14.14
288	UV	39	16.15	123	12.25	735	80015.65	-19.25	-44.32	0.07	2.06	-42.56	-14.12
289	UV	39	15.97	123	12.19	725	80016.07	-19.5	-44.23	0.05	2.03	-42.5	-14.15
290	UV	39	15.71	123	12.16	715	80016.2	-19.93	-44.31	0.77	2.73	-41.88	-13.72
291	UV	39	15.51	123	12.05	710	80016.91	-19.39	-43.61	0.08	2.04	-41.87	-13.78
292	UV	39	15.31	123	11.95	710	80016.79	-19.22	-43.43	0.18	2.12	-41.6	-13.58
293	UV	39	15.07	123	11.85	710	80016.09	-19.56	-43.78	0.1	2.03	-42.05	-14.13
294	LLV	39	27.54	123	22.35	1850	79968.57	21.69	-41.4	0.95	3.12	-38.99	-12.05
295	LLV	39	27.50	123	22.20	1810	79970.52	19.94	-41.79	1.38	3.5	-38.99	-11.88
296	LLV	39	27.40	123	22.05	1860	79968.39	22.66	-40.78	1.04	3.2	-38.29	-11.09
297	LLV	39	27.35	123	21.86	1880	79967.41	23.63	-40.49	1.26	3.44	-37.77	-10.37
298	LLV	39	27.36	123	21.70	1820	79971.01	21.58	-40.5	1.47	3.55	-37.65	-10.03
299	LLV	39	27.28	123	21.53	1740	79973.95	17.11	-42.23	1.83	3.83	-39.08	-11.29
300	LLV	39	27.25	123	21.38	1660	79978.47	14.15	-42.46	1.7	3.66	-39.45	-11.48
301	LLV	39	27.11	123	21.32	1590	79984.05	13.36	-40.87	0.87	2.81	-38.68	-10.74
302	LLV	39	27.54	123	22.38	1860	79967.71	21.77	-41.66	0.94	3.13	-39.25	-12.35
303	LLV	39	27.53	123	22.49	1950	79964.03	26.57	-39.94	1.45	3.77	-36.9	-10.17
304	LLV	39	27.42	123	22.59	1980	79960.31	25.83	-41.7	0.91	3.31	-39.14	-12.66
305*	LLV	39	27.40	123	22.73	2015	79959.42	28.27	-40.46	1.13	3.61	-37.61	-11.34
306	LLV	39	27.43	123	22.88	2010	79961.01	29.34	-39.21	1.2	3.67	-36.3	-10.2
307	LLV	39	27.52	123	23.01	1965	79960.86	24.83	-42.19	0.62	3.03	-39.91	-13.89

308	LLV	39	27.57	123	23.20	1980	79962.17	27.47	-40.06	0.46	2.93	-37.87	-12.05
309	LLV	39	27.58	123	23.39	2020	79959.33	28.38	-40.52	0.72	3.29	-37.99	-12.43
310	LLV	39	27.62	123	23.61	1930	79965.82	26.35	-39.48	0.82	3.28	-36.94	-11.61
311	LLV	39	27.59	123	23.95	2235	79946.81	36.06	-40.17	1.87	5.04	-35.95	-11.19
312	LLV	39	27.69	123	24.14	2340	79938.38	37.36	-42.45	1.99	5.53	-37.78	-13.21
313	UV	39	14.93	123	11.82	710	80016.74	-18.71	-42.92	0.12	2.04	-41.18	-13.34
314	UV	39	14.80	123	11.78	710	80017.21	-18.05	-42.26	0.14	2.05	-40.5	-12.73
315	UV	39	14.68	123	11.81	700	80017.54	-18.48	-42.35	0.16	2.08	-40.57	-12.93
316	UV	39	14.57	123	11.83	690	80017.94	-18.86	-42.39	0.21	2.13	-40.55	-13.03
317	UV	39	14.49	123	11.82	700	80017.64	-18.1	-41.97	0.33	2.23	-40.03	-12.58
318	UV	39	14.37	123	11.83	700	80016.78	-18.78	-42.65	0.52	2.41	-40.54	-13.2
319	UV	39	14.24	123	11.85	690	80016.16	-20.15	-43.68	0.37	2.27	-41.7	-14.49
320	UV	39	14.11	123	11.87	710	80016.01	-18.23	-42.44	0.3	2.17	-40.57	-13.48
321	UV	39	13.99	123	11.90	700	80017.14	-17.86	-41.73	0.42	2.31	-39.71	-12.76
322	UV	39	13.84	123	11.91	705	80016.68	-17.63	-41.67	0.83	2.71	-39.26	-12.44
323	UV	39	13.59	123	11.90	710	80017.25	-16.22	-40.43	0.43	2.29	-38.44	-11.84
324	UV	39	13.43	123	11.94	700	80016.93	-17.24	-41.12	0.37	2.26	-39.15	-12.72
325	UV	39	13.21	123	12.05	690	80016.95	-17.84	-41.37	0.36	2.25	-39.41	-13.27
326	UV	39	12.91	123	11.93	675	80016.56	-19.2	-42.22	0.77	2.68	-39.82	-13.81
327	UV	39	12.72	123	11.82	700	80016.12	-17	-40.88	0.25	2.13	-39.04	-13.08
328	UV	39	12.48	123	11.76	690	80016.79	-16.92	-40.45	0.19	2.09	-38.65	-12.82
329	UV	39	12.19	123	11.79	730	80013.71	-15.81	-40.71	0.12	1.97	-39.04	-13.49
330	UV	39	11.91	123	11.58	660	80018.19	-17.5	-40.01	0.64	2.63	-37.66	-12.11
331	Lay	39	41.26	123	28.87	1655	79997.02	11.49	-44.95	0.62	3.86	-41.74	-11.31
332	Lay	39	41.72	123	24.43	1920	79970.82	9.53	-55.95	3.13	6.05	-50.63	-14.11
333	Lay	39	41.72	123	24.80	1905	79973.86	11.16	-53.81	3.65	6.71	-47.83	-11.77
334	Lay	39	41.62	123	25.03	1980	79969.22	13.72	-53.81	2.79	5.83	-48.73	-13.06
335	Lay	39	41.54	123	25.26	2045	79964	14.73	-55.01	3.02	6.03	-49.76	-14.45
336	Lay	39	41.60	123	25.55	2110	79961.99	18.75	-53.22	3.13	6.15	-47.85	-12.87
337	Lay	39	41.63	123	25.82	2150	79960.87	21.34	-51.99	2.6	5.68	-47.11	-12.46
338	Lay	39	41.68	123	26.10	2180	79959.55	22.77	-51.58	2.59	5.76	-46.64	-12.32
339	Lay	39	41.61	123	26.37	2250	79956.04	25.95	-50.79	3.3	6.62	-45.01	-11.11
340	Lay	39	41.49	123	26.62	2265	79955.92	27.41	-49.84	2.21	5.65	-45.03	-11.57
341	Lay	39	41.30	123	26.81	2330	79953.46	31.35	-48.12	1.4	5.04	-43.94	-10.91
342	Lay	39	41.25	123	26.99	2350	79952.82	32.66	-47.49	1.29	5.1	-43.25	-10.5
343	Lay	39	41.17	123	27.20	2410	79950.33	35.93	-46.26	0.96	4.9	-42.25	-9.86

344	Lay	39	41.09	123	27.45	2525	79943.83	40.36	-45.75	0.89	5.39	-41.28	-9.32
345	Lay	39	41.17	123	27.67	2460	79947.13	37.43	-46.47	1.14	5.55	-41.81	-10.06
346	Lay	39	41.23	123	27.91	2350	79954.23	34.1	-46.05	1.77	5.92	-40.99	-9.48
347	Lay	39	41.37	123	28.10	2180	79964.07	27.75	-46.6	1.95	5.7	-41.71	-10.3
348	Lay	39	41.53	123	28.28	2020	79974.13	22.53	-46.37	1.89	5.25	-41.88	-10.53
349	Lay	39	41.55	123	28.47	1920	79981.06	20.02	-45.46	1.51	4.81	-41.38	-10.23
350*	Lay	39	41.48	123	28.68	1814	79987.26	16.36	-45.51	1.47	4.75	-41.45	-10.62
351	Lay	39	41.25	123	28.74	1680	79995.14	11.98	-45.32	0.95	4.2	-41.77	-11.18
352	Lay	39	41.27	123	29.18	1635	79997.61	10.19	-45.57	0.19	3.4	-42.81	-12.8
353	Lay	39	41.28	123	29.41	1610	79998.5	8.71	-46.2	0.1	3.29	-43.54	-13.84
354	Lay	39	40.85	123	29.64	1665	79993.88	9.9	-46.88	0.02	3.19	-44.34	-15.35
355	Lay	39	40.52	123	29.81	1690	79993.09	11.95	-45.69	0.03	3.17	-43.18	-14.75
356	Lay	39	40.40	123	30.11	1690	79993.04	12.08	-45.56	0.04	3.22	-42.99	-15.09
357	Lay	39	40.41	123	30.38	1715	79992.54	13.92	-44.58	0.09	3.3	-41.94	-14.43
358	Lay	39	40.39	123	30.65	1715	79992.36	13.77	-44.73	0.07	3.41	-41.98	-14.87
359	Lay	39	40.40	123	30.78	1725	79991.76	14.09	-44.74	0.09	3.52	-41.88	-14.96
360	Lay	39	40.47	123	30.99	1750	79991.82	16.4	-43.29	0.18	3.77	-40.19	-13.52
361	Lay	39	40.53	123	31.32	1780	79990.8	18.11	-42.6	0.41	4.13	-39.15	-12.91
362	Lay	39	40.51	123	31.61	1815	79988.72	19.35	-42.55	0.73	4.71	-38.54	-12.75
363	Lay	39	40.53	123	31.92	1930	79981.46	22.88	-42.95	1.23	5.63	-38.06	-12.74
364	Lay	39	40.27	123	31.94	2030	79975.1	26.3	-42.93	0.94	5.48	-38.22	-13.23
365	Lay	39	40.25	123	32.15	2270	79959.94	33.74	-43.68	1.9	7.08	-37.44	-12.85
366	Lay	39	40.29	123	32.49	2630	79936.78	44.37	-45.33	2.87	9.58	-36.69	-12.67
367	Lay	39	41.10	123	34.37	3700	79873.11	80.1	-46.09	3.13	18.33	-28.96	-7.38
368	Lay	39	40.93	123	34.24	3520	79882.07	72.39	-47.67	3.91	17.25	-31.57	-9.89
369	Lay	39	40.82	123	34.13	3440	79887.73	70.69	-46.63	3.91	16.52	-31.26	-9.5
370	Lay	39	40.67	123	33.98	3345	79896.74	70.99	-43.09	3.04	15.14	-29.08	-7.19
371	Lay	39	40.55	123	33.78	3180	79906.67	65.59	-42.87	2.56	13.44	-30.51	-8.37
372	Lay	39	40.48	123	33.56	3050	79915.25	62.05	-41.98	1.68	11.12	-31.91	-9.46
373	Lay	39	40.41	123	33.43	3100	79910.48	62.08	-43.65	2.02	11.72	-32.99	-10.43
374	Lay	39	40.30	123	33.32	3160	79906.67	64.08	-43.7	2.3	12.68	-32.1	-9.48
375	Lay	39	40.34	123	33.01	3080	79911.7	61.53	-43.52	3.21	12.8	-31.78	-8.63
376	Lay	39	40.32	123	32.73	2880	79924.95	56	-42.22	2.71	11.06	-32.18	-8.56
377	Lay	39	39.02	123	36.98	1610	80011.28	24.84	-30.07	1.14	5.66	-25.04	-9.25
378	Lay	39	38.75	123	36.93	1580	80012.64	23.78	-30.11	0.63	5.04	-25.68	-10.07
379	Lay	39	38.64	123	36.75	1600	80011.79	24.97	-29.6	0.71	5.17	-25.05	-9.23

380	Lay	39	38.53	123	36.39	1620	80008.6	23.83	-31.42	1.26	5.69	-26.37	-10.05
381	Lay	39	38.56	123	36.10	1610	80006.82	21.06	-33.85	1.11	5.69	-28.79	-11.94
382	Lay	39	38.36	123	36.01	1620	80005.28	20.76	-34.49	1.95	6.52	-28.6	-11.8
383	Lay	39	38.22	123	35.84	1620	80005.97	21.66	-33.6	2.06	6.53	-27.7	-10.74
384	Lay	39	38.08	123	35.52	1620	80004.64	20.53	-34.72	2.24	6.7	-28.65	-11.28
385	Lay	39	37.97	123	35.15	1660	80002	21.82	-34.8	2.19	6.64	-28.8	-10.93
386	Lay	39	37.84	123	34.92	1650	80001.18	20.25	-36.02	2.03	6.43	-30.24	-12.1
387	Lay	39	37.70	123	34.82	1660	80001.32	21.54	-35.08	1.74	6.17	-29.56	-11.38
388	Lay	39	37.58	123	34.55	1700	79999.67	23.83	-34.15	1.66	6.02	-28.79	-10.3
389	Lay	39	37.49	123	34.33	1690	79998.6	21.95	-35.69	1.59	5.9	-30.45	-11.7
390	Lay	39	37.45	123	33.94	1720	79995.09	21.32	-37.34	1.71	6.18	-31.83	-12.5
391	Lay	39	37.47	123	33.71	1720	79993.14	19.34	-39.32	2.09	6.31	-33.67	-13.94
392	Lay	39	37.42	123	33.46	1720	79993.98	20.26	-38.41	1.75	5.86	-33.21	-13.14
393*	Lay	39	37.27	123	33.18	1774	79992.05	23.63	-36.88	1.21	5.39	-32.17	-11.81
394	Lay	39	37.47	123	32.98	1740	79991.89	19.97	-39.37	2.16	6.38	-33.66	-12.78
395	Lay	39	37.52	123	32.81	1765	79991.62	21.98	-38.22	1.16	5.25	-33.65	-12.46
396	Lay	39	37.59	123	32.53	1770	79991.23	21.96	-38.41	1.13	5.11	-33.98	-12.3
397	Lay	39	37.63	123	32.33	1780	79990.11	21.72	-38.99	1.06	5.02	-34.66	-12.62
398	Lay	39	37.69	123	32.03	1790	79988.78	21.24	-39.81	0.86	4.79	-35.71	-13.13
399	Lay	39	37.86	123	31.84	1800	79987.42	20.57	-40.82	1.04	4.85	-36.67	-13.65
400	Lay	39	38.00	123	31.60	1830	79986.72	22.48	-39.93	0.92	4.62	-36.02	-12.51
401	Lay	39	38.12	123	28.07	1715	79990.09	14.86	-43.63	0.42	3.41	-40.89	-12.12
402	Lay	39	38.02	123	28.20	1815	79983.9	18.22	-43.68	0.57	3.59	-40.79	-12.31
403	Lay	39	38.04	123	28.43	1980	79973.34	23.15	-44.38	0.48	3.78	-41.35	-13.21
404	Lay	39	38.22	123	28.59	1980	79975.12	24.66	-42.87	0.62	3.94	-39.68	-11.61
405	Lay	39	38.14	123	28.81	1960	79976.36	24.14	-42.71	0.84	4.11	-39.34	-11.64
406	Lay	39	38.11	123	30.62	2290	79957.11	35.96	-42.14	0.7	5.25	-37.73	-12.79
407	Lay	39	38.06	123	30.39	2250	79959.25	34.41	-42.32	0.4	4.72	-38.44	-13.19
408	Lay	39	38.08	123	30.15	2260	79956.52	32.59	-44.49	0.4	4.67	-40.65	-15.03
409	Lay	39	38.05	123	29.90	2310	79955	35.82	-42.96	0.35	4.88	-38.94	-12.99
410	Lay	39	37.84	123	29.85	2340	79953.53	37.48	-42.33	0.34	4.94	-38.25	-12.43
411	Lay	39	37.62	123	29.88	2420	79948.19	39.99	-42.55	0.55	5.56	-37.87	-12.32
412	Lay	39	37.42	123	30.07	2420	79947.41	39.51	-43.03	1.43	6.41	-37.5	-12.42
413	Lay	39	37.22	123	29.97	2380	79950.76	39.39	-41.78	1.08	5.92	-36.73	-11.67
414	Lay	39	36.56	123	29.97	2260	79958.2	36.53	-40.55	0.34	4.82	-36.57	-12.09
415	Lay	39	36.74	123	29.92	2275	79957.12	36.59	-41	0.49	4.9	-36.95	-12.24

416	Lay	39	36.73	123	30.15	2200	79961.6	34.03	-41	0.55	4.81	-37.01	-12.62
417	Lay	39	36.67	123	30.36	2330	79955.71	40.45	-39.01	0.42	5.13	-34.74	-10.75
418	Lay	39	36.83	123	30.01	2270	79957.49	36.36	-41.07	0.44	4.82	-37.08	-12.42
419	Lay	39	36.98	123	29.90	2355	79952.65	39.29	-41.03	0.77	5.46	-36.44	-11.5
420	Lay	39	37.88	123	29.69	2350	79951.48	36.31	-43.84	0.36	4.98	-39.72	-13.63
421	Lay	39	37.90	123	29.50	2360	79949.59	35.33	-45.16	0.6	5.29	-40.73	-14.35
422	Lay	39	37.87	123	29.27	2340	79952.84	36.75	-43.06	0.67	5.09	-38.83	-12.14
423	Lay	39	38.05	123	29.01	2220	79960.82	33.18	-42.54	1.05	5.14	-38.22	-10.96
424	Lay	39	35.78	123	27.20	1350	80008.41	2.32	-43.72	2.81	5.92	-38.34	-10.34
425	Lay	39	36.21	123	27.19	1375	80007.35	2.97	-43.92	2.98	6.01	-38.46	-10.07
426	Lay	39	36.45	123	27.30	1400	80004.61	2.23	-45.52	3.69	6.68	-39.39	-10.95
427	Lay	39	36.86	123	27.45	1480	80000.7	5.24	-45.24	3.51	6.49	-39.34	-10.77
428	Lay	39	37.40	123	27.81	1670	79991.54	13.14	-43.81	0.86	3.83	-40.63	-12.13
429	Lay	39	37.63	123	27.67	1690	79991.32	14.46	-43.18	0.35	3.28	-40.55	-11.64
430	Lay	39	38.13	123	25.43	2250	79955.3	30.36	-46.38	0.79	3.77	-43.44	-11.23
431	Lay	39	38.19	123	25.67	2065	79965.53	23.11	-47.32	1.68	4.49	-43.61	-11.6
432	Lay	39	38.12	123	25.86	1935	79974.82	20.28	-45.72	1.43	4.22	-42.24	-10.52
433	Lay	39	38.07	123	26.05	1830	79981	16.66	-45.76	1.51	4.31	-42.15	-10.7
434	Lay	39	38.01	123	26.29	1820	79983.43	18.23	-43.84	0.83	3.66	-40.88	-9.8
435	Lay	39	38.09	123	26.48	1735	79986.81	13.5	-45.67	1.03	3.91	-42.43	-11.51
436	Lay	39	38.08	123	26.71	1735	79987.92	14.63	-44.55	0.64	3.55	-41.67	-11.07
437	Lay	39	38.06	123	26.97	1715	79988.9	13.76	-44.74	0.26	3.22	-42.18	-11.95
438	Lay	39	38.06	123	27.15	1710	79989.84	14.23	-44.09	0.15	3.05	-41.71	-11.72
439	Lay	39	38.02	123	27.37	1700	79990.66	14.17	-43.81	0.11	3.04	-41.43	-11.77
440	Lay	39	38.03	123	27.57	1700	79991.15	14.64	-43.34	0.11	3.04	-40.96	-11.58
441	Lay	39	37.99	123	27.77	1695	79991.4	14.48	-43.33	0.19	3.13	-40.86	-11.78
442	Lay	39	37.99	123	27.93	1700	79990.83	14.38	-43.6	0.4	3.39	-40.87	-12.01
443	Lay	39	38.79	123	28.49	1695	79992.37	14.27	-43.54	0.49	3.5	-40.7	-11.92
444	Lay	39	38.28	123	28.12	1710	79990.56	14.62	-43.7	0.39	3.39	-40.97	-12.13
445	Lay	39	38.62	123	28.37	1695	79991.19	13.34	-44.47	0.47	3.41	-41.73	-12.93
446	Lay	39	38.99	123	28.50	1675	79993.9	13.62	-43.51	0.2	3.26	-40.9	-11.95
447	Lay	39	39.18	123	28.53	1680	79995.04	14.95	-42.35	0.21	3.25	-39.75	-10.68
448	Lay	39	39.42	123	28.56	1675	79995.96	15.04	-42.09	0.49	3.49	-39.25	-10.02
449	Lay	39	39.70	123	28.54	1665	79995.52	13.25	-43.54	0.31	3.31	-40.88	-11.37
450	Lay	39	40.89	123	28.55	1665	79995.53	11.49	-45.29	1.01	4.25	-41.69	-11.14
451	Lay	39	40.71	123	28.49	1670	79995.5	12.2	-44.76	1.12	4.28	-41.13	-10.66

452	Lay	39	40.54	123	28.48	1670	79995.22	12.17	-44.78	1.15	4.27	-41.16	-10.82
453	Lay	39	40.32	123	28.48	1655	79995.34	11.21	-45.24	1.08	4.17	-41.71	-11.58
454	Lay	39	40.11	123	28.50	1650	79995.38	11.09	-45.19	0.6	3.75	-42.08	-12.15
455	Lay	39	39.81	123	28.52	1655	79995.63	12.25	-44.19	0.33	3.38	-41.45	-11.82
456	Lay	39	40.01	123	28.49	1660	79995.42	12.22	-44.4	0.47	3.61	-41.44	-11.59
457	Lay	39	41.08	123	28.64	1670	79995.63	11.78	-45.18	0.99	4.26	-41.56	-10.97
458	Lay	39	41.45	123	28.93	1660	79996.92	11.58	-45.03	0.61	3.92	-41.76	-11.25
459	Lay	39	41.73	123	29.00	1655	79996.92	10.7	-45.75	0.88	4.17	-42.22	-11.57
460	Lay	39	42.06	123	29.12	1675	79995.24	10.41	-46.72	1.16	4.39	-42.98	-12.23
461	Lay	39	42.28	123	29.20	1670	79995.21	9.58	-47.37	0.85	4.09	-43.93	-13.12
462	Lay	39	42.50	123	29.28	1690	79995.38	11.31	-46.33	0.66	3.83	-43.16	-12.28
463	Lay	39	42.75	123	29.37	1650	79997.38	9.18	-47.1	0.62	3.88	-43.86	-12.87
464	Lay	39	42.97	123	29.46	1605	80000.4	7.64	-47.1	0.77	4	-43.72	-12.67
465	Lay	39	43.17	123	29.93	1555	80004.54	6.78	-46.25	0.63	3.84	-43.02	-12.43
466	Lay	39	38.27	123	30.92	2170	79964.62	31.95	-42.06	0.41	4.79	-38.08	-13.4
467	Lay	39	38.38	123	31.14	2060	79972.33	29.15	-41.1	0.3	4.46	-37.42	-12.94
468	Lay	39	38.42	123	31.37	2045	79973.36	28.71	-41.03	0.29	4.37	-37.43	-13.25
469	Lay	39	38.51	123	31.62	2050	79974.42	30.11	-39.81	0.33	4.57	-36	-12.11
470	Lay	39	38.65	123	31.77	2010	79976.53	28.25	-40.3	0.44	4.71	-36.35	-12.55
471	LLV	39	26.94	123	20.39	1310	79997.49	0.72	-43.96	0.07	2.32	-42.17	-13.13
472	LLV	39	26.94	123	20.26	1315	79997.12	0.82	-44.03	0.07	2.33	-42.23	-13.02
473	LLV	39	26.94	123	20.13	1320	79996.85	1.02	-44	0.11	2.38	-42.15	-12.78
474	LLV	39	26.94	123	19.98	1320	79997.06	1.23	-43.79	0.18	2.46	-41.86	-12.32
475	LLV	39	26.94	123	19.83	1325	79997.53	2.17	-43.02	0.29	2.58	-40.97	-11.24
476	LLV	39	26.94	123	19.70	1325	79997.55	2.19	-43	0.44	2.73	-40.8	-10.92
477	LLV	39	26.94	123	19.53	1325	79997.18	1.82	-43.37	0.76	3.06	-40.84	-10.76
478	LLV	39	26.94	123	19.40	1340	79996.96	3.01	-42.69	1.11	3.39	-39.84	-9.6
479	LLV	39	26.94	123	19.28	1360	79996.19	4.12	-42.26	1.96	4.2	-38.6	-8.23
480	LLV	39	26.94	123	20.50	1310	79997.95	1.18	-43.5	0.08	2.31	-41.72	-12.81
481	LLV	39	26.94	123	20.63	1310	79998.52	1.75	-42.93	0.11	2.31	-41.14	-12.41
482	LLV	39	26.93	123	20.77	1310	79999.65	2.89	-41.78	0.19	2.37	-39.94	-11.39
483	LLV	39	26.85	123	20.93	1325	79999.86	4.63	-40.56	0.32	2.44	-38.65	-10.38
TOMKI	LM	39	19.59	123	13.42	865	80014.61	-13.14	-42.65	0.65	3.82	-39.18	-8.84
485	LM	39	20.09	123	15.23	2360	79926.42	38.51	-41.98	2.79	6.33	-36.51	-8.01
486	LM	39	20.13	123	15.08	2125	79942.95	32.89	-39.59	3.02	5.97	-34.41	-5.66
487	LM	39	20.07	123	14.95	2060	79944.99	28.9	-41.35	3.33	6.2	-35.93	-7.08

488	LM	39	20.00	123	14.78	2020	79945.77	26.03	-42.87	3.59	6.41	-37.22	-8.23
489	LM	39	19.90	123	14.70	1940	79951.83	24.71	-41.45	3.75	6.47	-35.73	-6.73
490	LM	39	19.69	123	14.47	1620	79968.08	11.18	-44.07	3.74	6.21	-38.49	-9.35
491	LM	39	19.66	123	14.31	1480	79976.66	6.64	-43.84	3.9	6.36	-38.06	-8.74
492	LM	39	19.59	123	14.15	1240	79989.35	-3.14	-45.43	3.45	6.11	-39.82	-10.34
493	LM	39	19.58	123	14.05	1220	79993.13	-1.22	-42.83	2.59	5.22	-38.1	-8.52
494	LM	39	19.56	123	14.00	1140	79998.3	-3.55	-42.43	2.02	4.77	-38.12	-8.48
495	LM	39	19.62	123	13.83	990	80007.53	-8.51	-42.28	1.32	4.36	-38.33	-8.42
496	LM	39	19.74	123	13.79	900	80011.66	-13.02	-43.72	1.08	4.4	-39.69	-9.61
497	LM	39	19.66	123	13.65	870	80012.94	-14.45	-44.12	0.76	4.06	-40.42	-10.26
498	LM	39	20.25	123	13.63	915	80011.32	-12.71	-43.91	0.53	3.87	-40.42	-9.7
499	LM	39	20.69	123	13.98	1260	79990.06	-2.17	-45.15	1.52	4.22	-41.43	-10.75
500	LM	39	20.16	123	12.72	1330	79985.09	0.22	-45.14	2.12	4.24	-41.43	-9.95
501	LM	39	20.16	123	12.89	1220	79992.99	-2.22	-43.83	1.72	4	-40.32	-8.99
502	LM	39	20.05	123	12.93	1110	80000.48	-4.91	-42.77	1.17	3.64	-39.58	-8.38
503	LM	39	19.99	123	13.01	980	80005.85	-11.68	-45.1	0.63	3.42	-42.09	-10.99
504	LM	39	19.98	123	13.12	910	80011.22	-12.88	-43.91	0.42	3.46	-40.83	-9.83
505	LM	39	20.05	123	13.23	875	80013.31	-14.18	-44.03	0.42	3.63	-40.75	-9.79
506	LM	39	20.08	123	13.29	860	80015.21	-13.74	-43.07	0.53	3.83	-39.59	-8.67
507	LM	39	20.08	123	13.39	915	80012.07	-11.71	-42.91	0.34	3.5	-39.79	-8.98
508	LM	39	20.67	123	13.71	960	80009.53	-10.89	-43.63	1.7	5.06	-38.96	-7.95
509	LM	39	21.11	123	13.82	970	80005.64	-14.49	-47.57	6.38	9.89	-38.08	-6.78
510	LM	39	21.64	123	13.92	1070	80001.5	-10	-46.5	3.3	6.6	-40.33	-8.67
511	LM	39	22.10	123	13.97	1260	79993.69	-0.63	-43.6	2.57	5.4	-38.7	-6.72
512	LM	39	22.49	123	13.97	1540	79977.41	8.85	-43.67	2.4	4.7	-39.58	-7.29
513*	LM	39	22.94	123	13.79	1968	79954.71	25.73	-41.39	2.25	4.31	-37.83	-5.03
513R	LM	39	22.93	123	13.84	1855	79954.71	15.12	-48.15	2.66	4.71	-44.15	-11.38
514*	LM	39	23.27	123	13.66	1887	79957.49	20.41	-43.95	1.3	3.31	-41.36	-8.08
515	LM	39	23.67	123	13.93	1840	79957.91	15.82	-46.94	1.64	3.65	-43.99	-10.61
516*	LM	39	24.11	123	14.16	1799	79963.47	16.87	-44.49	1.97	3.98	-41.2	-7.65
517	LM	39	24.56	123	14.24	1720	79965.89	11.2	-47.47	2.77	4.85	-43.29	-9.4
518	LM	39	24.94	123	14.46	1675	79969.92	10.43	-46.7	1.98	4.04	-43.31	-9.29
519	LM	39	25.24	123	14.30	1625	79970.79	6.16	-49.27	1.78	3.89	-46.02	-11.53
520	LM	39	25.78	123	14.55	1650	79969.76	6.68	-49.6	1.76	3.77	-46.47	-11.75
521	LM	39	26.08	123	14.65	1660	79969.08	6.5	-50.12	1.73	3.71	-47.06	-12.16
522	LM	39	19.97	123	17.90	1895	79960.07	28.62	-36.01	1.44	3.85	-32.89	-7.36

523	LM	39	19.99	123	16.12	3130	79879.62	64.26	-42.49	2.1	9.33	-34.24	-7.01
524	LM	39	19.81	123	16.21	3200	79874.57	66.06	-43.08	2.63	10.47	-33.7	-6.74
525	LM	39	19.68	123	16.28	3180	79875.35	65.15	-43.31	3.18	10.94	-33.45	-6.67
526	LM	39	19.57	123	16.31	3180	79876.39	66.35	-42.11	2.21	10.06	-33.13	-6.48
527	LM	39	19.48	123	16.47	3090	79880.53	62.16	-43.23	2.39	9.61	-34.67	-8.26
528	LM	39	19.53	123	16.63	3020	79886.36	61.34	-41.66	2.74	9.38	-33.33	-7.04
529	LM	39	19.61	123	16.77	2975	79891.06	61.69	-39.78	3.19	9.43	-31.38	-5.16
530	LM	39	19.53	123	16.99	2835	79896.36	53.94	-42.75	4.16	9.59	-34.15	-8.21
531	LM	39	19.56	123	17.17	2720	79904.1	50.83	-41.94	4.67	9.45	-33.46	-7.67
532	LM	39	19.55	123	17.32	2340	79928.02	39.03	-40.78	3.62	6.88	-34.76	-9.05
533	LM	39	19.57	123	17.46	2300	79931.81	39.03	-39.41	3.39	6.54	-33.72	-8.14
534	LM	39	19.63	123	17.62	2185	79938.9	35.22	-39.3	2.83	5.68	-34.43	-8.96
535	LM	39	19.51	123	17.82	1820	79960.88	23.05	-39.02	2.25	4.71	-35.01	-9.79
536	LM	39	19.33	123	17.89	1670	79971.16	19.49	-37.46	1.78	4.23	-33.88	-8.86
537	LM	39	19.27	123	18.02	1520	79978.18	12.5	-39.34	1.44	3.98	-35.96	-11.1
538	LM	39	19.16	123	18.22	1370	79985.63	6	-40.72	1.1	3.78	-37.48	-12.91
539	LM	39	19.08	123	18.42	1260	79995.7	5.85	-37.13	0.66	3.48	-34.16	-9.87
540	LM	39	19.03	123	18.60	1240	79998.28	6.62	-35.67	0.43	3.21	-32.96	-8.92
541	LM	39	19.14	123	20.13	1260	79999.32	9.38	-33.6	2.55	5	-29.1	-6.76
542	LM	39	18.94	123	19.91	1260	79999.44	9.79	-33.18	2.39	4.81	-28.88	-6.44
543	LM	39	18.88	123	19.56	1235	80000.45	8.54	-33.58	3.39	5.88	-28.19	-5.37
544	LM	39	18.95	123	19.21	1235	80001.15	9.14	-32.98	1.08	3.69	-29.79	-6.51
545	LM	39	18.90	123	19.00	1300	79996.1	10.28	-34.06	0.83	3.34	-31.24	-7.78
546	UV	39	19.23	123	13.35	850	80016.85	-11.78	-40.77	0.44	3.47	-37.65	-7.58
547	UV	39	18.77	123	13.12	825	80016.34	-13.96	-42.1	0.31	3.12	-39.32	-9.42
548	UV	39	18.44	123	12.63	805	80016.23	-15.47	-42.92	0.32	2.95	-40.31	-10.2
549	UV	39	18.10	123	12.43	780	80016.71	-16.84	-43.44	0.53	3.1	-40.66	-10.65
550	UV	39	17.75	123	12.29	780	80015.79	-17.24	-43.84	0.05	2.49	-41.68	-11.85
551	UV	39	17.35	123	12.21	760	80016.42	-17.9	-43.82	0.04	2.35	-41.78	-12.23
552	UV	39	17.00	123	12.28	760	80016.3	-17.5	-43.42	0.02	2.19	-41.55	-12.37
553	LM	39	18.68	123	15.90	2780	79898.67	52.34	-42.48	2.04	8.23	-35.23	-8.84
554	LM	39	18.50	123	15.91	2570	79910.78	44.97	-42.68	2.13	7.24	-36.37	-10.1
555	LM	39	18.37	123	15.92	2390	79923.08	40.54	-40.98	2.34	6.61	-35.24	-9.05
556	LM	39	18.23	123	15.93	2210	79933.31	34.05	-41.33	2.55	6.14	-36.01	-9.91
557	LM	39	18.12	123	15.97	2060	79940.81	27.61	-42.65	2.92	6.03	-37.4	-11.4
558	LM	39	17.97	123	15.92	1950	79948.95	25.62	-40.88	2.29	5.15	-36.48	-10.53

559	LM	39	17.85	123	15.77	1810	79957.54	21.23	-40.51	2.28	4.88	-36.32	-10.29
560	LM	39	17.70	123	15.61	1610	79969.3	14.4	-40.51	1.73	4.06	-37.07	-10.95
561	LM	39	17.52	123	15.57	1480	79977.27	10.41	-40.07	2.02	4.26	-36.39	-10.35
562	LM	39	17.38	123	15.47	1370	79983.67	6.67	-40.05	1.16	3.33	-37.27	-11.22
563	LM	39	16.70	123	14.80	1160	79994.93	-0.81	-40.37	1.12	3.04	-37.8	-11.58
564**	LM	---	---	---	---	---	---	---	---	---	---	---	---
565	LM	39	16.88	123	15.20	1200	79992.7	0.46	-40.47	1.51	3.52	-37.44	-11.48
566	LM	39	17.06	123	15.30	1240	79990.08	1.33	-40.96	1.58	3.65	-37.81	-11.81
567##	LM	---	---	---	---	---	---	---	---	---	---	---	---
568	LM	39	19.50	123	15.86	2880	79895.71	57.57	-40.66	1.74	7.83	-33.84	-6.7
569	LM	39	19.30	123	16.00	2920	79894.1	60.01	-39.58	1.56	8	-32.59	-5.8
570	LM	39	19.06	123	15.96	2930	79889.82	57.03	-42.9	1.44	8.2	-35.72	-9.1
571	LM	39	18.77	123	15.98	2880	79892.37	55.31	-42.92	2.17	8.89	-35.04	-8.6
572	LLV	39	27.80	123	19.91	1360.8	979997.5	4.2	-42.21	0.36	4.18	-38.57	-8.18
573	LLV	39	27.29	123	19.72	1346.3	979997.6	3.74	-42.18	0.17	3.45	-39.27	-9.1
574	LLV	39	25.87	123	19.94	1333.1	979991.9	-1.15	-46.61	0	2.03	-45.12	-16.51
575	LLV	39	26.19	123	19.91	1326.7	979993.6	-0.51	-45.76	0	2.13	-44.16	-15.2
576	LLV	39	26.46	123	19.91	1324	979994.9	0.19	-44.97	0	2.23	-43.27	-14.07
577	LLV	39	26.53	123	20.12	1328	979995.3	0.79	-44.5	0	2.19	-42.84	-13.84
578	LLV	39	26.93	123	20.12	1318.8	979997.2	1.26	-43.72	0	2.42	-41.83	-12.46
579	LLV	39	26.70	123	20.12	1320.9	979996.2	0.78	-44.27	0	2.28	-42.52	-13.36
580	LLV	39	19.44	123	18.06	1613.1	979975.5	18.29	-36.73	0.57	3.98	-33.37	-8.43
581	LLV	39	20.18	123	18.31	1886.4	979962.2	29.66	-34.68	0.37	3.29	-32.11	-6.87
582	LLV	39	20.92	123	19.05	1907	979960.4	28.64	-36.4	0.21	2.63	-34.5	-9.48
583	LLV	39	21.68	123	18.71	1752.3	979966.3	18.91	-40.85	0.49	2.75	-38.78	-12.63
584	LLV	39	22.34	123	19.20	1555.4	979976.8	9.91	-43.14	0.08	2.1	-41.65	-15.43
585	LLV	39	22.87	123	20.42	1425.1	979986.8	6.86	-41.74	0.08	2.2	-40.11	-14.84
586	LLV	39	22.20	123	19.54	1480	979983.8	10	-40.48	0.14	2.36	-38.71	-13.01
587	LLV	39	21.98	123	20.05	1570.6	979980.4	15.45	-38.12	0.28	2.55	-36.18	-11.32
588	LLV	39	21.68	123	20.62	1774.2	979971.4	26.03	-34.48	0.32	3.04	-32.13	-8.28
589	LLV	39	21.11	123	20.30	2035.1	979954.9	34.97	-34.44	0.27	2.99	-32.22	-8.54
590	LLV	39	21.55	123	19.86	1605.6	979979	17.99	-36.77	0.57	3.13	-34.27	-9.56
591	LLV	39	28.08	123	21.52	1333.1	979999.9	3.64	-41.83	0.78	3.61	-38.75	-10.13
592	LLV	39	27.43	123	20.86	1330	979999.8	4.22	-41.15	0.34	2.85	-38.83	-9.95
593	LLV	39	26.57	123	21.19	1339.8	979999.4	5.98	-39.72	0.08	2.45	-37.8	-10.13
594	LLV	39	26.15	123	21.39	1333.6	979999.1	5.7	-39.79	0.22	2.55	-37.77	-10.73

595	LLV	39	25.66	123	21.39	1347.9	979996.8	5.49	-40.49	0.42	2.56	-38.46	-11.87
596	LLV	39	25.47	123	22.97	1643.5	979978.7	15.42	-40.64	0.42	2.64	-38.63	-14.33
597	LLV	39	26.01	123	22.76	1500	979988.8	11.25	-39.91	0.39	2.76	-37.74	-12.63
598	LLV	39	25.65	123	22.03	1709.6	979974.5	17.18	-41.12	0.11	2.29	-39.5	-13.83
599	LLV	39	25.29	123	21.53	1624.3	979978.6	13.78	-41.62	0.23	2.3	-39.96	-13.97
600	LLV	39	28.60	123	18.37	1943.1	979960.5	20.82	-45.45	0.74	3.3	-42.9	-10.05
601	LLV	39	28.60	123	19.04	1981.3	979960.6	24.47	-43.1	0.44	2.99	-40.87	-8.84
602	LLV	39	28.06	123	19.37	2145.8	979951.1	31.27	-41.92	0.69	3.92	-38.8	-7.71
603	LLV	39	27.47	123	18.90	2223.5	979945.2	33.53	-42.31	0.74	4.27	-38.86	-7.75
604	LLV	39	28.08	123	20.12	1388.7	979995.7	4.67	-42.69	0.51	4.4	-38.84	-8.46
605	LLV	39	27.56	123	19.97	1335.2	979998.5	3.17	-42.37	0.02	3.32	-39.58	-9.48

Notes:
[#] Leading 9 omitted from absolute gravity value
Geographic coordinates in NAD27 per USGS
LLV: Little Lake Valley
LM: Laughlin Mountain
UV: Ukiah Valley and northern Ukiah Valley
Lay: Laytonville
* Elevation interpolated from U. S. Geological Survey 30-m DEM
** Data omitted by U. S. Geological Survey due to poor DEM coverage
[##] Data omitted by U. S. Geological Survey due to poor observed gravity value

Appendix 2: National Geodetic Survey benchmarks used as gravity station locations

Station ID	Stamped Benchmark Designation	PID Number	Latitude Degrees	Latitude minutes	Longitude Degrees	Longitude minutes	Elevation (feet)	Elevation (meters)	Calculated Absolute Gravity (mGal)
120	NN 959	KT1279	39	25.67	123	19.46	1339	408	79992.59
189	H 104	KT1115	39	23.50	123	20.25	1390	424	79984.01
263	W 104	KT1165	39	9.57	123	12.27	610	186	80018.83
519	USGS 27 S	NA*	39	25.24	123	14.30	1625	495	79970.79
522	L 104	KT1127	39	19.97	123	17.90	1895	578	79960.07

PID: Permanent Indentifier
*Station 519 (USGS 27 S) not located on National Geodetic Survey benchmark database (http://www.ngs.noaa.gov/cgi-bin/datasheet.prl).
Benchmark is located on the Foster Mountain Quadrangle 7 1/2 minute series at the bridge intersection of Tomki Road and Redwood Valley Road, southwest of Cave Creek and Tomki Creek confluence.